Preparation and properties of nano-structures fabricated from porphyrin polymers with inorganic nano-materials

Department of Functional Molecular Scinece

School of Mathematical and Physical Science

The Graduate University for Advanced Studies

Hiroaki Ozawa

2007

Contents

Chapter 1. General Introduction

In this Chapter, the background and molecular electronics and the review of this Thesis are described.

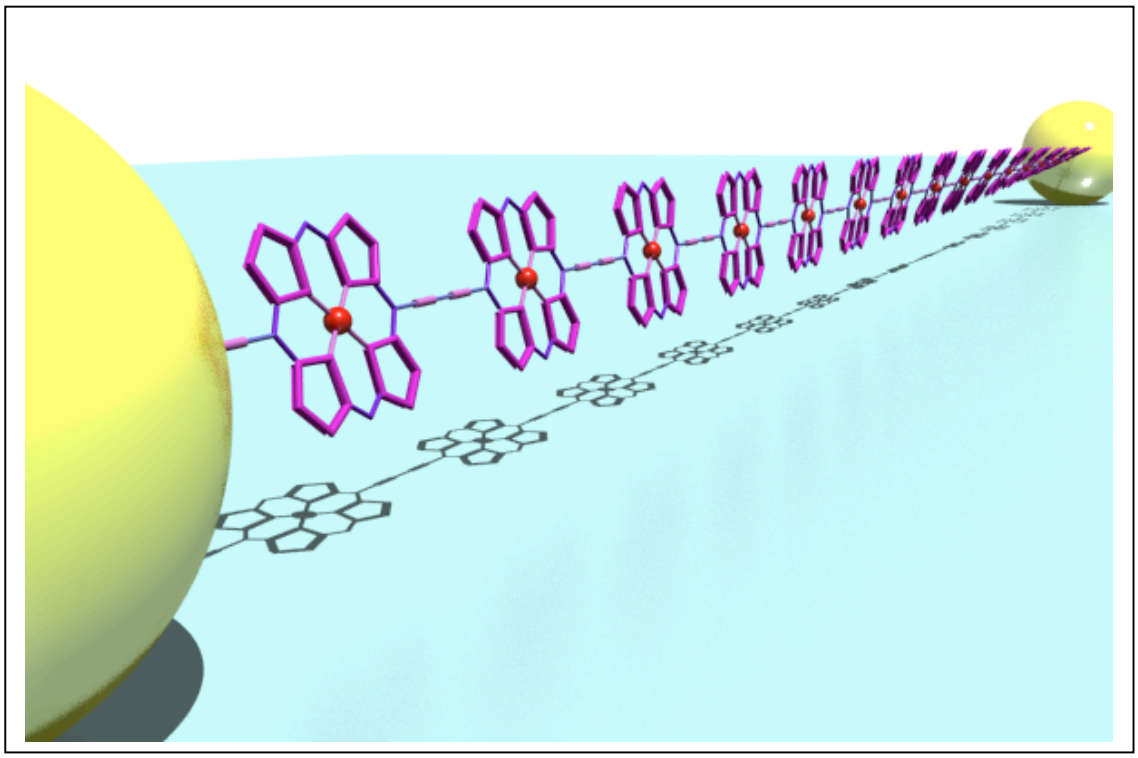

1-1. Background

The idea of molecular electronics comes from a theoretical proposal of Aviram and Ratner in 1974, predicting that single molecules with a donor-bridge-acceptor structure would have rectifying properties when placed between two electrodes.[1] Their theoretical calculation results from a study of molecule **1** (Figure 1-1), composed of a donor moiety tetrathia fulvalene (TTF) connected by a triple methylene bridge to and acceptor moiety, 7,7,8,8-tetracyanoquino-dimethane (TCNQ), showed a rectification of current should be possible. The rectification behavior can be explained by the energy-level diagrams for the system (Figure 1-1).

At positive bias (Figure 1-1(b)), when the applied field become enough for the cathode levels to overlap the acceptor LUMO (A) and for the anode levels to overlap the HOMO (D), the passage of electron current begins with the electron transfer from the cathode to the acceptor and from the donor to the anode (these transfers are represented by "A" and "C" in Figure 1-1(b), respectively), and the internal tunneling process from the acceptor LUMO (A) to the donor HOMO (D) (this transfer is represented by "B" in Figure 1-1(b)). On the other hand, in reverse bias (Figure 1-1(c)), the donor LUMO (D) would have to be lowered to the Fermi level of the metal on the right and the Fermi level of the metal on the left would have to be lowered below the acceptor HOMO (A) in order to occur electron transfer. This allows an electron to tunnel from LUMO (D) to HOMO (A). Another mechanism must be considered, in which the first step is an internal process of tunneling from HOMO (D) to LUMO (A). Then, electron transfer can occur from LUMO (A) to the metal and from the metal to HOMO (D).

However, the proposal was premature in that both the chemical synthesis of such a rectifying molecule and the fabrication of such a device. With recent developments in chemical synthesis and micro-fabrication, many of these challenging experiments have been done. For example, Metzger et al. realized the D-A rectification through Langmuir-Blodgett (LB) multi layers and mono layers of hexadecylquinolinium trixyanoquinodimethanide in 1997.[2]

Instead of using LB films, Reed proposed conjugated oligomers with precisely controlled length as molecular devices using self-assembly techniques.

Mechanically controllable break junctions were originally used to study conductance quantization.[3] In 1997, Reed et al. first applied these technique to measure electronic transport through a single molecules.[4] Using similar technique, Kergueris et al. employed a micro-fabricated break junction to study transport through oligothiophene molecules.[5] Zhou et al. applied a vertical electrode method,[6] first developed by Ralls et al.,[7] to characterize molecular junctions. This technique realized direct and robust metal-molecule contacts and allows for variable-temperature measurements, leading to further understanding of metal-SAM contact[8,9] and nonlinear molecular devices.[9]

In the meantime, the discovery of the scanning tunneling microscopy (STM) opened a new horizon for the study of molecular scale electronics. It allows for imaging, probing, and manipulation of single molecules.[10-13] The first demonstration of conduction through single molecule was made by Bumm et al. who measured electron transport through individual molecules isolated in an insulating alkanethiol matrix using STM.[12] Dorogi et al. succeeded in extracting the conductance of vinylene-dithiol by measuring current-voltage I(V) characteristics with an STM tip placed above gold cluster on a xylene-dithiol SAM covered gold surface.[13]

In addition, the search for individual molecules with the ability to behave as switches and memories has been performed.[9]

Combination of molecular elements such as wires, switches, and memories to created devices with more complex functionality are the logical next step in further development of molecular electronics.

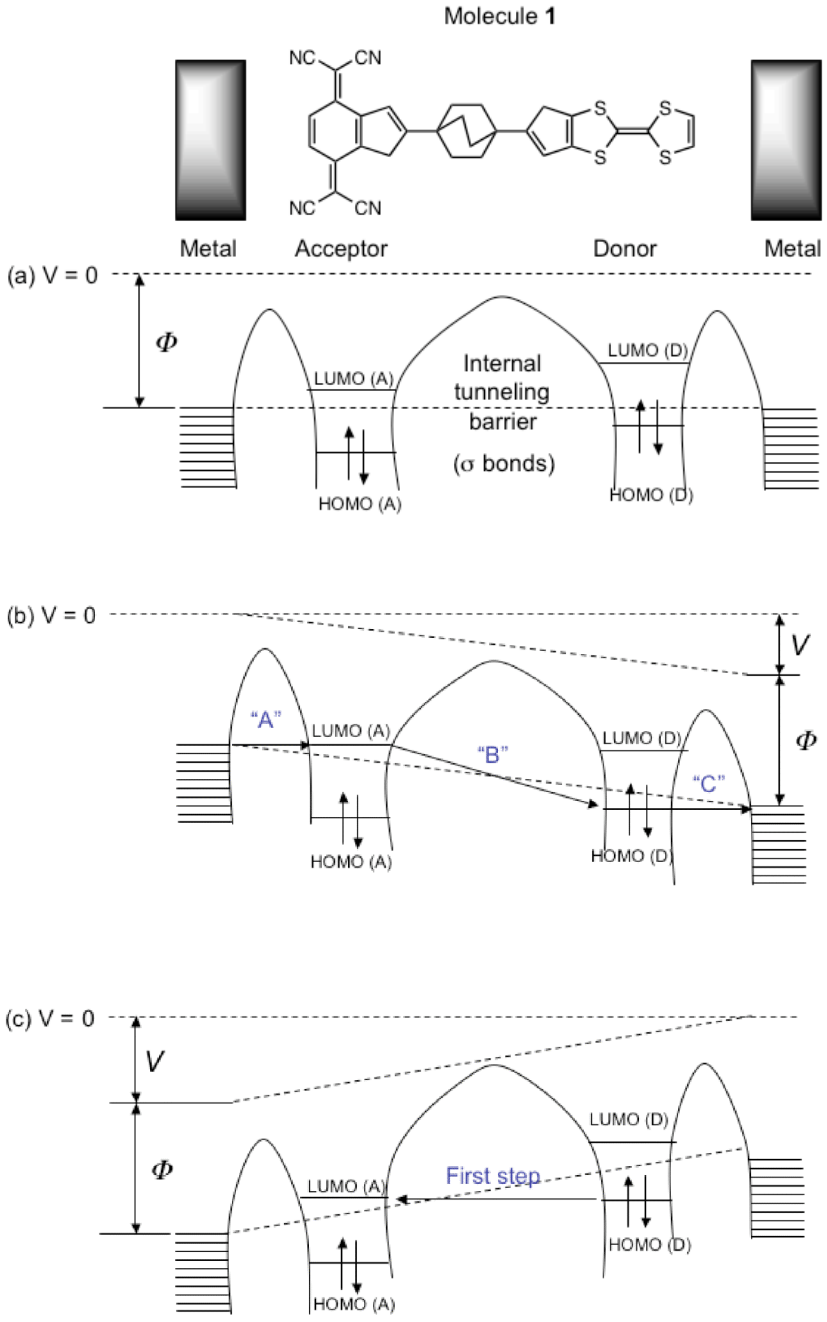

Figure 1-1. (a) Energy-level diagrams of **1**, the donor-acceptor systems, between two metal electrodes, (b) under positive applied bias (c) under reverse applied bias. ϕ = Fermi energy, V = applied bias. Modified the figure in ref. 15.

1-2. Molecular electronics

Molecular electronics involves the use of single molecules, small groups of molecules, or carbon nanotubes in device-based structures, that can be used as the fundamental units for electronics components such as wires, switches, memories and gain elements.[14-17] From the broader definition, it can be suggested that any device utilizing molecular properties is a molecular electronic devices.

Molecular electronics is conceptually different from conventional solid state semiconductor electronics.[18] It allows chemical engineering of organic molecules with their physical and electronic properties tailored by synthetic methods, bringing a new dimension in design flexibility that does not exist in typical inorganic electronic materials. It is well known that semiconductor devices are fabricated from the "top-down" approach that employs a variety of sophisticated lithographic and etch techniques to pattern a substrate. This approach has become increasingly challenging as feature size decreases. In particular, at nanometer scale, the electronic properties of semiconductor structures fabricated via conventional lithographic processes are increasingly difficult to control. In contrast, molecules are synthesized from the "bottom-up" approach that builds small structures from the atomic, molecular, or single device level. It in principle allows a very precise positioning of collections of atoms or molecules with specific functionalities. For example, one can selectively add an oxygen atom to a molecule with a precision far greater that an oxidation step in micro-fabrication using state of the art lithography and etching. Chemical synthesis makes it possible to make large quantities of nanometer size molecules with the same uniformity but at significantly less cost, compared to other batch-fabrication processes such as microlithography. One can envision that in assembling molecular circuits, instead of building individual components on a chip one will synthesize molecules with structures possessing desired electronic configurations and attach/interconnect them into an electronic circuit

using surface attachment techniques like self-assembly. Self-assembly is a phenomenon in which atoms, molecules, or groups of molecules arrange themselves spontaneously into regular patterns and even relatively complex systems without outside intervention.

Basic charge transport mechanisms of bulk organic materials

Electron transport in bulk organic materials can be characterized by the macroscopic conductivity. Most conjugated polymer systems are electrically non-conducting unless they are doped.

In the case of poly(*p*-phenylene) (Figure 1-2), when an electron is removed from the system of its backbone (chemical oxidation), an unpaired electron with spin 1/2 (a free radical) and a spinless positive charge (cation) are created. The radical and cation are coupled to each other via a local bond rearrangement, creating a polaron which appears in the band structures as localized electronic states symmetrically located within the gap with the lower energy states being occupied by a single unpaired electron. Further oxidation creates dications in the polymer. An electron can be removed from either the polaron or the remaining neutral portion of the chain. In the former case, the free radical of the polaron is removed and a dication is created comprised of two positive charges coupled through the lattice distortion, creating a new spinless defect bipolaron. Removal of an additional electron from a neutral portion of the chain would create two polarons. Because the formation of a bipolaron produces a larger decrease in ionization energy compared to the formation of two polarons, the former process is thermodynamically favorable. These new empty bipolaron states are also located symmetrically within the bandgap. Further doping creates additional localized bipolaron states, which eventually overlap to form continuous bipolaron bands at high enough doping levels.

In the case of conjugated polymers with degenerate ground state structures, the situation is different. The initial oxidation of trans-polyacetylene also creates polarons as discussed previously. When it is further oxidized, since its ground state is twofold degenerate, the bonding configurations

on either side of the charged defects only differ by a reversed orientation of the conjugated system and are energetically equivalent resonance forms. It in turn creates isolated, non-interacting charged defects that form domain walls separating two phases of opposite orientation but identical energy. Such defects are called solitons, which result in the creation of new localized electronic states that appear in the middle of the energy gap. As the doping level increases, these states can overlap to form soliton bands.

It is now well accepted that in conducting polymer, transport occurs by the movement of charge carriers between localized states or between soliton, polaron, or bipolaron states. Conjugated polymers have a bulk conductivity limited not by carrier mobility in a molecule but by inter chain hopping, and, macroscopic conductivity measurements do not directly probe single molecule properties. The mechanism of bulk conductivity involves incoherent diffusive.

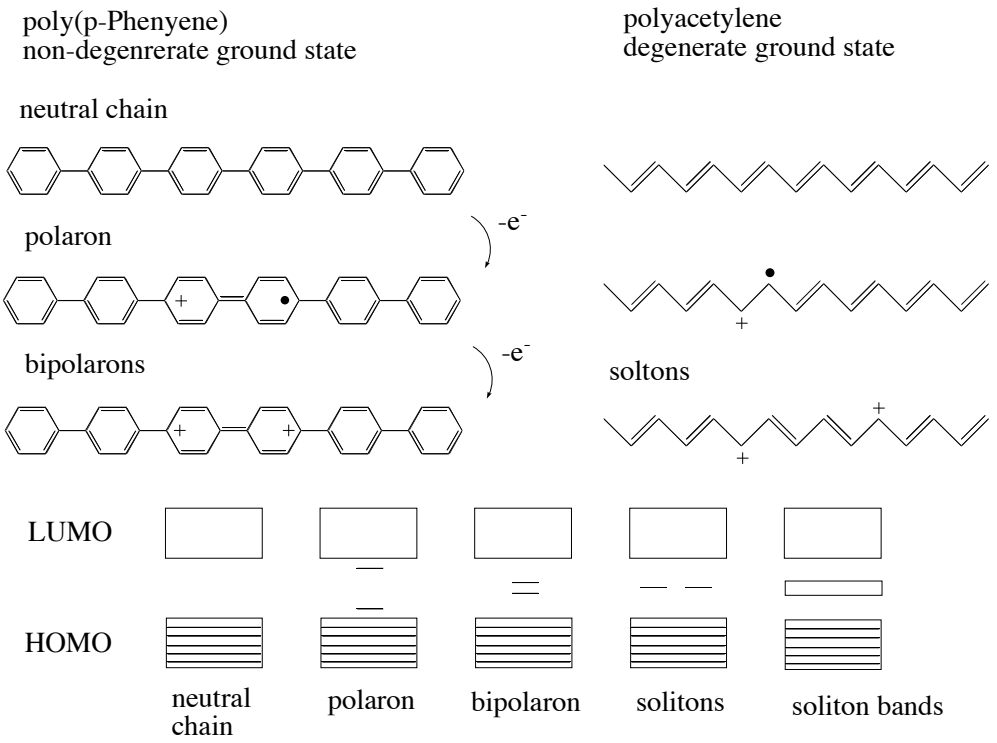

Figure 1-2. Neutral chain and oxidation of poly(p-phenylene)(left) and polyacetylene (right) and the creation of polaron, bipolaron and solitons states. (Modified the table in ref. 19)

The mechanisms of electron transport in single or a little of molecule

The possible conduction mechanisms in the single or a little of molecule-metal junction are listed in Table 1-1, with their characteristic behavior, temperature dependence, Voltage dependence and schematic diagrams.[19] Five mechanisms are reported along with more classical process for bulk materials.

Schottky emission is a process in which carriers overcome the molecule/contact barrier by thermionic emission, whose current is a strong function of temperature. The Schottky barrier usually arises from partial charge transfer from one phase to another at an interface.

Frankel-Pool conduction is due to field-enhanced thermal excitation of trapped electrons into the conduction band, a process similar to Schottky emission. A trap in this context is a "Coulombic" site whose potential well depth varies in an electric field. The energy barriers for Frankel-Pool conduction are within the molecule rather than at the molecule/ contact interface. Its current has the same temperature dependence as that of Schottky emission, but with different voltage dependence.

Hopping conduction usually refers to the thermally activated electron transfer that follows a classical Arrhenius relation, whose conductance also depends strongly on temperature.

Fowler-Nordheim tunneling refers to an enhanced tunneling rate that occurs in high electric fields, being also called "field emission. High means that the applied voltage exceeds the barrier height and is well beyond the linear voltage behavior implied by the Simmons relation.

Direct tunneling (classical or coherent tunneling) is based on the probability of and electron transition through a barrier of some thickness and height, and maintains the phase of the electron. The tunneling processes (Fowler-Nordheim and direct) have not the temperature dependence but strongly depend on distances of the single-molecule junction and applied voltage.

Table 1-1. Conduction mechanisms[a]

Conduction mechanism		Temperature dependence	Voltage dependence	Schematic band diagram
Schottky emission	$I = A_s T^2 \exp\left(-q\dfrac{\Phi - \sqrt{\dfrac{qV}{4\pi\varepsilon d}}}{kT}\right)$	$\ln\left(\dfrac{I}{T^2}\right) \sim \dfrac{I}{T^2}$	$\ln(I) \sim \sqrt{V}$	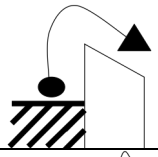
Frankel-Pool Conduction	$I = A_{FP} V T^2 \exp\left(-q\dfrac{\Phi - \sqrt{\dfrac{qV}{\pi\varepsilon d}}}{2kT}\right)$	$\ln\left(\dfrac{I}{T^2}\right) \sim \dfrac{I}{T^2}$	$\ln\left(\dfrac{I}{V}\right) \sqrt{V}$	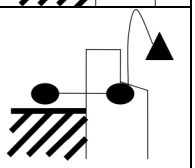
Hopping conduction	$I = A_H V \exp\left(\dfrac{\Delta E}{kT}\right)$	$\ln\left(\dfrac{I}{V}\right) \sim \dfrac{I}{T^2}$	$I \sim V$	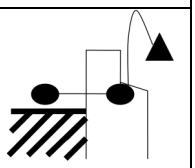
Fowler-Nordheim tunneling	$I = A_{FN} V^2 \exp\left(-\dfrac{4d\sqrt{2m}}{3qhV}(q\Phi)^{3/2}\right)$	—	$\ln\left(\dfrac{I}{V^2}\right) \sim \dfrac{I}{V}$	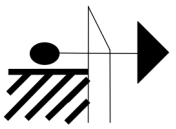
Direct tunneling	$I = A_T V \exp\left(-\dfrac{4\pi d}{h}\sqrt{2m\Phi}\right)$	—	$I \sim V$	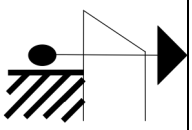

[a] I = Current, V = applied voltage, T = Temperature, A_x = proportionality constant, q = electron charge, Φ = energy barrier, ε = dielectric constant, d = molecular length, k = Boltzmann constant, E = activation barrier, m = electron mass and h = plank constant. (Modified the table in ref. 19)

1-3. Thesis overview

The overall objective of this thesis is to clarify the properties of nano-structures fabricated from porphyrin polymers with inorganic nano-materials. The studies in electric conduction of single molecules have been performed extensively, and interesting phenomena were reported. However, it is difficult to construct practical devices only by molecules because they have relatively low conductance. Thus, we have attempted to prepare nano-structures fabricated from organic molecules and conductive nano-materials such as gold nano-particles or carbon nanotubes.

In Chapter 2, synthesis, characterization of dendron protected porphyrin polymers and observation of the structures on various solid surfaces are described. The porphyrin polymers are useful for construction of nanostructures.

In Chapter 3, the preparation of 4-pyridineethanethiol capped gold nano-particles and one-dimensional assemblies of gold nanoparticles chemically linked to porphyrin polymers are described. 4-Pyridineethanethiol capped AuNPs were connected to porphyrin polymer, which were deposited on substrate surfaces. The assemblies were observed by AFM and SEM to clarify the structures.

In Chapter 4, the one-dimensional assemblies of gold nanoparticles linked to porphyrin polymers were made between nano-gapped electrodes, and then electric properties were studied to show a photo-response of the devices.

In Chapter 5, the synthesis of end-functionalized porphyrin oligomers is described. A series of porphyrin oligomers were end-functionalized by 1-[4-(S-acetylthiomethyl)phenyl]ethynyl groups or 2-pyrenylethynyl groups. Spectroscopic studied of oligomers were performed, to clarify the effects of the end-functional groups on the main π-conjugated electronic systems. Porphyrin oligomers end-functionalized by thiol groups can be connected to gold nanorods or nanoparticles, and those which end-functionalized by pyrenyl groups can be adsorbed to the surface of carbon nanotubes efficiently through π-π interactions.

Chapter 6 will summarize the results and discussions.

Reference

1. Aviram, A.; Ratner, M. A. *Chem. Phys. Lett.* **1974,** *29*, 277-283.
2. Metzger, R. M.; Chen, B.; Hopfner, U.; Lakshmikantham, M. V.; Vuillaume, D.; Kawai, T.; Wu, X. L.; Tachibana, H.; Hughes, T. V.; Sakurai, H.; Baldwin, J. W.; Hosch, C.; Cava, M. P.; Brehmer, L.; Ashwell, G. J. *J. Am. Chem. Soc.* **1997,** *119*, 10455-10466.
3. Muller, C. J.; Krans, J. M.; Todorov, T. N.; Reed, M. A. *Phys. Rev. B* **1996,** *53*, 1022-1025.
4. Reed, M. a.; Zhou, C.; Muller, C. J.; Burgin, T. P.; Tour, J. M. *Science* **1997,** *278*, 252-254.
5. Kergueris, C.; Bourgoin, J. P.; Palacin, S.; Esteve, D.; Urbina, C.; Magoga, M.; Joachim, C. *Phys. Rev. B* **1999,** *59*, 12505-12513.
6. Zhou, C.; Deshpande, M. R.; Reed, M. A.; Jones, L.; Tour, J. M. *Appl. Phys. Lett.* **1997,** *71*, 611-613.
7. Ralls, K. S.; Buhrman, R. a.; Tiberio, R. C. *Appl. Phys. Lett.* **1989,** *55*, 2459-2461.
8. Chen, J.; Calvet, L. C.; Reed, M. A.; Carr, D. W.; Grubisha, D. S.; Bennett, D. W. *Chem. Phys. Lett.* **1999,** 313, 741-748.
9. Chen, J.; Reed, M. A.; Rawlett, A. M.; Tour, J. M. *Science* **1999,** *286*, 1550-1552.
10. Binnig, G.; Rohrer, H.; Gerber, C.; Weibel, E. *Phys. B & C* **1982,** *110*, 2075-2077.
11. Eigler, D. M.; Schweizer, E. K. *Nature* **1990,** *344*, 524-526.
12. Bumm, L. a.; Arnold, J. J.; Cygan, M. T.; Dunbar, T. D.; Burgin, T. P.; Jones, L.; Allara, D. L.; Tour, J. M.; Weiss, P. S. *Science* **1996,** *271*, 1705-1707.
13. Dorogi, M.; Gomez, J.; Osifchin, R.; Andres, R. P.; Reifenberger, R. *Phys. Rev. B* **1995,** *52*, 9071-9077.
14. Joachim, C.; Gimzewski, J. K.; Aviram, A. *Nature* **2000**, *408*, 541.
15. Carrol, R. L.; Gorman, C. B. *Angew. Chem. Int. Ed.* **2002**, *41*, 4379.
16. Heath, J. R.; Ratner, M. A. *physics Today* **2003**, *56*, 43.

17. Maruccio, G; Cingolani, R.; Rinaldi, R. *J. Mater. Chem.* **2004**, *14*, 542.
18. Sze, S. M. Eds. Physics of Semiconductor Devices, 2nd ed.: Wiley: New York, 1981.
19. Reed, M. A.; Lee, T., Eds. Molecular Nanoelectronics: American Scientific Publisher: California, 2003.

Chapter.2 Dendron protected porphyrin polymers

In this chapter, dendron protected porphyrin polymers are described

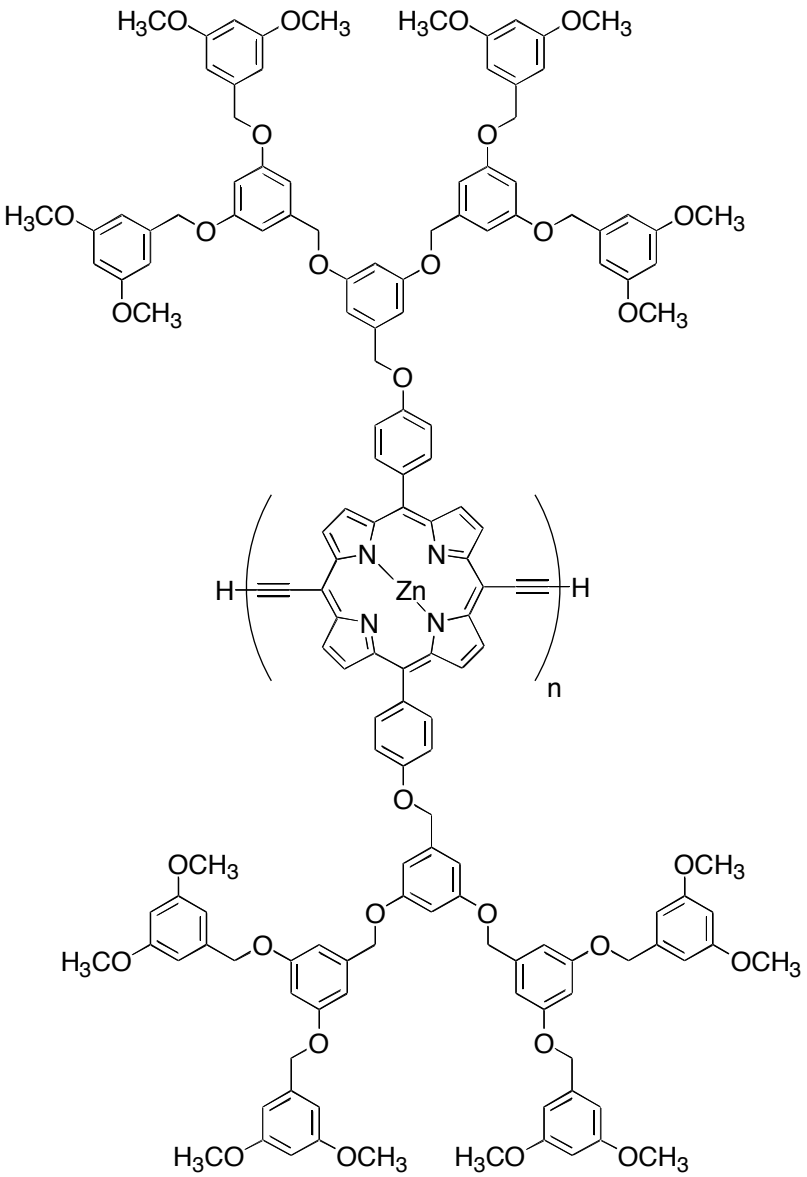

2-1. Introduction

π-Conjugated porphyrin systems have been attracted much attentions as potential materials because they have specific electronic and optical properties.[1-5] Particularly, one-dimensional porphyrin oligomers were interesting for optical and electric wires.[1, 6-8] However, most of these studies have been performed in solutions or for aggregates or for a large number of molecules on solid states. I am interested in measuring the conductance of single molecules using scanning probe microscopic techniques. In order to realize it, it is necessary to synthesize long and thick molecules, which is visible even on the rough surface and can be deposited on solid surfaces without making aggregates.

Highly oriented pyrolytic graphite (HOPG) is suitable substrate for molecular observation by AFM and STM. However, it is not suitable for electric measurement in lateral direction because of its electric conductance. Insulative substrate such as SiO_2/Si or glass substrates are suitable for electric or optical measurements. But these substrates have roughness of *ca.* 1 nm. In order to observe individual molecules on such rough surfaces, thick molecular wires are required whose diameter is more than 2 nm.

Deposition of isolate porphyrin polymer on solid surfaces were difficult because of the affinity between substrates and porphyrin polymers and difference of surface-dried condition when sample preparation on solid surfaces. It is necessary to deposit on solid surfaces without making aggregates.

We report the synthesis of dendron protected porphyrin polymers whose diameters are expected to be ca. 4.5 nm based on the MM calculation. To deposit isolated porphyrin polymer on surfaces, we use Langmuir-Blodgett (LB) techniques and modification of solid surfaces. The structures of dendron protected porphyrin polymers on various substrates, which have rough surface, are confirmed by AFM observations.

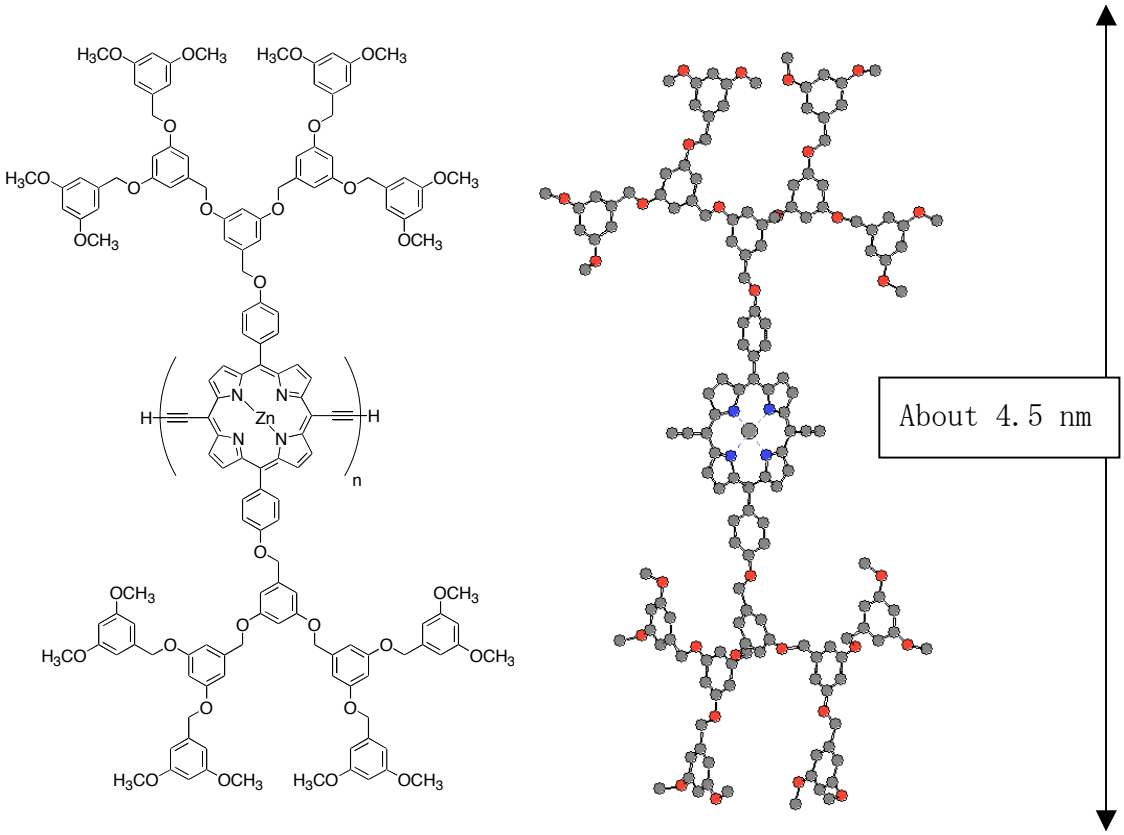

Figure 2-1. The structure of dendron protected porphyrin polymer (left). The optimized structure by MM calculation (right).

2-2. Synthesis of dendron protected porphyrin polymers

Synthetic scheme of the dendron protected porphyrin polymers is shown in Scheme 2-1. 5,15-Bis(4-methoxyphenyl)porphyrin (**1**) was synthesized by a reported procedures. Bromination of **1** was performed by N-bromosuccinimide (NBS) to give **2**.[9,10] Compound **3** was obtained by demethylation of **2** with BBr_3.[11] By introduction of zinc atom and dendron functionality, porphyrin **4** was obtained.[9-11] Ethynyl groups were introduced by the Sonogashira coupling to give **5**,[9] whose trimethylsilyl groups (TMS) was removed by tetrabutylammonium fluoride (TBAF) to afford the porphyrin monomer **6**[9]. Dendron protected porphyrin polymer **7** were prepared by the copper oxidative coupling of the monomer **6**.[12]

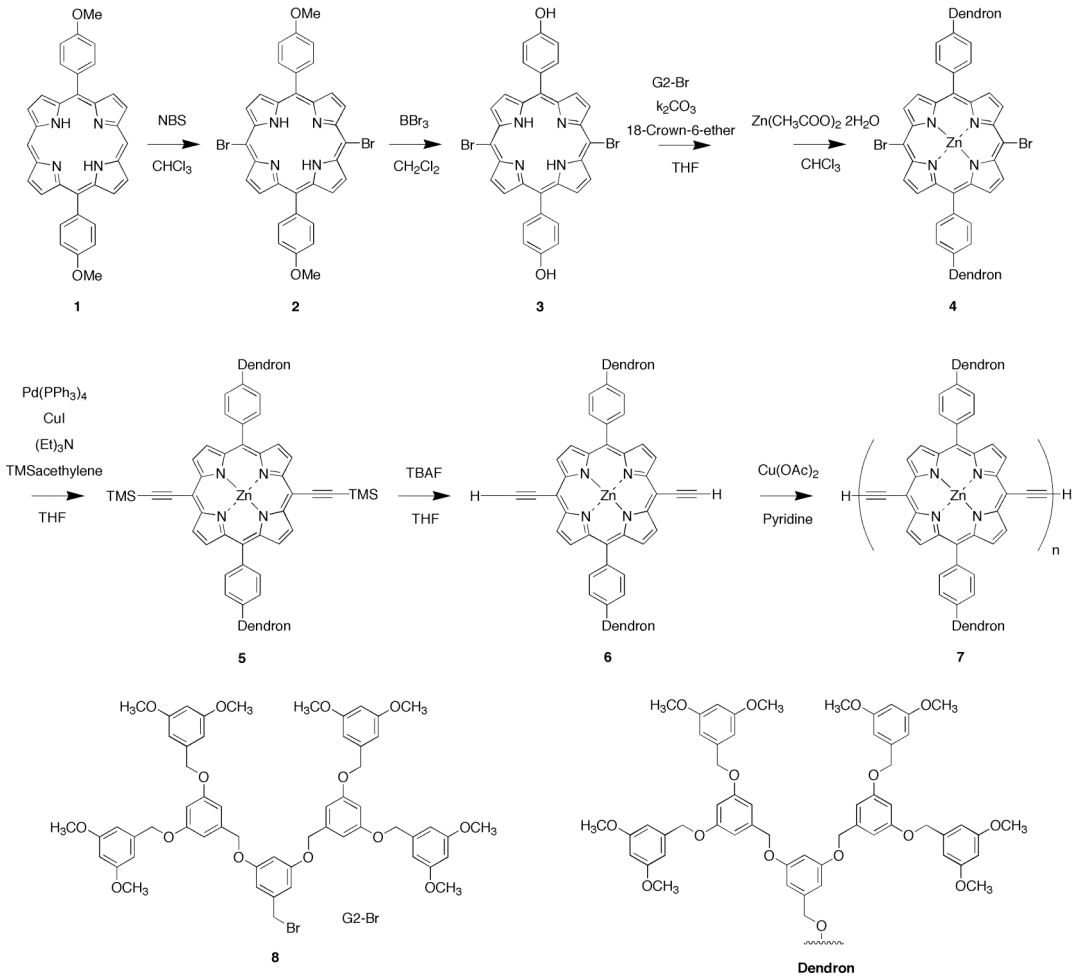

Scheme 2-1. Synthetic scheme of the dendron protected porphyrin polymer.

2-3. Characterization of the dendron protected porphyrin polymers

2-3-1. Molecular weight analysis of the dendron protected porphyrin polymers 7

The molecular weights of the porphyrin polymers were determined by matrix assisted laser desorption/ionization time of flight mass spectroscopy (MALDI-TOF-MS). The mass spectra of the polymers were shown in Figure 2-2. From the mass spectra of monomer to 13 mer could be identified. However, it was difficult to determine the molecular weights of the longer porphyrin polymers more than 13 mer by MALDI-TOF-MS, because of both the limitation of the instrumentation and the difficulty for ionization of these high molecular weight species.

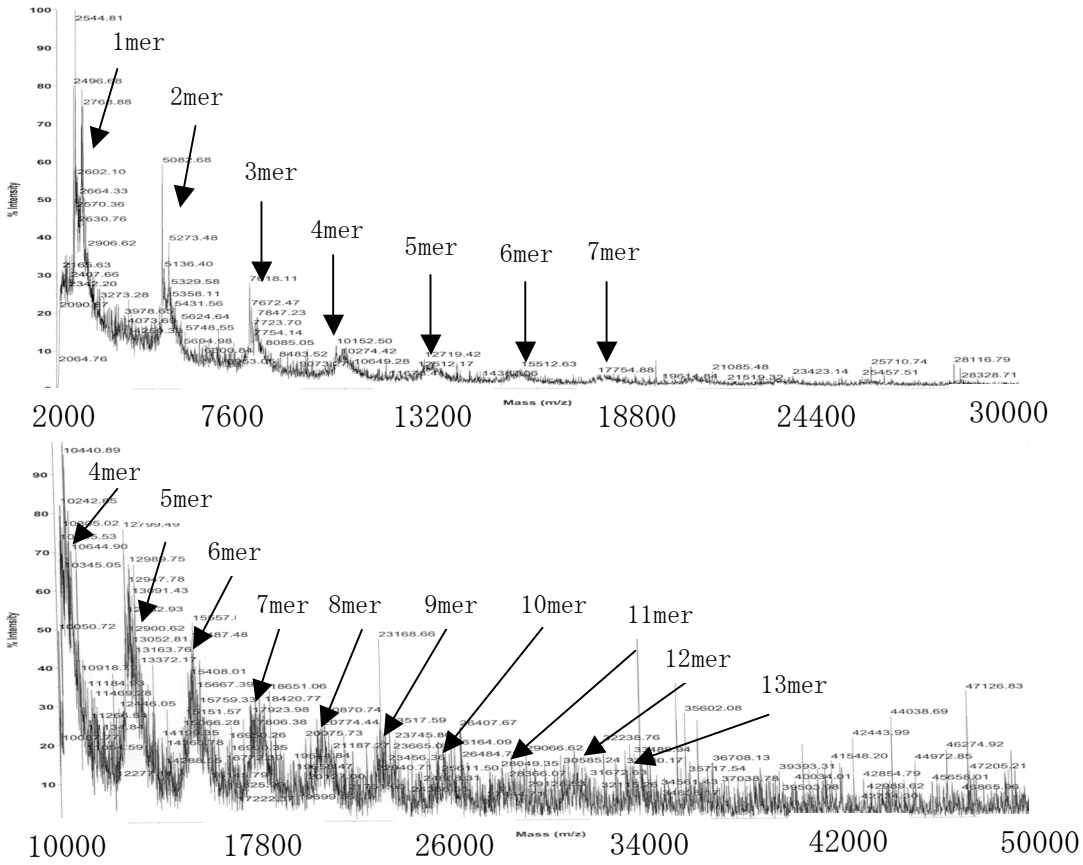

Figure 2-2. MALDI-TOF-MS spectra of the porphyrin polymers. 9-Nitroanthracene was used as a matrix.

Molecular weight distribution of the porphyrin polymers was analyzed by the analytical GPC calibrated by standard polystyrenes (Figure 2-3). Analytical GPC data clearly indicated the presence of porphyrin polymers whose molecular weights are more than 500,000 Dalton. The molecular weight corresponded to about 200 units of the porphyrin, as calculated from the molecular weight of one unit (2,536).

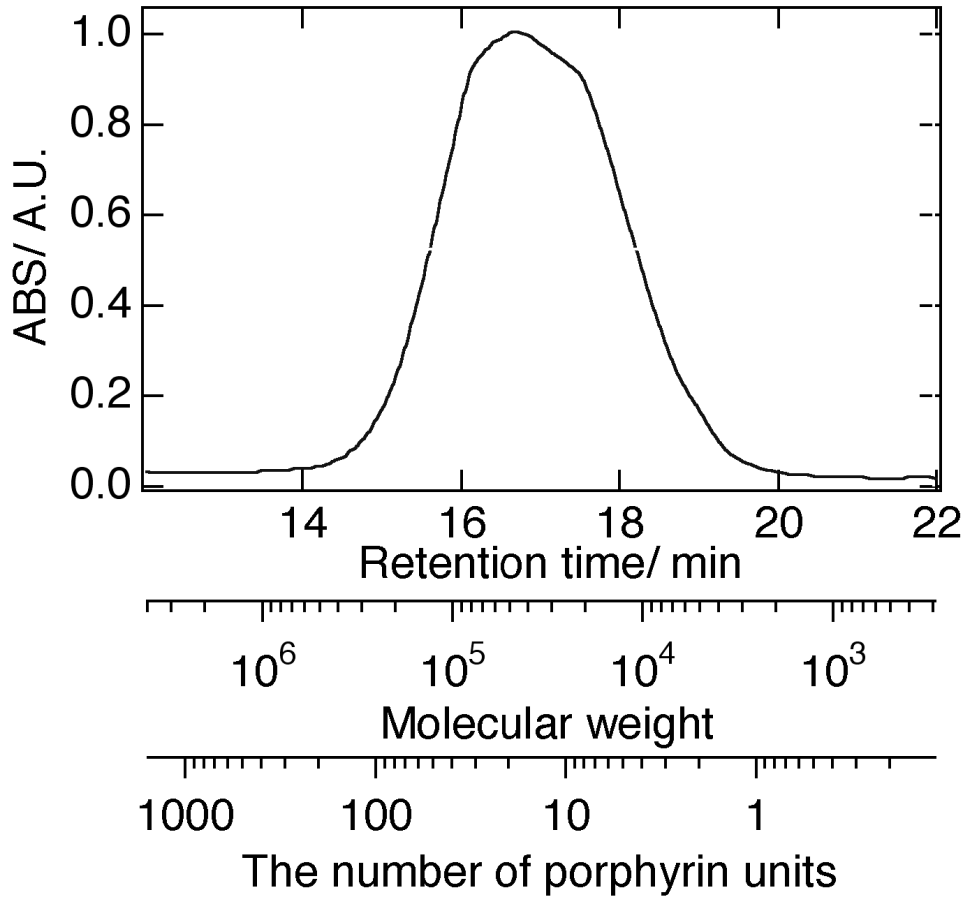

Figure 2-3. Analytical GPC data of the porphyrin polymers. Molecular weight was calibrated by standard polystyrene.

2-3-2. ^{1}H NMR spectrum of the dendron protected porphyrin polymers

^{1}H NMR spectrum of the dendron protected porphyrin polymer **7** taken in dimethylformamide (DMF) at room temperature was shown in Figure 2-4. In the spectrum, the broad peaks of β-protons (H^1 and H^2) appeared at 9.98 and 9.05 ppm. The broad peaks at 8.30 and 7.30 ppm were H^p and H^m protons of the phenyl rings. Protons (H^4, H^5, H^7, H^8, H^{10}, and H^{11}) of phenyl rings in dendron appear between 7.06 and 6.20 ppm. The broad peaks of H^3, H^6, and H^9 exhibited at 5.45, 5.20, and 5.09 ppm, respectively. The broad peaks of protons H^{12} of methoxy group are appears at 3.78 ppm. The peaks corresponding to the β-position of the terminal porphyrin units were not observed, because the relative number of the β-protons is very smaller compared with the inner β-protons.

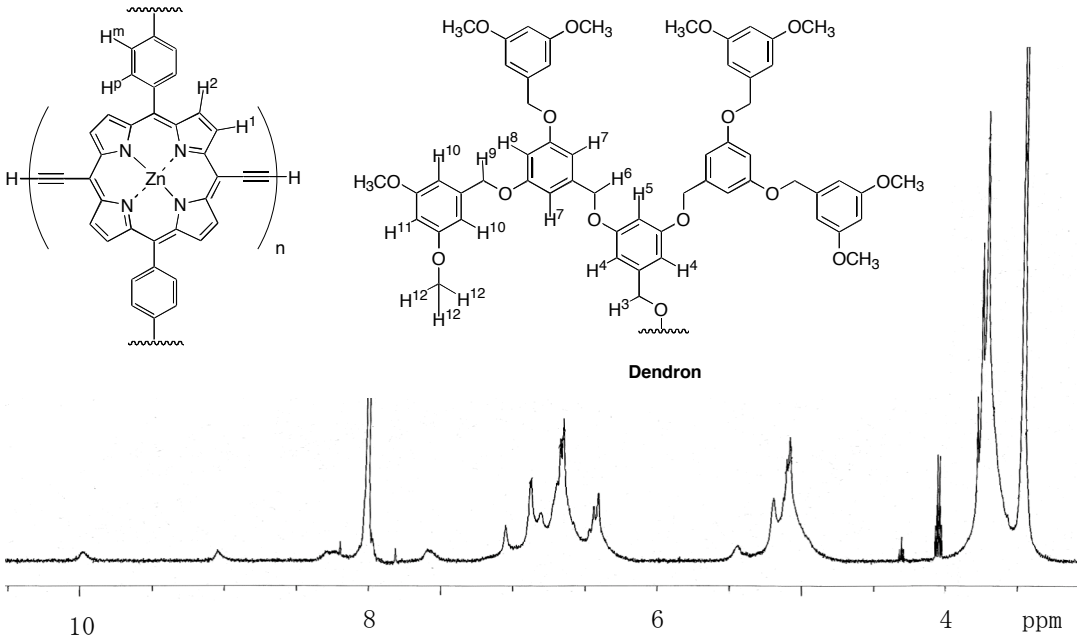

Figure 2-4. ^{1}H NMR spectrum of the dendron protected porphyrin polymers in DMF.

2-3-3. UV absorption and fluorescence spectra of dendron protected porphyrin polymer

UV-Vis absorption spectra of the porphyrin polymers **7** and the monomer **5** were shown in Figure 2-5. The Soret and Q bands of the porphyrin polymers exhibited at 466 nm and 805 nm, respectively. Compared with monomer **5**, the Soret band and Q band of porphyrin polymers were red shifted about 30 nm and 160 nm. Absorption spectra of the porphyrin polymer **7** showed large redshifts in both the Soret band and Q band compared with the monomer **5**, which indicated the high degree of conjugation in **7**.

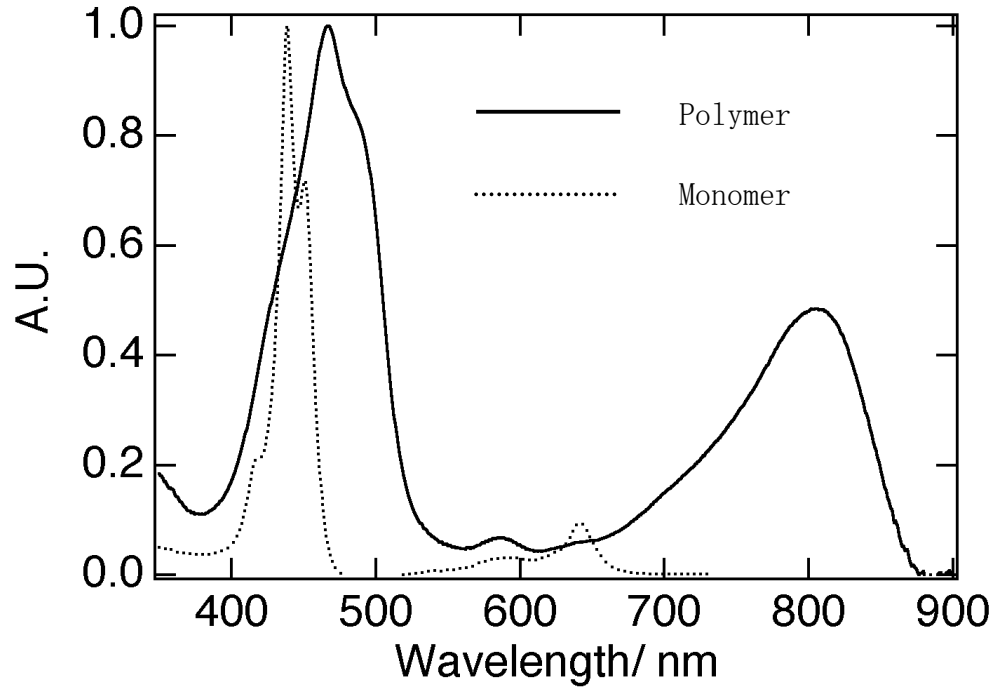

Figure 2-5. UV-Vis absorption spectra of the porphyrin polymers **7** (Soret band, λ_{max} = 495 nm; Q band, λ_{max} =805 nm) in DMF and the monomer porphyrin **5** (Soret band, λ_{max} = 439; Q band, λ_{max} = 590, 642 nm) in DMF.

The fluorescence spectrum of porphyrin polymer **7** was shown in Figure 2-6. The spectrum was taken after excitation of a DMF solution at 465 nm. The fluorescence peak of **7** was observed at ca. 841 nm.

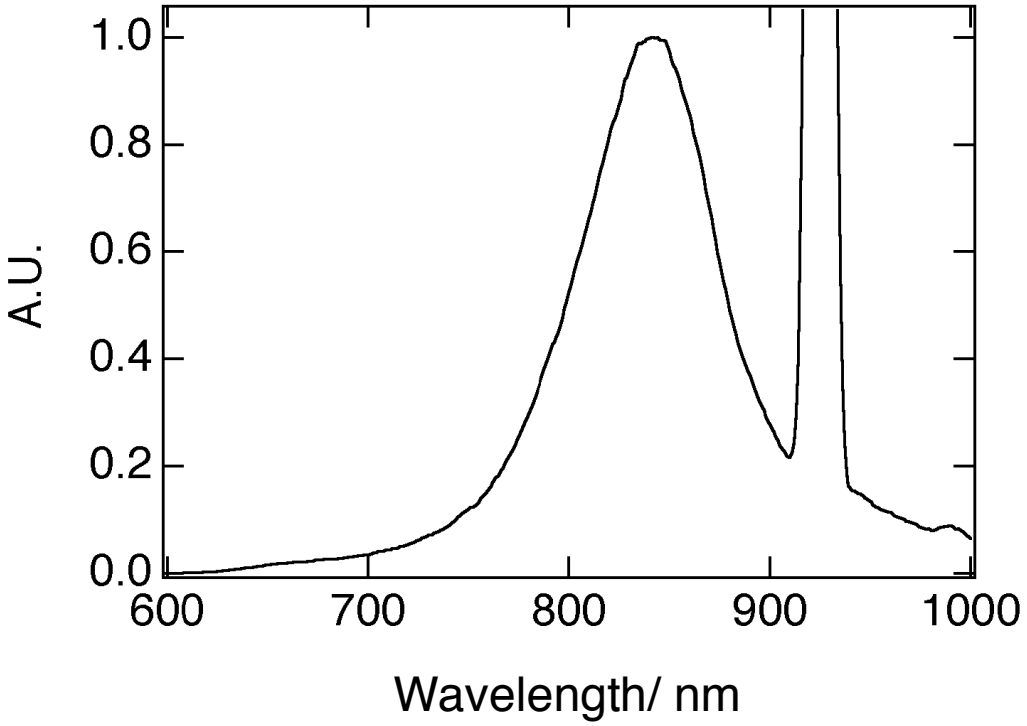

Figure 2-6. Fluorescence spectra of the porphyrin polymers in DMF (λ_{max} = 841 nm, excitation at 465 nm).

2-4. The effects of the dendron groups

The effect of dendron groups on aggregation behavior was investigated by comparing absorption spectra of dendron protected polymer **7** and non-dendron protected **9** in solution. Molecule **9** was synthesized as described in the literature.[10] As shown in Figures 2-7 (a), spectrum of **7** in tetrahydrofuran (THF) was very similar to that of **7** in $CHCl_3$. But spectrum of **9** in THF was not similar to that of **9** in $CHCl_3$ (Fig. 2-7 (b)). The difference can be attributed to the fact that **9** associate with themselves more easily to form aggregates. These results imply that stacking between porphyrin polymers was prevented by the sterical protection of the dendron groups.

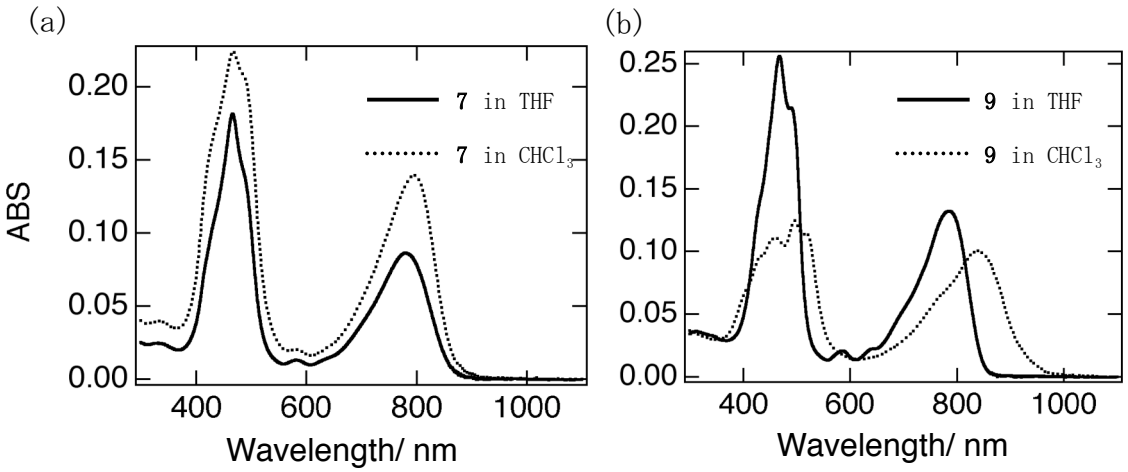

Figure 2-7. UV-Vis spectra of (a) dendron protected (**7**) and (b) non-dendron protected porphyrin polymers (**9**).

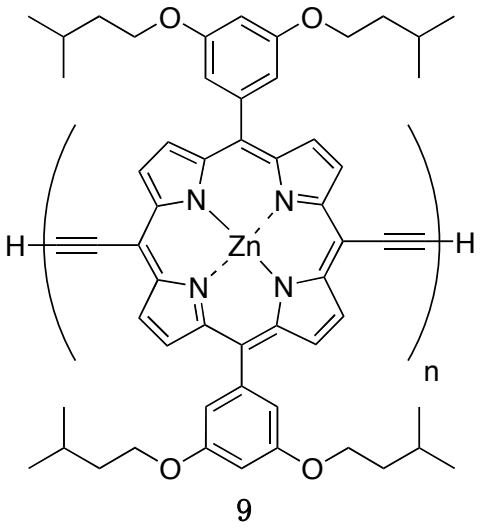

9

2-5. Deposition of the dendron protected porphyrin polymers using Langmuir-Blodgett method.

Dendron protected porphyrin polymers were deposited on solid surfaces using the Langmuir-Blodgett (LB) methods. This method can deposit homogeneously the isolated porphyrin polymers on a solid surface. By adjusting barrier pressure, it is possible to change density of porphyrin polymers on a substrate. The procedure is shown in Figure 2-8.

Step. 1 Disperse porphyrin polymers on water surface and then increase the surface pressure.

Step. 2 Deposit the porphyrin polymers on substrates.

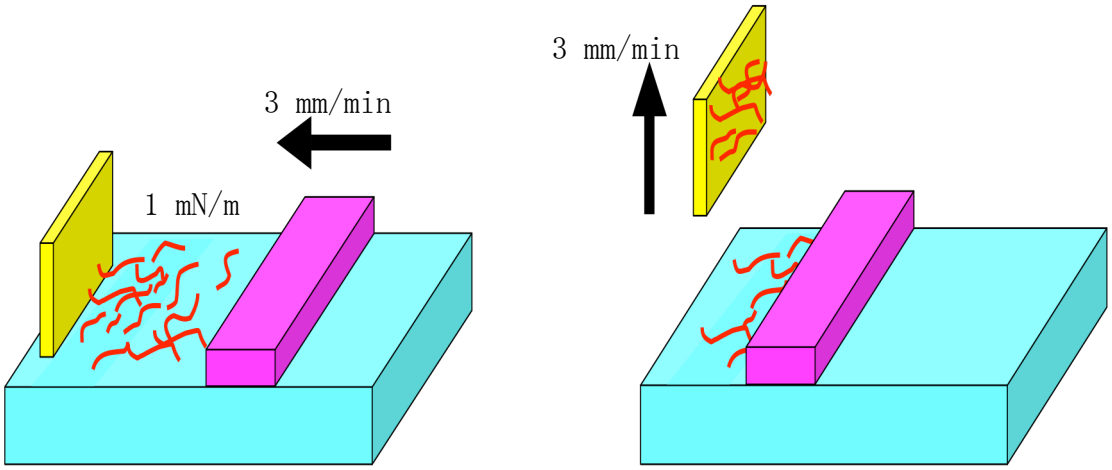

Figure 2-8. Scheme of the procedure for deposition of isolated porphyrin polymers on solid surfaces.

2-6. AFM images of the dendron protected porphyrin polymers

2-6-1. AFM imaged of dendron protected porphyrin polymer on HOPG surface.

The porphyrin polymers were dispersed on HOPG surface using the LB method. An AFM image of the porphyrin polymer was shown in Figure 2-9 (a). The height histogram (Figure 2-9 (b)) was obtained from the line profiles of the image to show the average as 1.0 ± 0.3 nm, which smaller than that obtained by the MM calculation (4.5 nm). The possible reason is strong π-π interaction between the porphyrin polymer and aromatic HOPG, or hydrophobic interaction of the dendron groups with the hydrophobic HOPG.

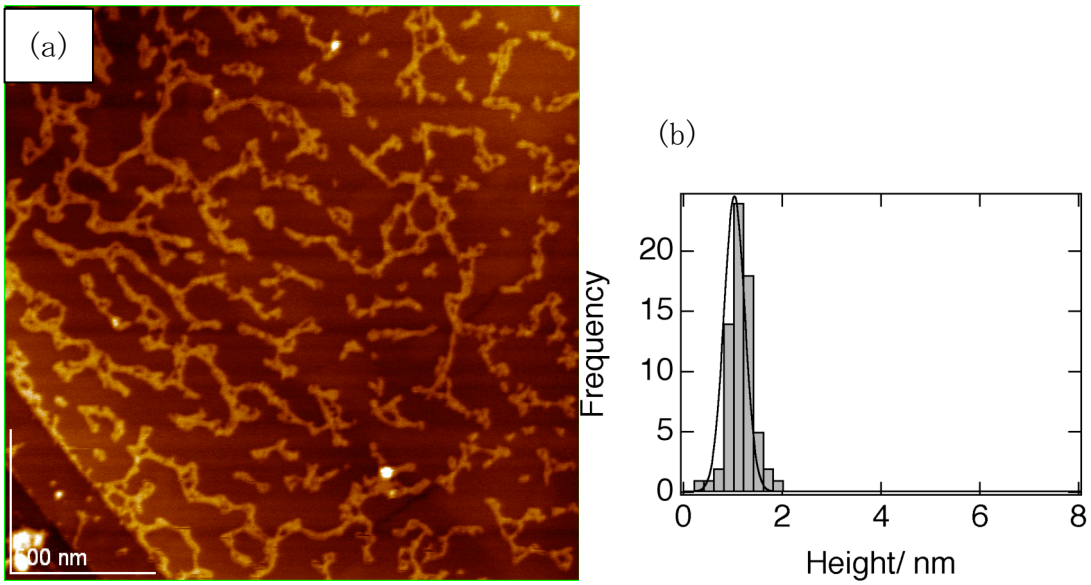

Figure 2-9. AFM image of dendron protected porphyrin polymer on HOPG surface (a) and this histogram (b).

2-6-2. AFM images of the dendron protected porphyrin polymers on thermally oxidized silicon wafer surface.

The porphyrin polymers formed network structures on a SiO_2/Si wafer surface (Figure 2-10 (a)). The height histogram (Figure 2-10 (b)) showed that the average height of the porphyrin polymers was 4.3 ± 0.8 nm, which was consistent with the height obtained by MM calculation. From the AFM image, you can see that porphyrin polymers on the SiO_2 were shrunken and curl up, probably because hydrophobic porphyrin polymer molecules have little affinity with hydrophilic SiO_2 surface, which has hydroxyl groups.

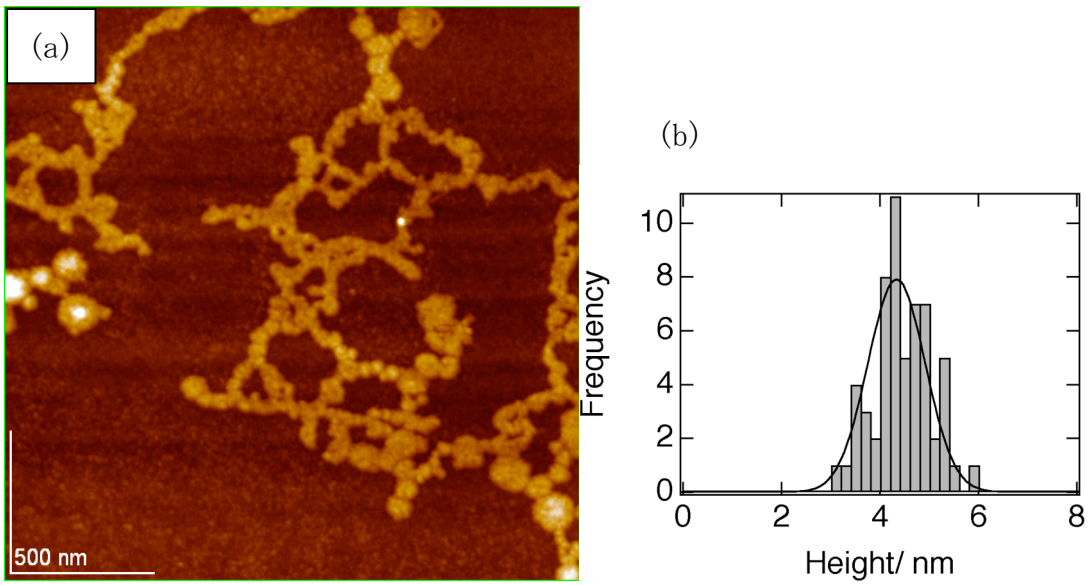

Figure 2-10. AFM image of dendron protected porphyrin polymers on thermally oxidized silicon wafer surface (a) and this histogram (b).

2-6-3. AFM images of the dendron protected porphyrin polymers on modified glass surface.

Glass is a convenient substrate for both electronic and optical measurements because it is electrically insulating and transparent to visible light. However, untreated glass surfaces are hydrophilic, and hydrophobic porphyrin polymers cannot be dispersed homogeneously on such surfaces. In order to make the glass surfaces hydrophobic, they were treated with N-phenyl-3-aminopropyltrimethoxysilane (Figure 2-11 (c)).

The porphyrin polymers on modified glass formed network structures and the histogram (Figure 2-11 (a) and (b)) were indicated that height was 3.1 ± 0.4 nm. The structures were shrink a little. This side of HOPG, modified glass and dendron porphyrin polymers exhibit stronger adaptation than that on SiO_2 surface.

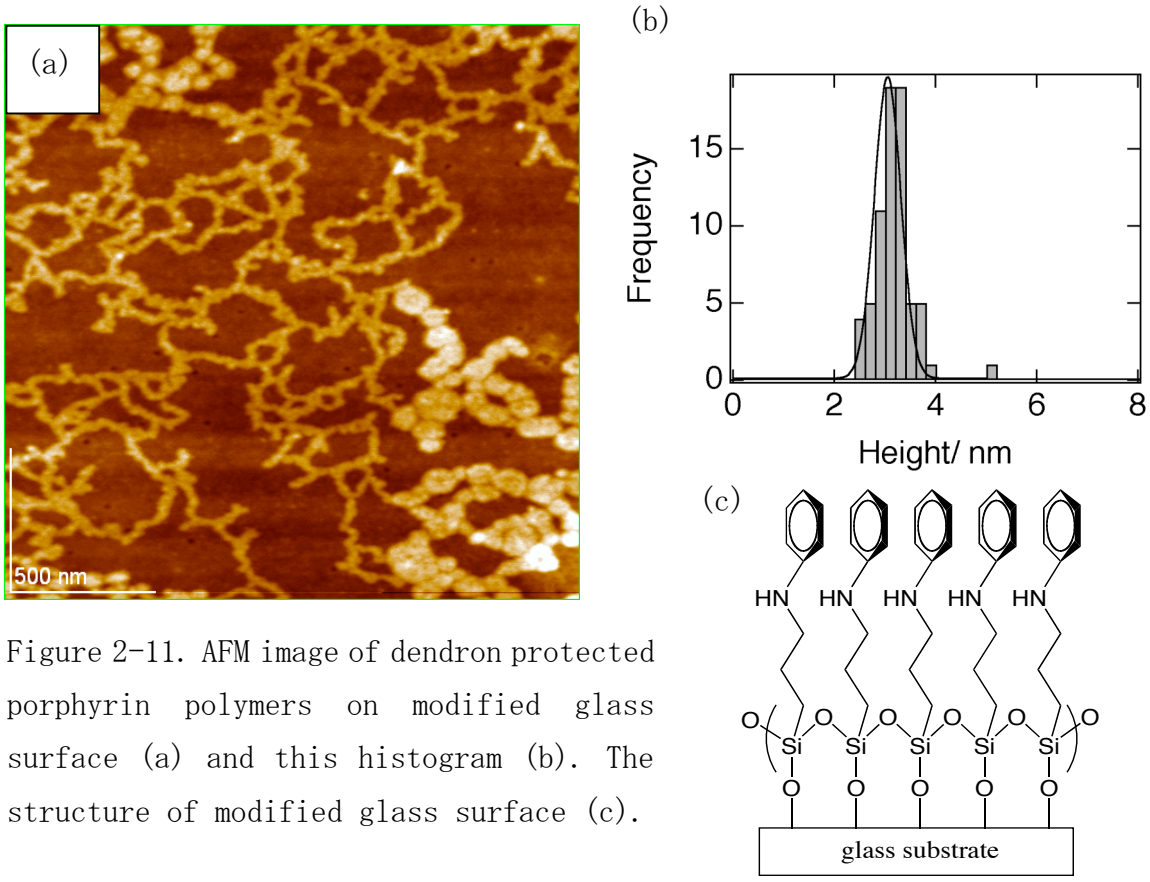

Figure 2-11. AFM image of dendron protected porphyrin polymers on modified glass surface (a) and this histogram (b). The structure of modified glass surface (c).

2-7. Conclusion

Dendron protected porphyrin polymers with more than 50 nm in length were synthesized. By sterical protection of the dendron groups, porphyrin polymer chains were prevented to aggregation in solution and observed easily using AFM on various substrates, which has rough surface such as SiO_2/Si and modified glass substrates. From AFM measurements, the average heights of porphyrin polymers on HOPG, SiO_2/Si and modified glass surface were 1.0 ± 0.3 nm, 4.3 ± 0.8 nm and 3.1 ± 0.4 nm, respectively. These results implied that porphyrin polymers might be isolated on surfaces. The measurements of conductance in the single polymer using SPM techniques are in progress.

Experimental

Instrumentation

UV-Vis absorption spectra were recorded with a Shimadzu UV-3150 double-beam spectrophotometer and fluorescence spectra were recorded with a JASCO FP-6600 spectrometer. Analytical gel permeation chromatography (GPC) data were recorded on a JASCO MD-2015 plus and column was applied Shodex GPC KF-805L. THF was the mobile phase and the flow rate was 1 ml/min. NMR spectra were recorded on a JEOL JNM-LA400 spectrometers and chemical shifts were reported in the delta scale relative to internal standard of TMS (δ = 0.00). Matrix assisted laser desorption ionization time of flight mass spectrometry (MALDI-TOF-MS) was performed on an Applied Biosystems Voyager DE-STR spectrometer with 2-aminopyridine and dithranol as the matrices. Depositions of wires on substrates were performed with a Langmuir-Blodget film system Nihon Laser, NL-LB 400. Atomic force microscopic (AFM) observation was performed with a JEOL JSPM-4210. All images were collected in tapping mode in air with silicon cantilever (Mikromasch, silicon cantilevers NSC35/AIBS/50).

Materials

Dendron molecule **8** was synthesized according to literatures.[13,14]

[5,15-Dibromo-10,20-bis((4-dendron)phenyl)porphyrinato]zinc(II) (4)

5,15-dibromo-10,20-bis-(4-hydroxyphenyl)porphyrin **(3)** (900 mg, 1.38 mmol), G2-Br **(8)** (4.62 g, 3.40 mmol), K_2CO_3 (3 g, 21.7 mmol) and 18-crown-6-ether (800 mg, 3.03 mmol) was dissolved in 150 ml of THF. Chloroform (400 ml) was added in the reaction solution, which was washed several times by water (300 ml). The organic layer was filtered by a column of alumina to remove the crown ether. The solvent was evaporated off, and the residue was dissolved in 100 ml of $CHCl_3$, in which $Zn(CH_3COO)_2 2H_2O$ (3 g , 13.7 mmol) was added and stirred for 12 hours. The solution was washed

several times with water (300 ml), and the organic layer was roughly purified by passing a column of alumina using chloroform as the eluent. The product was isolated as purple solid by passing an open column of GPC (2.67 g, 73.2 %).

^{1}H NMR (400 MHz, $CDCl_3$): 9.61 (d, J = 5 Hz, 4H, β-position of the porphyrin ring), 8.87 (d, J = 5 Hz, 4H, β-position of the porphyrin ring), 7.96 (d, J = 8 Hz, 4H, Ph), 7.28 (d, J = 8 Hz, 4H, Ph), 6.80~6.00 (m, 42H, dendrimer-ArH), 5.27 (s, 4H, CH_2), 5.01 (s, 8H, CH_2), 4.89 (s, 16H, CH_2), 3.60 (s, 96H, OCH_3). MALDI-TOF-HRMS (m/z): M^+ calcd for $C_{146}H_{134}Br_2N_4O_{30}Zn$, 2644.6735; found, 2644.6793. UV-Vis ($CHCl_3$): λ_{max} = 430, 564, 606 nm. IR (KBr): 2928, 2837, 1597, 1155 cm^{-1}.

[5,15-bis-((4-dendron)phenyl)-10,20-bis-(trimethylsilylethynyl)porphyrinato]zinc(II) (5)

Compound **4** (460 mg, 174 μmol), CuI (4 mg, 21.1 μmol)、$Pd(PPh_3)_4$ (21 mg, 18.2 μmol)、1 ml of Et_3N and 0.3 ml of trimethylsilylacetylene were dissolved in 10 ml of THF, which was refluxed for 24 hours. The reaction solution was washed several times by water (200 ml). The organic layer was dried and evaporated. The product was purified by passing through a silica gel chromatography ($CHCl_3$: hexane= 5: 5) to give a dark green solid (321 mg, 68.8%).

^{1}H NMR (400 MHz, $CDCl_3$): 9.65 (d, J = 5 Hz, 4H, β- position of the porphyrin ring), 8.89 (d, J = 5 Hz, 4H, β- position of the porphyrin ring), 8.02 (d, J = 8 Hz, 4H, Ph), 7.23 (d, J = 8 Hz, 4H, Ph), 6.85~6.15 (m, 42H, dendrimer-ArH), 5.30 (s, 4H, CH_2), 5.08 (s, 8H, CH_2), 4.92 (s, 16H, CH_2), 3.62 (s, 96H, OCH_3), 0.59 (s, 18H, $(CH_3)_3Si$). MALDI-TOF-HRMS (m/z): M^+ calcd for $C_{156}H_{152}N_4O_{30}Si_2Zn$, 2680.9316; found, 2680.9349. UV-Vis ($CHCl_3$): λ_{max} = 439, 577, 636 nm. IR (KBr): 2930, 2837, 2138, 1597, 1156 cm^{-1}.

[5,15-diethynyl-10,20-bis-((4-dendron)phenyl)porphyrinato]zinc(II) (6)

Compound **5** (100 mg, 37 μmol) and THF solutions of tetrabutylammonium

fluoride (1M, 0.1 mmol, 0.1 ml) were dissolved in 50 ml of $CHCl_3$ and the mixture solution was stirred for 5 min. The solvent was evaporated and the residue was purified by passing through a silica gel chromatography ($CHCl_3$: AcOEt= 9: 1) to give green solid (90 mg, 94.8 %).

^{1}H NMR ($CDCl_3$): 9.67 (d, J = 5 Hz, 4H, β-position of the porphyrin ring), 8.90 (d, J = 5 Hz, 4H, β-position of the porphyrin ring), 8.01 (d, J = 8 Hz, 4H, Ph), 7.29 (d, 4H, Ph), 6.84~6.12 (m, 42H, dendrimer-ArH), 5.31(s, 4H, CH_2), 5.08 (s, 8H, CH_2), 4.91 (s, 16H, CH_2), 4.15 (s, 2H, CCH), 3.61 (s, 96H, OCH_3). MALDI-TOF-HRMS (m/z): M^+ calcd for $C_{150}H_{136}N_4O_{30}Zn$, 2536.8525; found, 2536.8455. UV-Vis ($CHCl_3$): λ_{max} = 433, 575, 625 nm. IR (KBr): 3276, 2927, 2838, 2095, 1596, 1155 cm^{-1}.

Porphyrin polymer 7

To the pyridine solution (1 ml) of compound **6** (12mg, 4.7 μmol), $Cu(OAc)_2$ (10 mg, 55 μmol) was added, which was stirred for 12 hours. To the solution water (50 ml) was added, the precipitate was filtrated, which was washed with water and methanol. The precipitate was dissolved in DMF and then filtrated to remove insoluble solids. The solvent was evaporated to dryness and the solid was washed by methanol, to give black green solid (9 mg). Analytical GPC should that the molecular weight distributed from 4×10^3 to 4×10^5, centered at 4×10^4 dalton.

^{1}H NMR (400 MHz, DMF): 9.98 (m, β-position of the porphyrin ring), 9.05 (m, β-position of the porphyrin ring), 8.30 (m, Ph), 7.30 (m, Ph), 7.06~6.20, (m, dendron), 5.45 (m, CH_2), 5.20 (m, CH_2), 5.09 (m, CH_2), 3.78 (m, OCH_3). UV-Vis (DMF): λ_{max} =467, 587, 805 nm. Fluorescence (DMF, λ_{ex} = 460 nm) λ_{em} 841 nm.

Surface treatment of glass

Cover glass (MATSUNAMI, micro cover glass, 18 x 18 mm, thickness No.1 0.12-0.17 mm) was treated with (N-phenyl-3-aminopropyltrimethoxysilane (98 %, Shin-Etsu Silicone Co.) to prepare a hydrophilic glass surface as follows; N-phenyl-3-aminopropyltrimethoxysilane (0.5 ml) was dissolved in

40 ml of 5 % acetic acid aqueous solution, and stirred for 5 min. Cover glasses were soaked in the solution for 15 min, followed by washing with water, acetone and ethanol, and were dried with nitrogen gas.

Reference

1. Tsuda, A.; Osuka, A. *Science* **2001**, *293*, 79-82.
2. Taylor, P. N.; Huuskonen, J.; Rumbles, G.; Aplin, R. T.; Williams, E.; Anderson, H. L. *Chem. Commun.* **1998**, 909-910.
3. Hajjaj, F.; Yoon, Z. S.; Yoon, M. C.; Park, J.; Satake, A.; Kim, D. H.; Kobuke, Y. *J. Am. Chem. Soc.* **2006**, *128*, 4612-4623.
4. Izumi, T.; Kobashi, S.; Takimiya, K.; Aso, Y.; Otsubo, T. *J. Am. Chem. Soc.* **2003**, *125*, 5286-5288.
5. Tour, J. M.; Rawlett, A. M.; Kozaki, M.; Yao, Y. X.; Jagessar, R. C.; Dirk, S. M.; Price, D. W.; Reed, M. A.; Zhou, C. W.; Chen, J.; Wang, W. Y.; Campbell, I. *Chem. Eur. J.* **2001**, *7*, 5118-5134.
6. Screen, T. E. O.; Thorne, J. R. G.; Denning, R. G.; Bucknall, D. G.; Anderson, H. L. *J. Mater. Chem.* **2003**, *13*, 2796-2808.
7. Holten, D.; Bocian, D. F.; Lindsey, J. S. *Acc. Chem. Res.* **2002**, *35*, 57-69.
8. Kang, B. K.; Aratani, N.; Lim, J. K.; Kim, D.; Osuka, A.; Yoo, K. H. *Chem. Phys. Lett.* **2005**, *412*, 303-306.
9. Screen, T. E. O.; Lawton, K. B.; Wilson, G. S.; Dolney, N.; Ispasoiu, R.; Goodson, T.; Martin, S. J.; Bradley, D. D. C.; Anderson, H. L. *J. Mater. Chem.* **2001**, *11*, 312-320.
10. Kawao, M.; Ozawa, H.; Tanaka, H.; Ogawa, T. *Thin Solid Films* **2006**, *499*, 23-28.
11. Jiang, D. L.; Aida, T. *J. Am. Chem. Soc.* **1998**, *120*, 10895-10901.
12. Ozawa, H.; Kawao, M.; Tanaka, H.; Ogawa, *Tetrahedron* **2006**, *62*, 4749-4755.
13. Hawker, C. J.; Frechet, J. M. J. *J. Am. Chem. Soc.* **1990**, *112*, 7638-7647.
14. Hawker, C.; Frechet, J. M. J. *J. Chem. Soc., Chem. Commun.* **1990**, 1010-1013.

Chapter 3. Preparation of One-Dimensional Assembly of Gold Nanoparticles Chemically linked to π-Conjugated Porphyrin Polymers

---

In this chapter, preparation of one-dimensional assembly of gold nanoparticles chemically Linked to π-conjugated porphyrin polymers are des

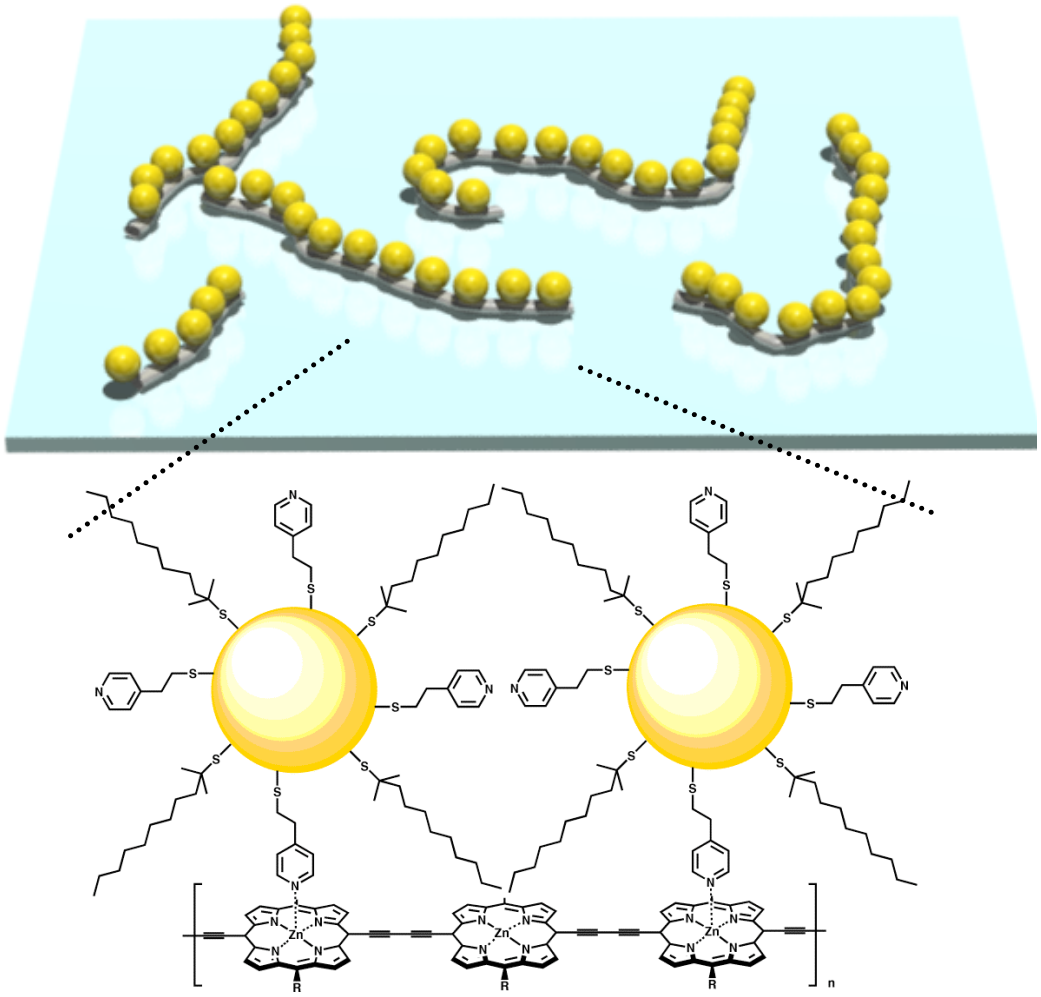

Ozawa, H.; Kawao, M.; Tanaka, H.; Ogawa, T., Synthesis of Dendron Protected Porphyrin Wires and Preparation of a One-Dimensional Assembly of Gold Nanoparticles Chemically Linked to the π-Conjugated Wires. *Langmuir*, in press.

3-1. Introduction

Metal nanoparticles have attracted considerable recent interest as materials due to their characteristic optical and electronic properties.[1-8] The electrical properties of assembled gold nanoparticles (AuNPs) are strongly influenced by the dimensionality of the structures.[9] In particular, one-dimensional structures have gathered a great deal of attention due to their potential for applications in areas such as sensors; catalysis; medical diagnostics; and electric and optical devices.[10-18] These assemblies have been prepared in various ways, the most straightforward method being the use of dimensional templates. These templates include copolymers, modified carbon nanotubes and DNA.[19-27] However, AuNPs were physically adsorbed on these templates. We are interested in the physical properties of assemblies in which AuNPs are chemically bonded to their templates. Here we report the preparation of a one-dimensional array of AuNPs chemically linked to π-conjugated systems (Figure 1). Porphyrin polymers with dendron groups were used as templates, to increase the solubility of the long polymer molecules, and to enlarge the diameter of the molecular chains for easy observation by AFM. AuNPs were capped with 4-pyridineethanethiol (py-AuNPs), whose pyridinyl moiety could bind chemically to zinc atoms of the porphyrin units. After porphyrin polymers were deposited by the Langmuir-Blodgett (LB) method on substrates, they were soaked in a solution of the py-AuNPs. This procedure was expected to form one-dimensional arrays of AuNPs on the conjugated porphyrin polymers. These assemblies were observed by atomic force microscopy (AFM) and scanning electron microscopy (SEM). Spectroscopic studies of the assemblies were performed to study the interactions between the AuNPs and the π-conjugated porphyrin system.

3-2. Preparation of one-dimensional assembly of gold nanoparticles chemically Linked to π-conjugated porphyrin polymers

3-2-1. Preparation of assemblies of porphyrin polymer with py-AuNPs

Assemblies of py-AuNPs on porphyrin polymer were prepared by the procedure shown in Figure 3-1. Porphyrin polymers were dispersed on the substrate surfaces by using LB method, which showed network structures of the polymer

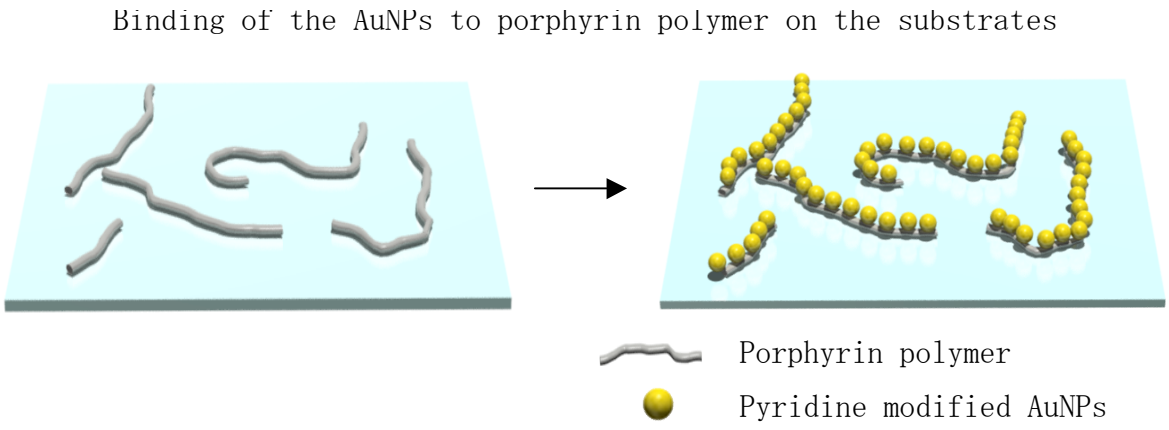

molecules as observed by AFM. These substrates were immersed in the py-AuNPs solution (10 mg/ml, methanol) for 2 min, and were rinsed by methanol.

Figure 3-1. Procedure of assemblies of AuNPs on porphyrin polymer. Porphyrin polymer was dispersed on the substrates modified glass or silicon wafer by LB method.

3-2-2. Materials

Synthesis of dendron protected porphyrin polymers and modification of glass substrates were described in chapter 2. Non-doped naturally oxidized silicon wafers (silicon substrate) were used without this treatment.

3-3. Preparation of the pyridineethanethiol capped gold nanoparticles

Syntheses of pyridineethanethiol capped gold nanoparticles (py-AuNPs) were performed by ligand exchange methods[28] (Scheme 3-1). Firstly, alkanethiol capped gold nanoparticles were prepared by modification of a reported method.[29] Py-AuNPs were prepared by ligand exchange of *t*-dodeAuNPs with 4-pyridineethanethiol in toluene.[31] As the ligand exchange progressed, the solubility of AuNPs in toluene gradually decreased and precipitates appeared. Py-AuNPs were characterized by ^{1}H NMR, UV-Vis and IR spectra, elemental analysis and TEM.

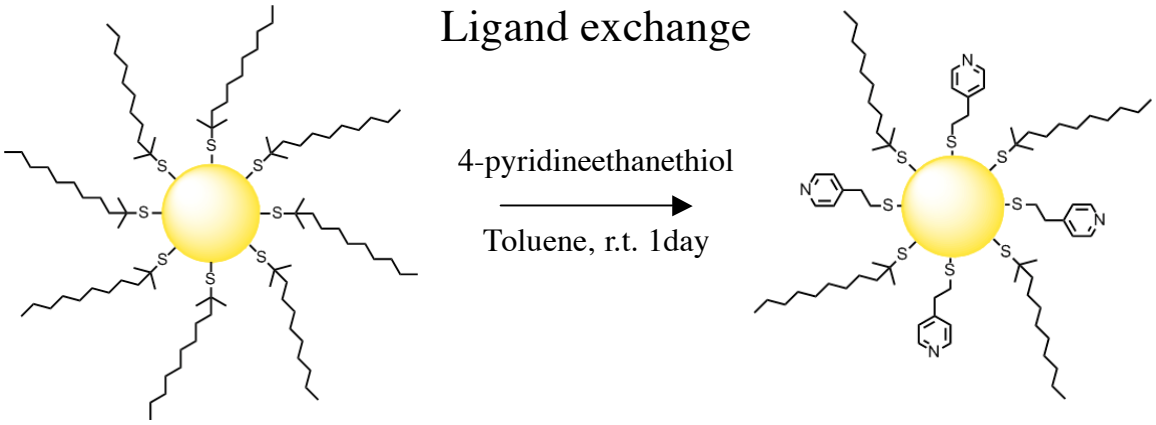

Scheme 3-1. The ligand exchange procedure.

3-4. Characterizations of the pyridineethanethiol capped gold nanoparticles

3-4-1. Fourier Transform Infrared (FT-IR) absorption spectra of pyridineethanethiol capped gold nanoparticles

FT-IR absorption spectrum of py-AuNPs was shown in Figure 3-2. Ring stretching of six-membered ring present characteristic peak. The IR spectra of py-AuNPs exhibited 1601 cm^{-1} peak, which could be assigned as the ring stretching of the pyridine ring. *t*-Dodecanethiol capped gold nanoparticles did not exhibit 1601 cm^{-1} peak, which derived from pyridine ring.

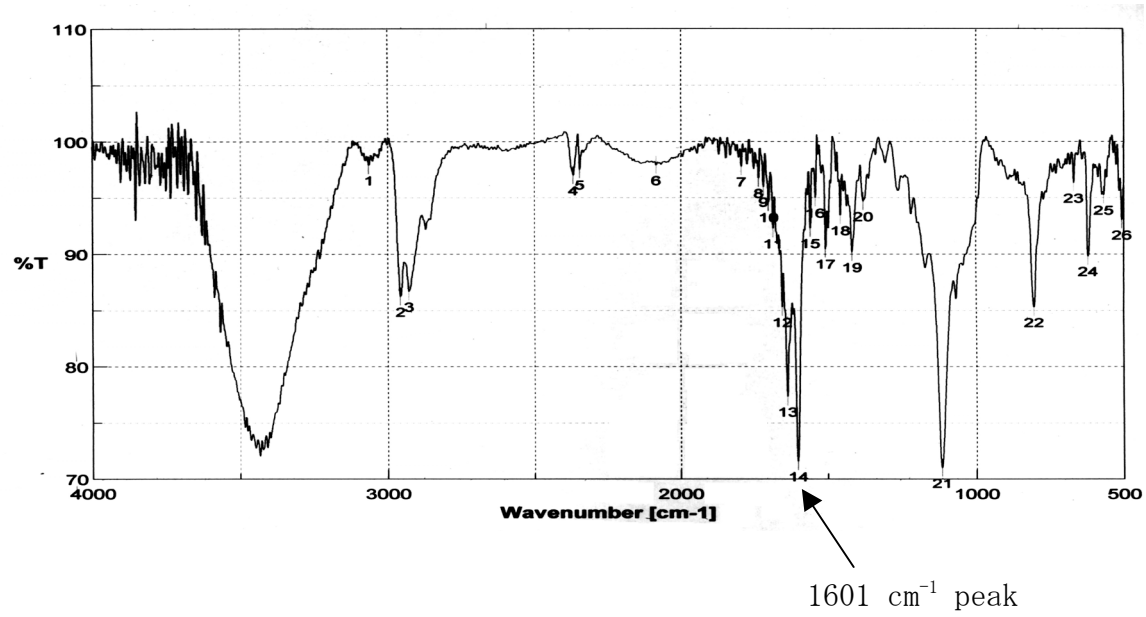

Figure 3-2. FT-IR absorption spectra of py-AuNPs.

3-4-2. ^{1}H NMR spectra of pyridineethanethiol capped gold nanoparticles

^{1}H NMR spectra of py-AuNPs in $CDCl_3$ (Figure 3-3) taken at room temperature. In this spectrum of py-AuNPs, broad peaks derived from protons of pyridine ring appear at 7.1 and 8.4 ppm. This result implies that the surface of AuNPs was coated by 4-pyridineethanethiol.

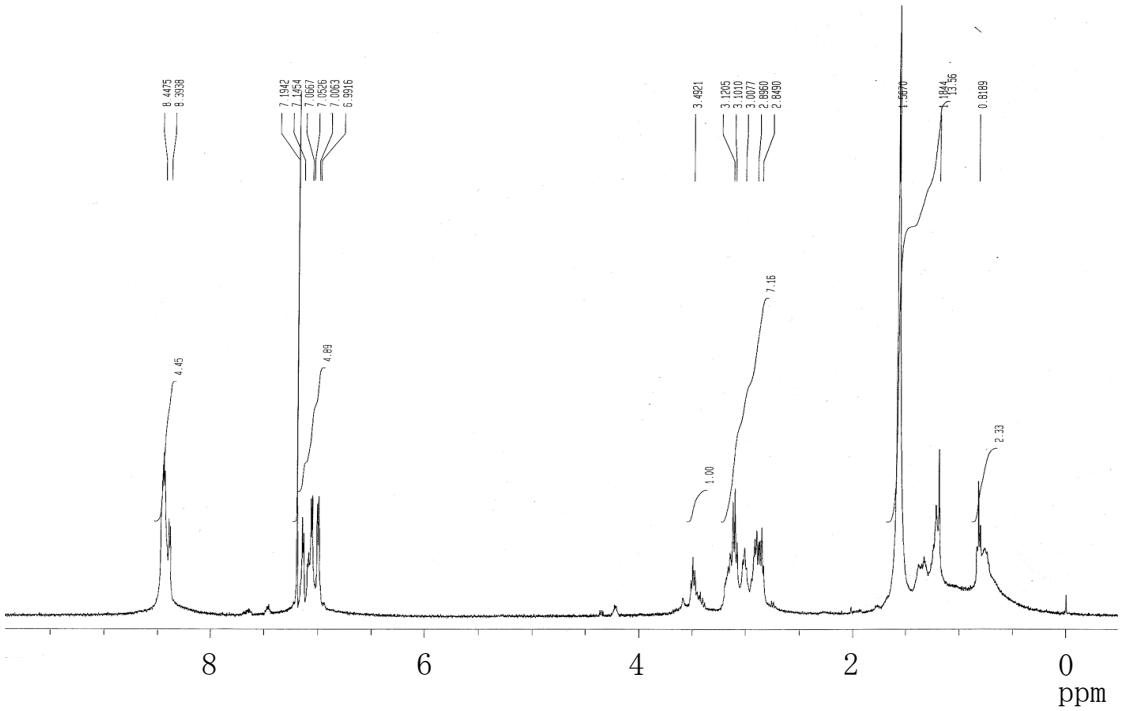

Figure 3-3. ^{1}H NMR spectra of py-AuNPs in $CDCl_3$ at room temperature.

3-4-3. Elemental analysis of pyridineethanethiol capped gold nanoparticles

Elemental analyses of py-AuNPs were carried. The atomic ratio of sulfur to nitrogen was estimated to be 1.32 from the elemental analysis. If we assume only *t*-dodecanethiol and pyridineethanethiol are present as the organic molecular in AuNPs, the molar ratio pyridneethanethiol/*t*-dodecanethiol is ca 3.1.

Found: C, 7.22; H, 0.95; N, 0.94; S, 2.84%.

3-4-4. Transmission electron microscopy observation of pyridineethanethiol capped gold nanoparticles

Core diameter of AuNPs was determined by TEM observations. TEM grids were covered by collodion. From the TEM images (Figure 3-4), core diameter of AuNPs were determined to be 2.7 ± 0.8 nm. Compared with *t*-dodecanethiol capped AuNPs, Core diameter of py-AuNPs didn't changed after ligand exchange method.

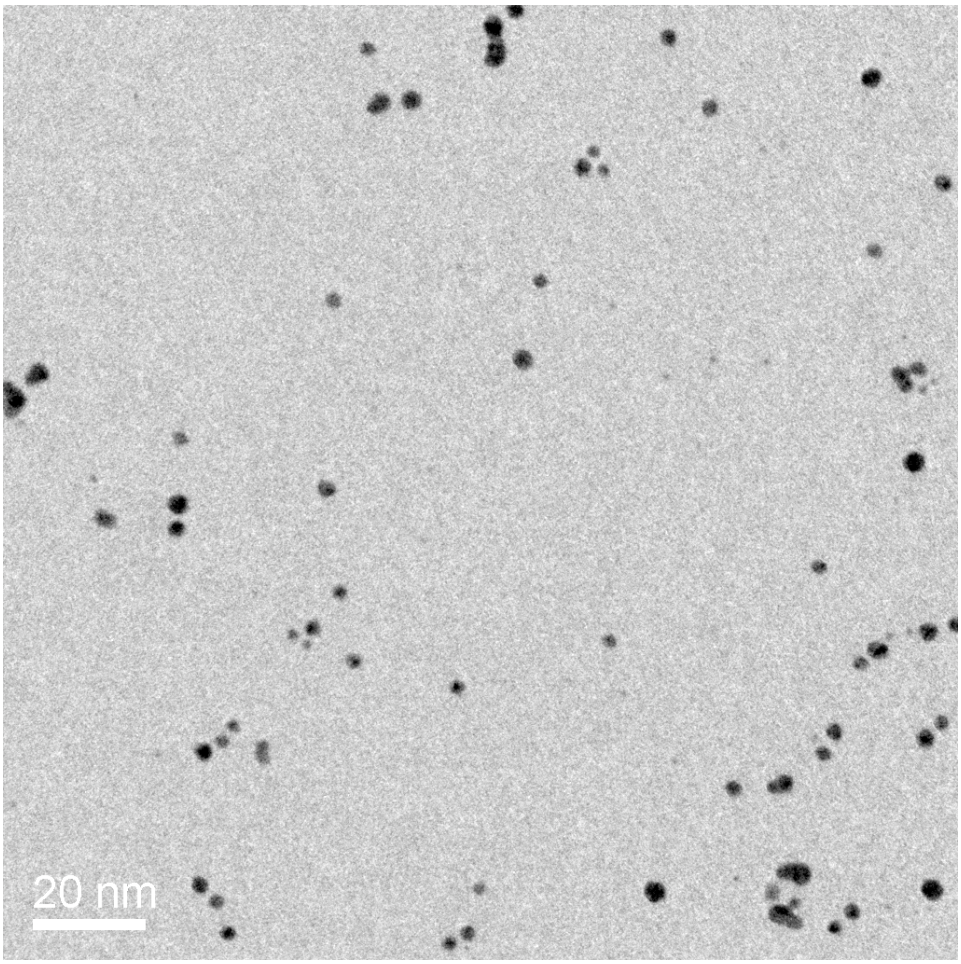

Figure 3-4. TEM images of py-AuNPs.

3-5. Characterization of py-AuNPs assemblies connected to porphyrin polymers.

3-5-1. UV-Vis absorption spectra of py-AuNPs assemblies connected to porphyrin polymers

UV-Vis spectra of the assemblies in solution and on the glass substrate were measured (Figure 3-5 and 3-6). When *t*-dodecaneAuNPs was added to the porphyrin polymers solution, the Soret and Q bands in the assembly did not shifted. When py-AuNPs was added, the Soret and Q band were broad ended. The Soret band of the porphyrin polymers on the solid surface (Figure 3-6), λ_{max} = 495 nm) appeared at longer wavelength than that of the porphyrin polymers in solution (Figure 3-5, λ_{max} = 463 nm). The redshift of porphyrin

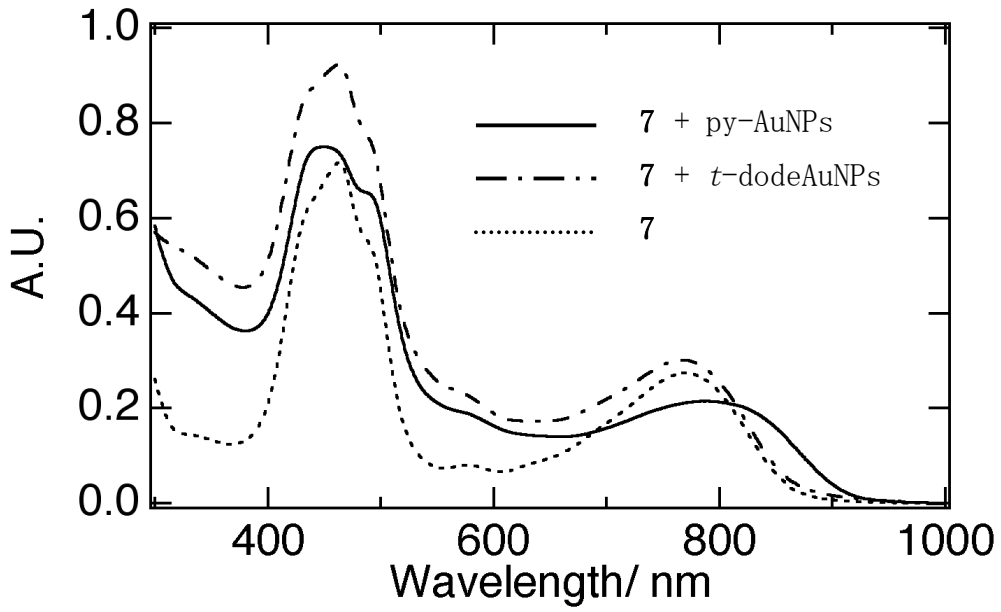

Figure 3-5. UV-Vis absorption spectra of porphyrin polymers (dashed line, Soret band, λ_{max} = 463 nm; Q band, λ_{max} = 769 nm), a mixture of porphyrin polymers and py-AuNPs (solid line, Soret band, λ_{max} = 450 nm; Q band, λ_{max} = 790 nm) and a mixture of porphyrin polymers and *t*-dodeAuNPs (dashed dotted line, Soret band, λ_{max} = 463 nm; Q band, λ_{max} = 770 nm) in $CHCl_3$.

polymers on the solid surface is probably due to the adoption of more ordered planar conformations, with small torsional disorder.[30,31]
Additionally, UV-Vis spectra of the Soret band of porphyrin polymers/py-AuNPs assemblies red-shifted about 5 nm in comparison with that of porphyrin polymers. This redshift could attribute to the extension of resonance between the pyridine molecules with the porphyrin units.[31,32] However, this effect was not so significant due to the small number of AuNPs attached to the porphyrin polymers.

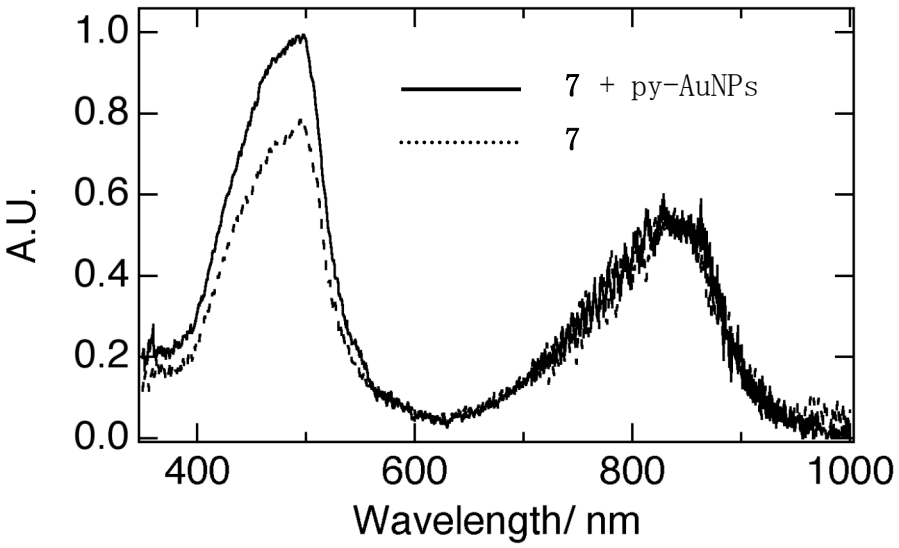

Figure 3-6. UV-Vis absorption spectra of py-AuNPs assemblies on the porphyrin polymers **7** (solid line, Soret band, λ_{max} = 498 nm; Q band, λ_{max} = nm) and the porphyrin polymers **7** (Soret band, λ_{max} = 495 nm; Q band, λ_{max} = nm) on the modified glass substrates.

3-5-2. Fluorescence spectra of py-AuNPs assemblies connected to porphyrin polymers

Emission and excitation spectra of the porphyrin polymers, py-AuNPs, and the assemblies were shown in Figure 3-7 and 3-8, respectively. The peak of porphyrin polymers **7** (Figure 3-7, Solid line) in $CHCl_3$ was 780 nm. Py-AuNPs assemblies with porphyrin polymers **7** exhibit a peak (767 nm, Figure 3-7, broken line), which differ from that of porphyrin polymers **7** and py-AuNPs. These results imply two hypotheses. 1) Py-AuNPs interacts with porphyrin polymers and this interaction creates new electronic state. 2) The spectral change of py-AuNPs assemblies connected with porphyrin polymers **7** compared to that of porphyrin and py-AuNPs is probably due to the change conformations, with small torsional disorder. These data confirm the binding of nanoparticles to the porphyrin polymers to influence of AuNPs on π-systems.

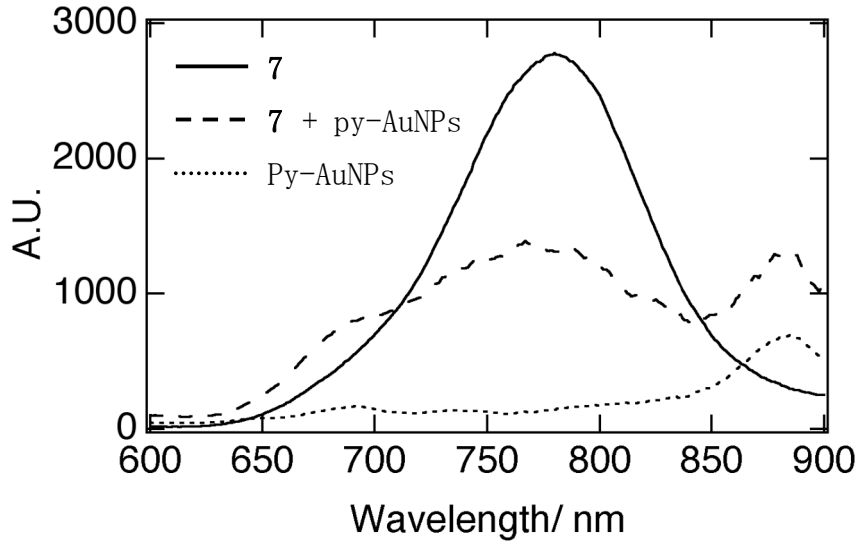

Figure 3-7. Fluorescence spectra of porphyrin polymers **7** (solid line, λ_{max} = 780 nm), py-AuNPs (dotted line) and py-AuNPs assemblies connected to the porphyrin polymers **7** (broken line, λ_{max} = 767 nm) in $CHCl_3$ (excitation at 460 nm).

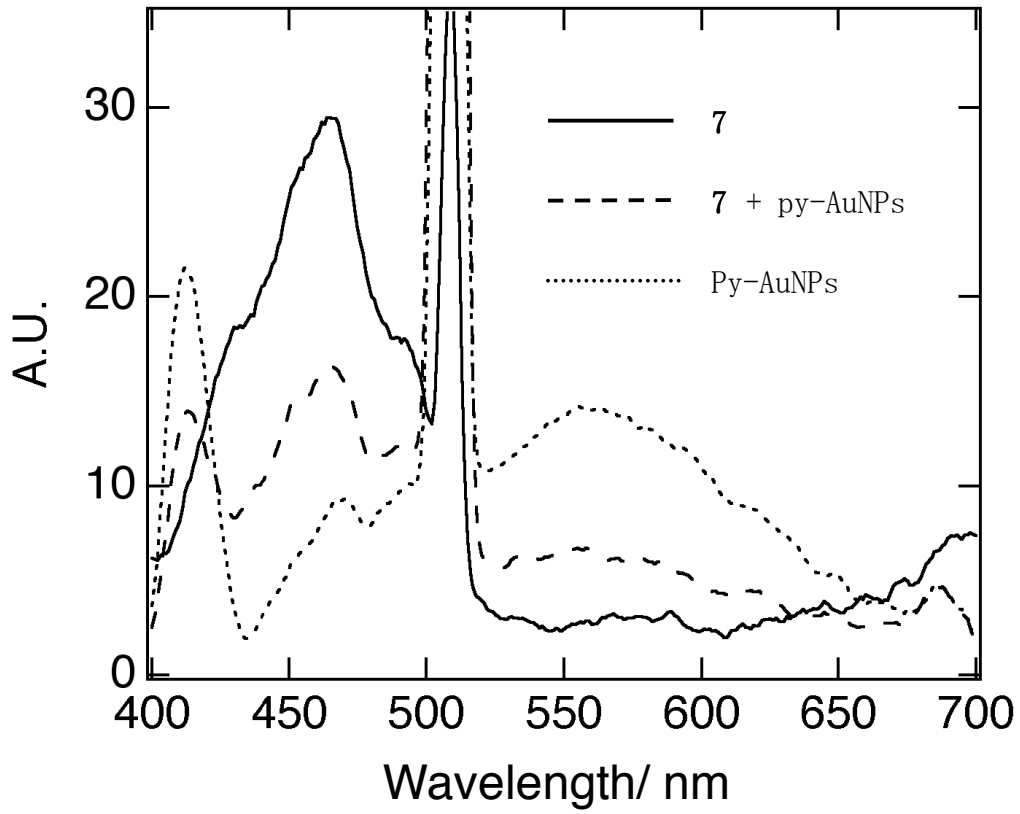

Figure 3-8. Excitation spectra of porphyrin polymers **7** (solid line), py-AuNPs (dotted line), and py-AuNPs assemblies connected to the porphyrin polymers **7** (broken line) in $CHCl_3$ (observation at 760 nm).

3-6. AFM and SEM observations.

3-6-1. AFM observations of assemblies on modified glass surface.

Figure 3-9(a) shows AFM images of the porphyrin polymers on modified glass surface, and that after the treatment with py-AuNPs (Figure 3-9(b)). The AFM observations showed similar topographic pattern in both samples, however, the height of porphyrin polymers treated with the py-AuNPs (5.3 ± 0.5 nm, Figure 3-9(d)) was ca. 2.5 nm higher than that of the non-treated porphyrin polymer (2.8 ± 0.5 nm, Figure 3-9(c)). The height difference was almost consistent with the diameter of the core of AuNPs (2.7 ± 0.8 nm). This result strongly supported that the py-AuNPs was connected to the porphyrin polymer molecules on the surface.

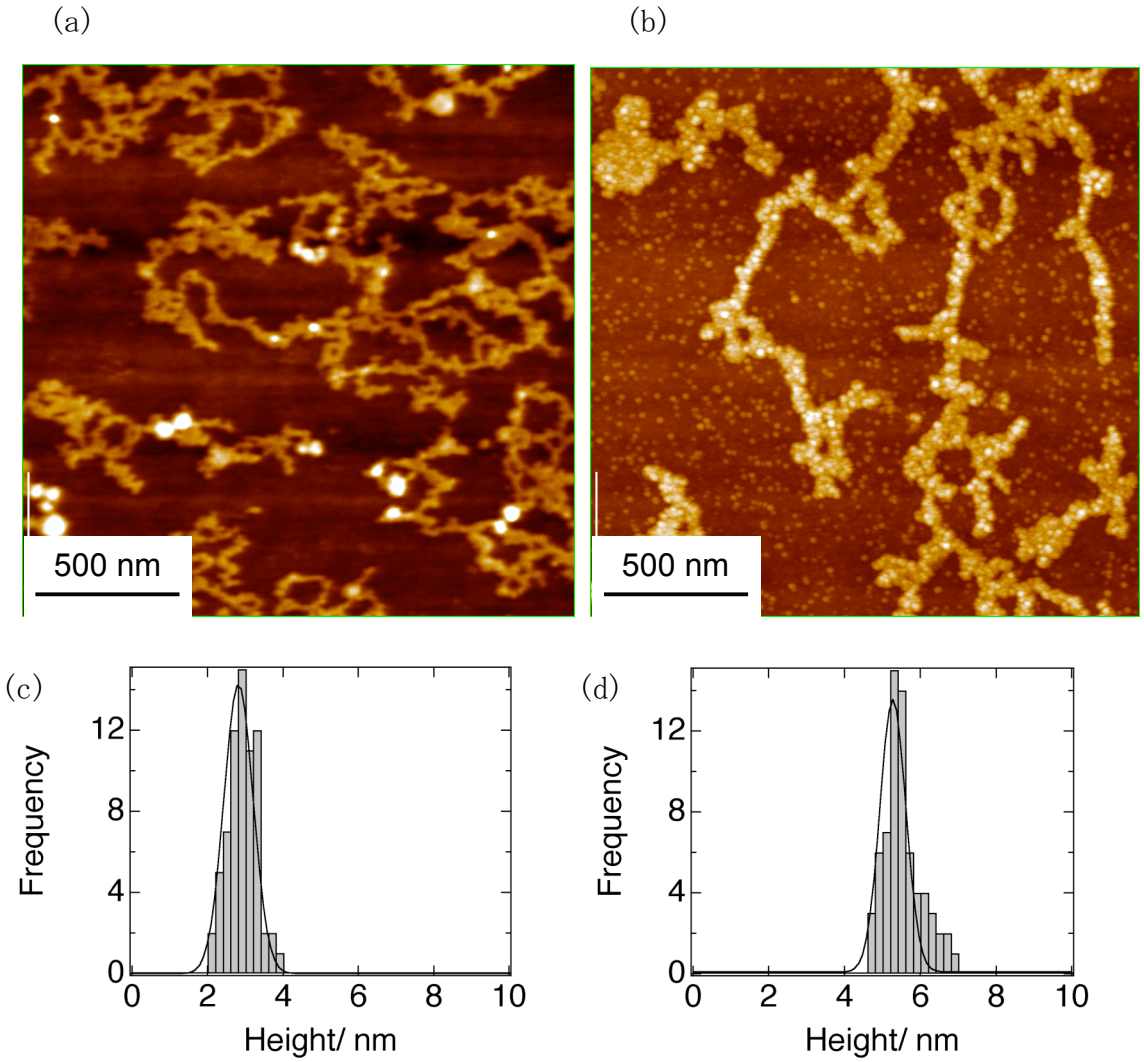

Figure 3-9. AFM images of (a) porphyrin polymers on modified glass surface and (b) py-AuNPs assemblies connected to the porphyrin polymers **7** on modified glass surface. Histograms of (c) the height of the porphyrin polymer (2.8 ± 0.5 nm) and (d) the height of the py-AuNPs assemblies connected to the porphyrin polymers **7** (5.3 ± 0.5 nm).

3-6-2. AFM and SEM observations of assemblies on silicon surface.

Figure 3-10 (a) and (b) shows AFM image of porphyrin polymers on silicon surface and that after the treatment with py-AuNPs. The structures and the heights of porphyrin polymer were similar to that of the porphyrin polymer on modified glass surface. On the silicon surface also, the height difference (ca. 2.3 nm) between the height of the polymer after the py-AuNPs treatment (5.4 ± 0.7 nm, Figure 3-10(d)) and that before the treatment (3.1 ± 0.5 nm, Figure 3-10(c)), was in good agreement with the diameter of the AuNPs.

Shown in Figure 3-11(a) are representative SEM images of the assembly on silicon surface. Since the individual AuNPs could be confirmed by SEM, the average center-to-center distances between adjacent AuNPs could be determined as about 5 nm (Figure 3-11(b)). It has been reported that for the close packed AuNPs protected by *n*-dodecanethiol, the average gap (1.3 nm) between each AuNPs is substantially less than twice of the thickness of the alkylthiol (2.4 nm); alkylthiols attached to adjacent AuNPs interpenetrate in the region between AuNPs.[33] In the present assemblies the average gap was ca. 2.3 nm (5 - 2.7 nm) that was significantly more than sum of the thickness of *t*-dodecanethiol (2 x 1.0 = 2.0 nm). This observation shows that the assemblies are not the closed packed structure. The most probable structure is that the pyridine nitrogen of py-AuNPs coordinate to zinc atom of every form porphyrin units of the porphyrin polymer, since the distance between the zinc atoms of the neighboring porphyrin units is ca. 1.3 nm and four times of it (4 □ 1.3 nm = 5.2 nm) well match with the observed center-to-center distance between adjacent AuNPs.

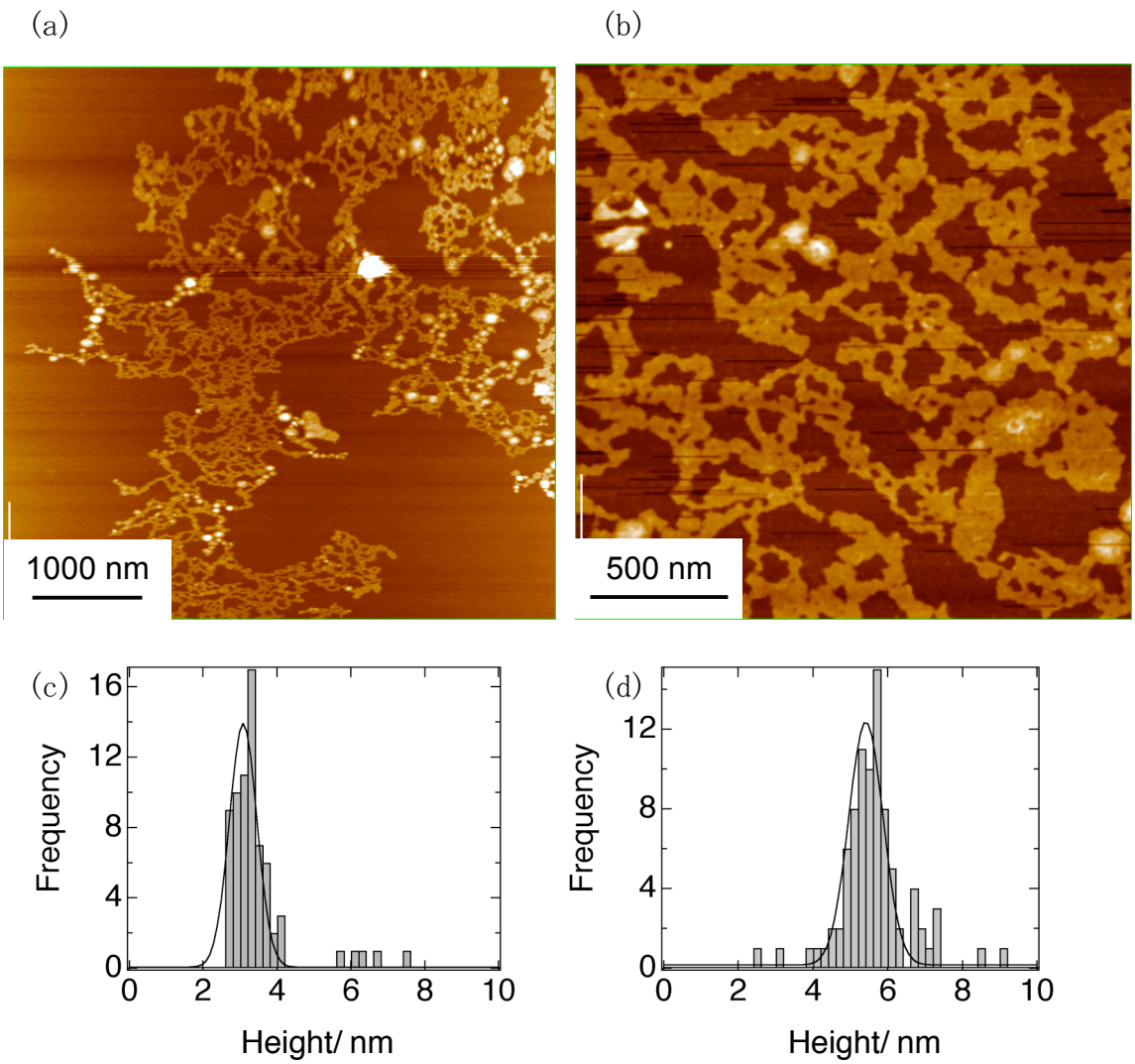

Figure 3-10. AFM images of (a) porphyrin polymers on silicon surface and (b) py-AuNPs assemblies connected to the porphyrin polymers **7** on modified glass surface. Histograms of (c) the height of the porphyrin polymers (3.1 ± 0.5 nm) and (d) the height of the py-AuNPs assemblies connected to the porphyrin polymers **7** (5.4 ± 0.7 nm).

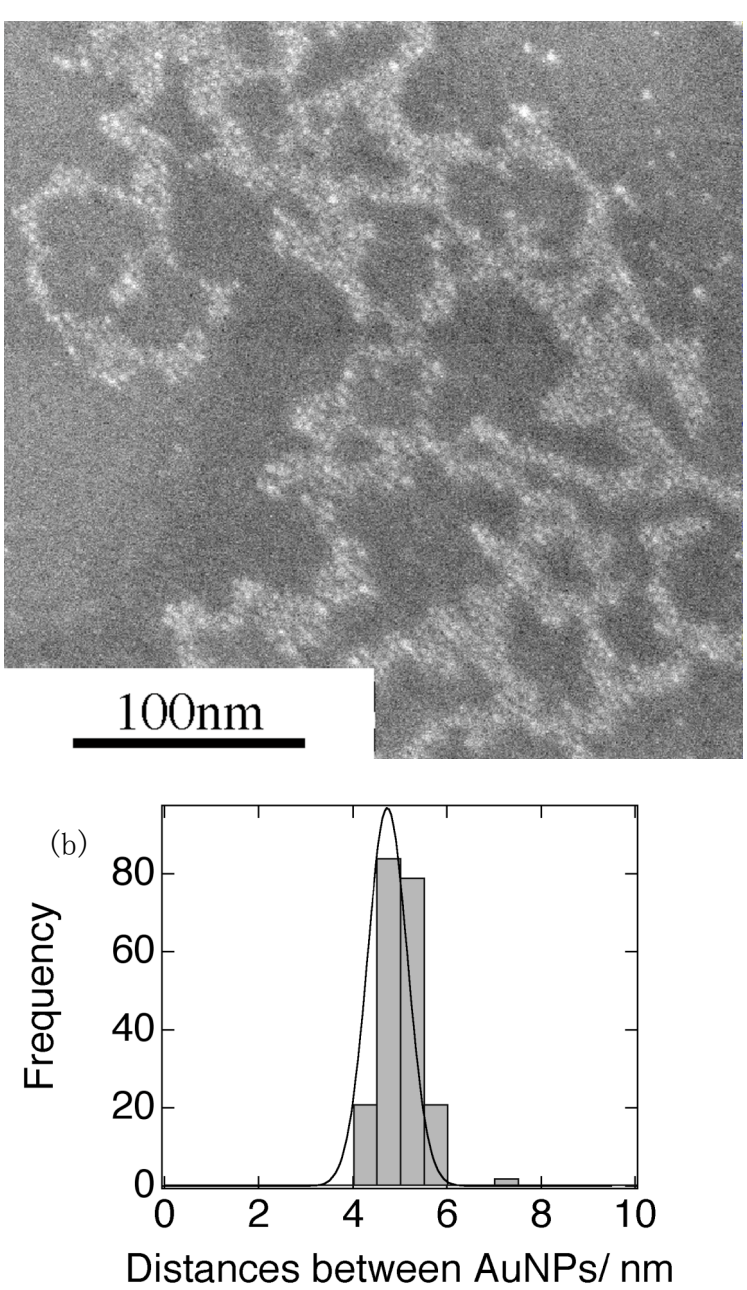

Figure 3-11. (a) SEM images of py-AuNPs assemblies connected to the porphyrin polymer 7 on silicon substrates. (b) Distances between AuNPs on porphyrin polymers measured by SEM (4.7 ± 0.6 nm).

Conclusion

One-dimensional assemblies can be fabricated by the binding of py-AuNPs onto conjugated porphyrin polymers. The structures of assemblies were observed by AFM and SEM on glass or silicon surfaces. Distances between AuNPs were about 5 nm and each AuNPs connected to every four porphyrin units. Spectroscopic studies of the assemblies of py-AuNPs with porphyrin polymers showed the presence of electronic interaction between these two moieties. Nano-scale conductance measurements of the assemblies are in progress.

Experimental section

Synthesis of pyridineethanethiol-capped gold nanoparticles

t-Dodecanethiol-modified AuNPs (*t*-dodeAuNPs) were prepared by modification of a reported method.[28] The pyridineethanethiol-capped AuNPs (py-AuNPs) were synthesized by ligand exchange methods.[29] To a t-dodeAuNP (10 mg) solution in 10 ml of toluene, 4-pyridineethanethiol (10 mg, 0.72 μmol) was added with stirring for 1 day. The reaction solution was centrifuged (1450 g, 30 min) and the supernatant was removed. The residue was dissolved in MeOH and centrifuged (1450 g, 30 min) again. The precipitate was removed and the solvent was evaporated. The solid was washed three times with toluene and dried to give the product as a black powder (8 mg).

Elem. Anal. Found: C, 7.22; H, 0.95; N, 0.94; S, 2.84 %. IR (KBr) $\tilde{\nu}$ (cm^{-1}): 2956, 2927, 1637, 1601, 1116, 803, 620 cm^{-1}. The TEM image (Figure S3) showed the average diameter of py-AuNPs to be 2.7 ± 0.8 nm.

Surface treatment of glass and silicon substrate

Cover glass (MATSUNAMI, micro cover glass, 18 x 18 mm, thickness No.1 0.12-0.17 mm) was treated with (N-phenyl-3-aminopropyltrimethoxysilane (98 %, Shin-Etsu Silicone Co.) to prepare a hydrophilic glass surface as follows; N-phenyl-3-aminopropyltrimethoxysilane (0.5 ml) was dissolved in 40 ml of 5 % acetic acid aqueous solution, and stirred for 5 min. Cover glasses were soaked in the solution for 15 min, followed by washing with water, acetone and ethanol, and were dried with nitrogen gas.

Non-doped naturally oxidized silicon substrates were washed with acetone and isopropanol, and dried by nitrogen gas.

Deposition of porphyrin polymers

Porphyrin polymers were deposited on the substrates by LB method. Porphyrin polymers with more than 100,000 Dalton (about 40 mer) were collected by analytical GPC instrumentation. They were dissolved in DMF/chloroform (1

/ 1), and diluted with the same solvent to adjust the absorbance about 0.1 at 461 nm. The droplets of the solution were spread on the water surface of the LB trough. After leaving undisturbed for 10 min, barrier was moved to compress at 3 mm/ min, while the dipper with the substrates was vertically moved up at 3 mm/ min and interface pressure was kept at 1 mN/m. Substrates deposited with the porphyrin wires were dried in air.

Assembly of py-AuNPs on porphyrin polymers

The substrates deposited with porphyrin polymer were soaked in methanol solution of py-AuNPs (0.5 mg/ml) for 5 min, which were washed with methanol and dried with nitrogen gas.

REFERENCES

1. Barton, M. I. *Synthesis, Fictionalization and Surface Treatment of Nanoparticles*; American Scientific Publishers: Los Angeles, California, 2003.
2. Schmidt, G. *Nanoparticles*; WILEY-VCH, Wenham, 2004.
3. Chi, L. F.; Hurting, M.; Dresser, T.; Schwas, T.; Seidel, C.; Fuchs, H.; Schmidt, G. *Apple. Phys. A.* **1998,** *66*, S187-S190.
4. Brust, M.; Bethel, D.; Schifrin, D. J.; Kiel, C. J. *Adv. Mater.* **1995,** *7*, 795-797.
5. Ogawa, T.; Kobayashi, K.; Masuda, G.; Takes, T.; Maeda, S. *Thin Solid Films* **2001,** *393*, 374-378.
6. Huang, W.; Masuda, G.; Maeda, S.; Tanaka, H.; Ogawa, T. *Chem. Euro. J.* **2006**, *12*, 607-619.
7. Sato, T.; Ahmed, H.; Brown, D.; Johnson, B. F. G. *J. Apple. Phys.* **1997,** *82*, 696-701.
8. The Lander, C.; Magnusson, M. H.; Depart, K.; Samuelson, L.; Paulsen, P. R.; Niggard, J.; Berggren, J. *Apple. Phys. Let.* **2001,** *79*, 2106-2108.
9. Grabert, H.; Devoret, M. H. *Single charge tunneling : Coulomb blockade phenomena in nanostructures*; Plenum Press: New York, 1992.
10. Remacle, F.; Levine, R. D. *Nano Lett.* **2002,** *2*, 697-701.
11. Remacle, F.; Beverly, K. C.; Heath, J. R.; Levine, R. D. *J. Phys. Chem. B* **2002,** *106*, 4116-4126.
12. Sample, J. L.; Beverly, K. C.; Chaudhari, P. R.; Remacle, F.; Heath, J. R.; Levine, R. D. *Adv. Mater.* **2002,** *14*, 124-128.
13. Beverly, K. C.; Sampaio, J. F.; Heath, J. R. *J. Phys. Chem. B* **2002**, *106*, 2131-2135.
14. Haiss, W.; Nichols, R. J.; Higgins, S. J.; Bethell, D.; Hobenreich, H.; Schiffrin, D. J. *Faraday Discuss.* **2004,** *125*, 179-194.
15. Hassenkam, T.; Moth-Poulsen, K.; Stuhr-Hansen, N.; Norgaard, K.; Kabir, M. S.; Bjornholm, T. *Nano Lett.* **2004,** *4*, 19-22.
16. Fan, H. Y.; Yang, K.; Boye, D. M.; Sigmon, T.; Malloy, K. J.; Xu,

H. F.; Lopez, G. P.; Brinker, C. J. *Science* **2004,** *304*, 567-571.

17. Snow, a. W.; Ancona, M. G.; Kruppa, W.; Jernigan, G. G.; Foos, E. E.; Park, D. *J. Mater. Chem.* **2002,** *12*, 1222-1230.
18. Imura, K.; Nagahara, T.; Okamoto, H. *J. Am. Chem. Soc.* **2004,** *126*, 12730-12731.
19. Reuter, T.; Vidoni, O.; Torma, V.; Schmid, G. *Nano Lett.* **2002,** *2*, 709-711.
20. Correa-Duarte, M. A.; Sobal, N.; Liz-Marzan, L. M.; Giersig, M. *Adv. Mater.* **2004,** *16*, 2179-2184.
21. Quinn, B. M.; Dekker, C.; Lemay, S. G. *J. Am. Chem. Soc.* **2005,** *127*, 6146-6147.
22. Fullam, S.; Cottell, D.; Rensmo, H.; Fitzmaurice, D. *Adv. Mater.* **2000,** *12*, 1430-1432.
23. Kimura, M.; Kobayashi, S.; Kuroda, T.; Hanabusa, K.; Shirai, H. *Adv. Mater.* **2004,** *16*, 335-338.
24. Berry, V.; Rangaswamy, S.; Saraf, R. F. *Nano Lett.* **2004,** *4*, 939-942.
25. Patolsky, F.; Weizmann, Y.; Willner, I. *Nature Materials* **2004,** *3*, 692-695.
26. Fu, X. Y.; Wang, Y.; Huang, L. X.; Sha, Y. L.; Gui, L. L.; Lai, L. H.; Tang, Y. Q. *Adv. Mater.* **2003,** *15*, 902-906.
27. Harnack, O.; Ford, W. E.; Yasuda, A.; Wessels, J. M. *Nano Let.* **2002,** *2*, 919-923.
28. Brust, M.; Walker, M.; Bethel, D.; Schifrin, D. J.; Whyman, R. *J. Chem. Soc., Chem. Commun.* **1994**, 801-802.
29. Hostetler, M. J.; Green, S. J.; Stokes, J. J.; Murray, R. W. *J. Am. Chem. Soc.* **1996**, *118*, 4212-4213.
30. Taylor, P. N.; Huuskonen, J.; Rumbles, G.; Aplin, R. T.; Williams, E.; Anderson, H. L. *Chem. Commun.* **1998**, 909-910.
31. Anderson, H. L. *Inorg. Chem.* **1994,** *33*, 972-981.
32. Screen, T. E. O.; Thorne, J. R. G.; Denning, R. G.; Bucknall, D. G.; Anderson, H. L. *J. Mater. Chem.* **2003,** *13*, 2796-2808.

33. Andres, R. P.; Bielefeld, J. D.; Henderson, J. I.; Janes, D. B.; Kolagunta, V. R.; Kubiak, C. P.; Mahoney, W. J.; Osifchin, R. G. *Science* **1996**, *273*, 1690-1693.

Chapter. 4 Electric properties of one-dimensional assembly of gold nanoparticles chemically linked to π-conjugated porphyrin polymers

---

In this chapter, Photo-response behavior of AuNPs/porphyrin polymers composite device with nano-gapped electrodes is described.

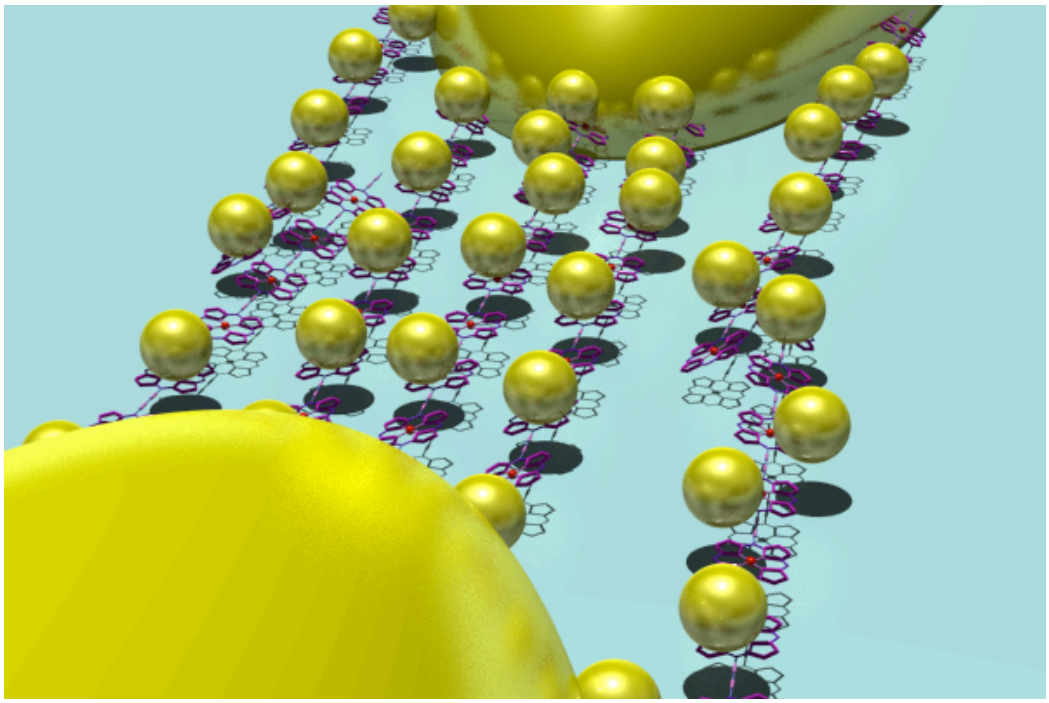

Ogawa, T.; Ozawa, H.; Kawao, M.; Tanaka, H.,Photo-response behavior of Au nano-particle/porphyrin polymer composite device with nano-gapped electrodes. *J. Mat. Sci.*, in press.

4-1. Introduction

Electrical conductance of individual molecules has attracted considerable attention, in both the fundamental sciences and as the basis for potential practical applications in molecular nano-electronics. Recently, efficient electron transport for small molecule is known to perform by the usual tunneling mechanisms.[1,2] However, theoretical predictions show that longer range conduction is possible by resonant tunneling mechanisms. Actual clear observations of conduction has not yet been reported for large moelcules.[3] Consequently, at present, the use of conductive nano-materials such as metal nano-particles, metal nano-rods, and carbon nanotubes as carrier transport materials together with molecules as functional parts is the most practical choice for realization of molecular nano-electronics. In previous reports, we have demonstrated that by using a simple combination of carbon nano-tubes with porphyrin molecules, a molecular-scale rectifier can be realized as confirmed by PCI-AFM (point contact current imaging atomic force microscopy).[4-7] In chapter 4, we have shown that AuNPs/organic molecule composites are very useful materials for nano-scale electronics.[8,9] In this report, we attempt to demonstrate that quasi-one-dimensional assemblies of AuNPs on porphyrin polymers show characteristic electrical properties as measured using nano-gap electrodes.

4-2. Preparation of py-AuNPs assemblies connected to porphyrin polymers between gold electrodes

In this experiment, dendron protected porphyrin polymers and 4-pyridineethaenthiol capped AuNPs were used (Figure 4-1). By using Gel permeation chromatography, porphyrin polymers can be bridged between electrodes collected. The distribution of porphyrin polymers is from 40 to 230 mer (50 ~ 300 nm in length). Py-AuNPs were synthesized by the reported method in chapter 3.

The AuNPs/porphyrin polymer composite devices were prepared by modification of method in chapter 3. The preparation procedure of Au NPs/porphyrin polymer composite device with nano-gapped electrodes is shown in Figure 4-2. 1) Porphyrin polymers were trapped between nano-gap electrodes and 2) py-AuNPs were connected to porphyrin polymers. It is well known that one dimensional nano structures such as organic polymers, carbon nanotubes, and inorganic nanowires can be aligned between electrodes by applying the alternating potential between them, which is used to trap these nano materials.[10,11] The porphyrin polymers were trapped between the gold nano-gap electrodes by applying an alternating potential (1 MHz, 1 Vp-p) in the presence of a droplet of dimethylformamide (DMF) solution of the polymer for about 1 hour. The device of only porphyrin polymers was soaked in a solution of py-AuNPs (0.1 mg/ml) for 1 h followed by washing and drying with organic solvents.

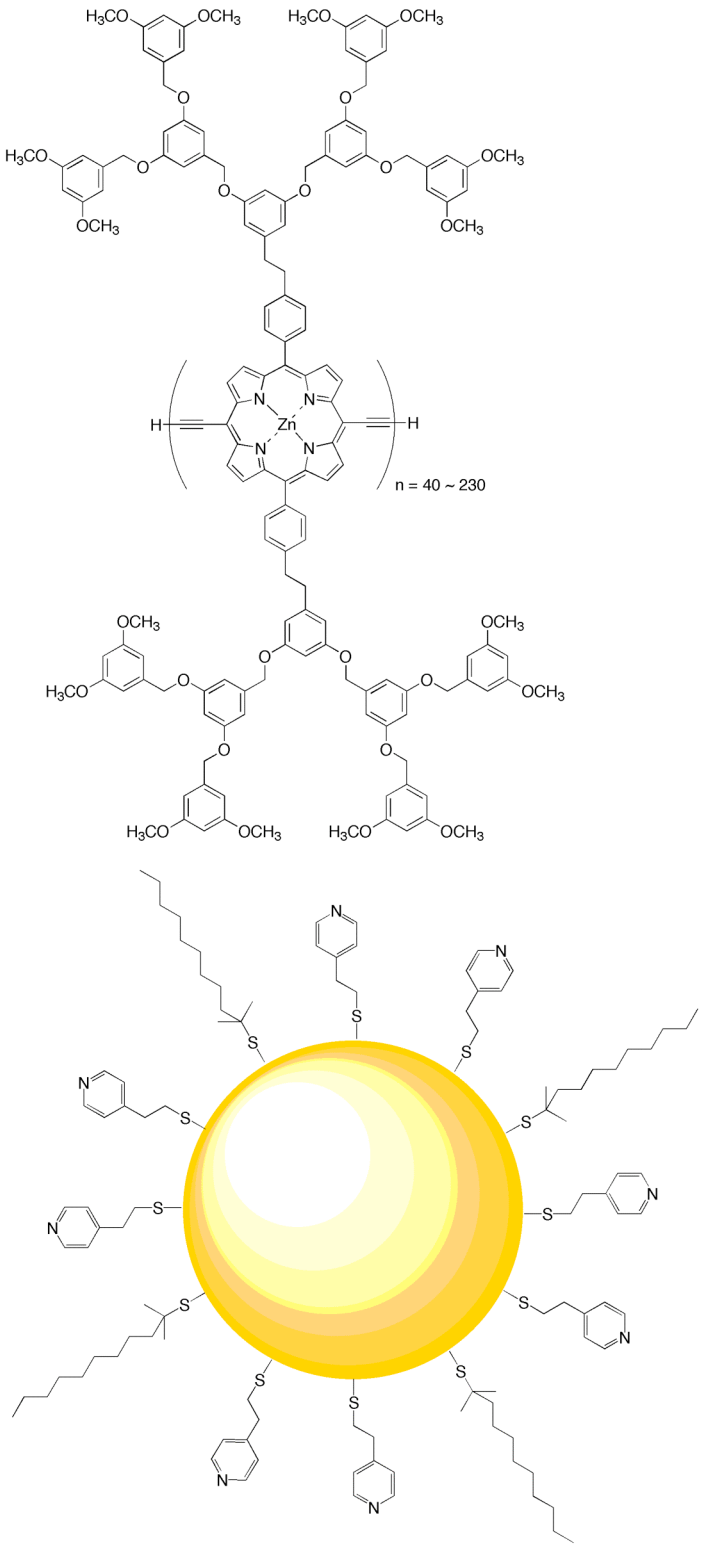

Figure 4-1. the structures of dendron protected porphyrin polymers and pyridineethanethiol capped AuNPs.

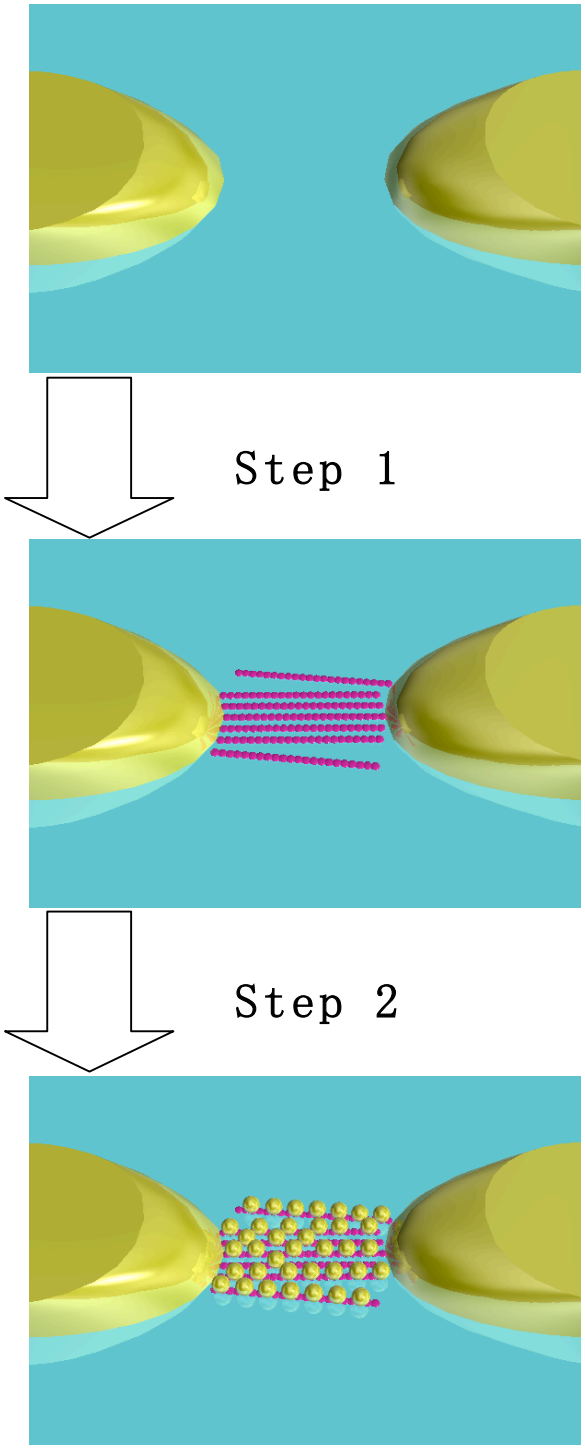

Step 1. Molecules Trapping

The porphyrin polymers were trapped between the gold nano-gap electrodes by applying an alternating potential (1 MHz, 1 Vp-p) in the presence of a droplet of dimethylformamide (DMF) solution of the polymer for about 1 hour.

Step 2. Py-AuNPs connecting

The device was then soaked in a solution of py-Au nano-particles for 1 h followed by washing and drying with organic solvents.

Figure 4-2. Preparation procedure of AuNPs/porphyrin polymers composite device with nano-gapped electrodes

4-3. Current-Voltage measurements and photo response of py-AuNPs assemblies connected to porphyrin polymers

4-3-1. I-V characterization of AuNPs/porphyrin polymers composite device

The *I-V* curves of a representative device were measured at room temperature at a pressure of 10^{-4} Pa, and the results are shown in Figure 4-3. Prior to the deposition of the polymers, SEM images were shown in Figure 4-4 (a) and, almost no current was observed (Fig. 4-3, dotted lines). After the deposition, using the alternating potential method, sigmoidal *I-V* curves with 20 nA at 1 V were obtained (Figure 4-3, broken lines). The device was then soaked in a solution of py-AuNPs for 1 h, and after washing and drying, the *I-V* curves were measured, as shown in Fig. 4-3 (solid lines). The results indicate that by adding the Au nanoparticles to the device, the conductance increased. The SEM image of the device (Figure 4-4, (b)) shows the presence of aggregates of Au nanoparticles around the nano-gap, based on the fact that pure organic molecules do not have such high contrast as the Au nano-particles in SEM images. It is likely that the pyridinyl part of the Au nano-particles formed a coordination bond with the Zn atom of the porphyrin unit in the polymer.

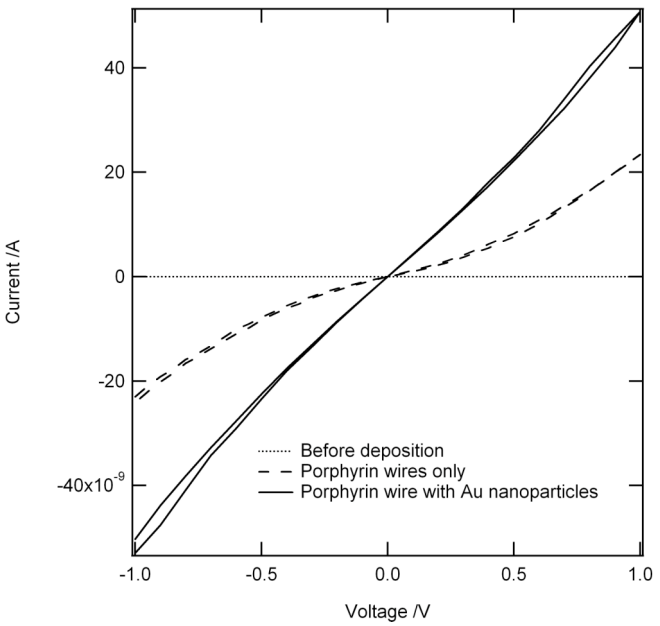

Figure 4-3. *I-V* curve measured at room temperature for the gap electrodes as-cleaned (dotted lines), after deposition of porphyrin polymers (broken lines), and for the device treated with py-AuNPs (solid lines).

(a)

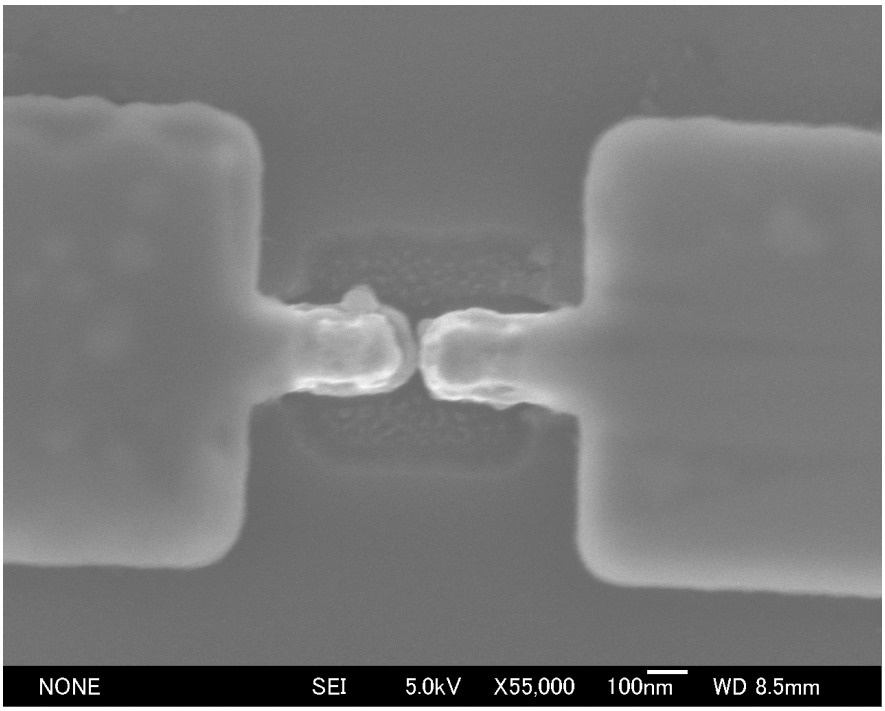

(b)

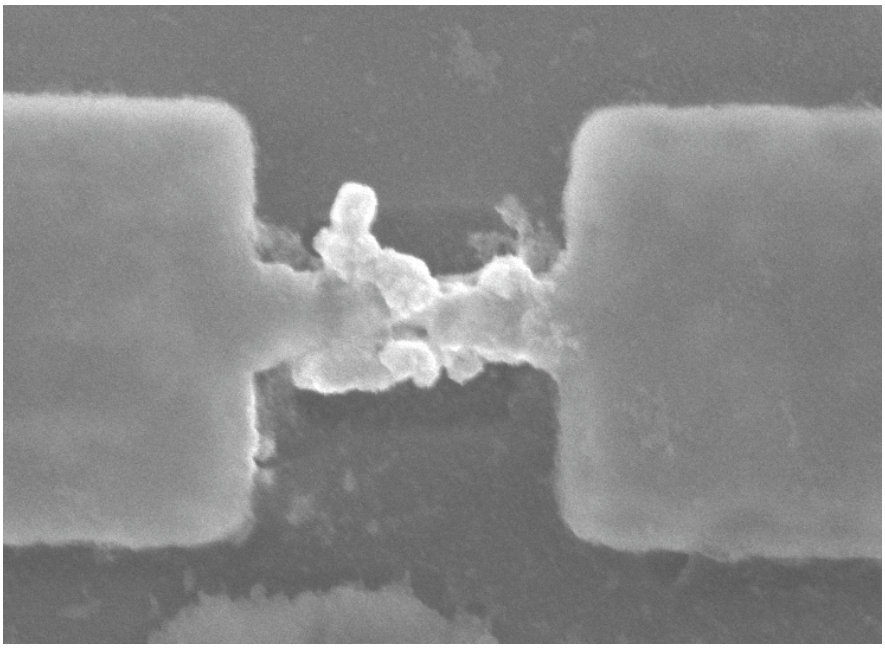

Figure 4-4. (a) Scanning electron microscope (SEM) image of the gold nano-gap electrodes prior to the deposition of the porphyrin polymers. (b) SEM image of the electrodes after deposition of the porphyrin polymers followed by incorporation of py-AuNPs.

4-3-2. Photo-response behavior of Au nano-particle/porphyrin polymer composite device

An interesting finding was that the nano-gap device with porphyrin polymers adsorbed by Au nano-particles showed photo-response characteristics, as shown in Figure 4-5. Photo-response was not observed prior to the deposition of the Au nano-particles. The possibility of thermal effects due to irradiation could be excluded by the fact that the device with only the porphyrin polymer did not show any photo-response (Figure 4-5(a). A possible mechanism involves photo-electron transfer from the porphyrin units to the Au nano-particles or vice versa. Porphyrin units were photo-chemically doped by the electron transfer to increase conductivity.

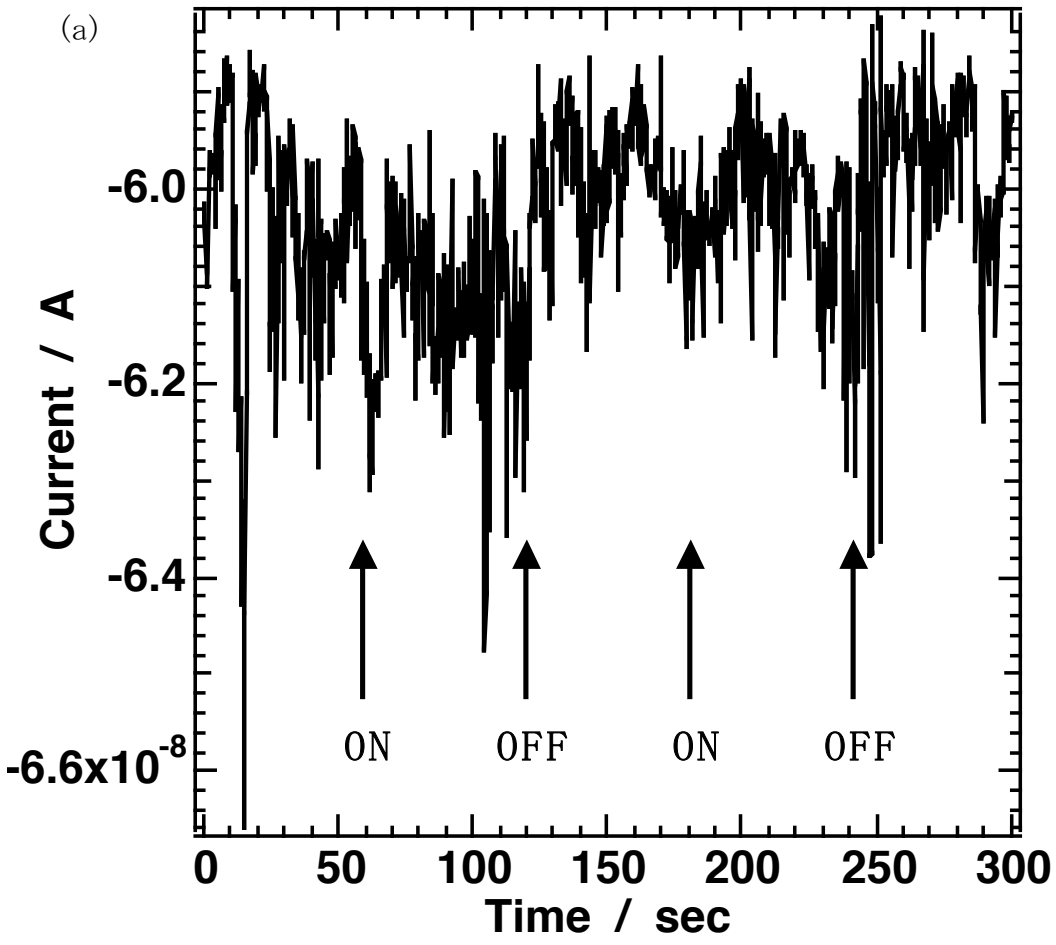

(b)

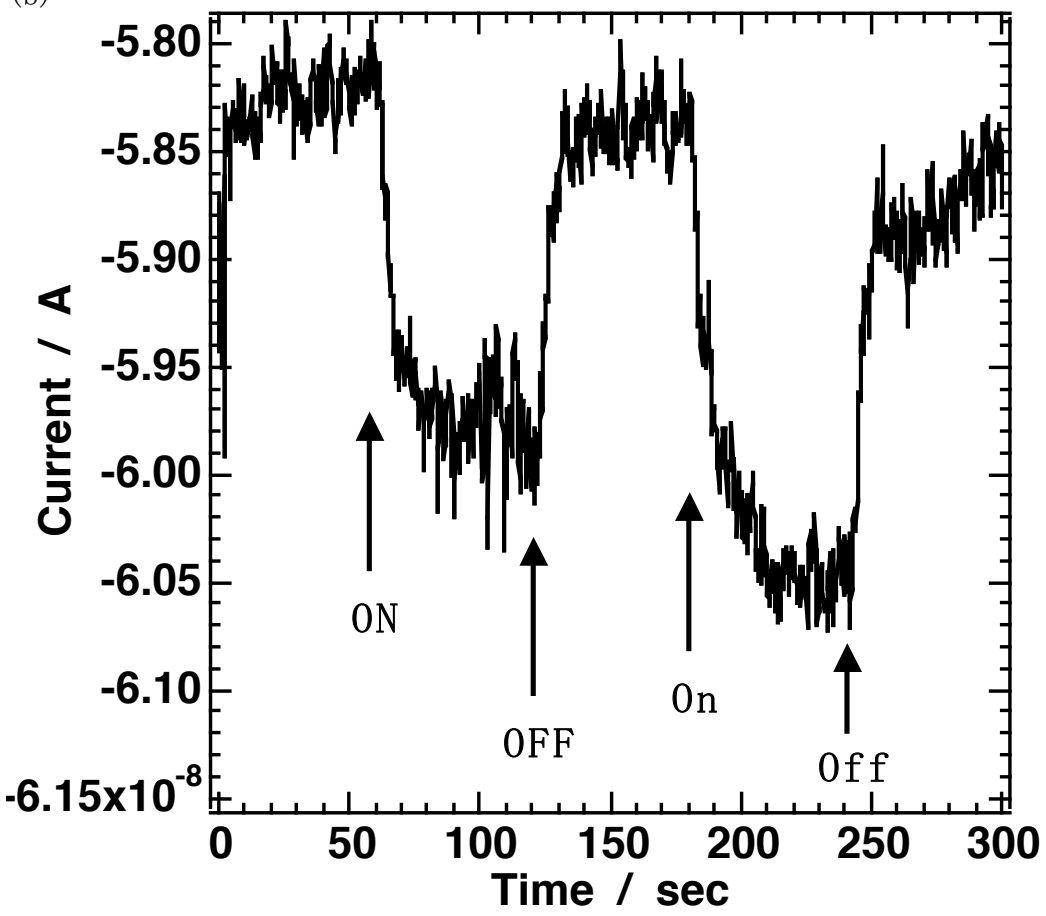

Figure 4-5. Photo-response behavior of the device. (a) Porphyrin polymers. (b) Porphyrin polymers with Py-AuNPs. The light source was a metal halide lamp; room temperature; ambient conditions.

5-4. Conclusion

Electrodes with a gap size size of 15 ~ 80 nm could be bridged by porphyrin molecular wires with 50 ~ 300 nm length. The porphyrin units could be coordinated with Au nano-particles having pyridinyl moiety. The device with both the porphyrin and Au nano-particles showed photo-response characteristics while those without the Au nano-particles showed no response. The finding indicates the good potential for developing nano-materials composed of both organic and inorganic composites for highly functional devices.

Experimental

Nano-gap electrodes

Gold electrodes with a gap of 15 ~ 80 nm were fabricated on silicon wafers with a SiO_2 insulating layer; the scanning electron microscopic (SEM) image of the electrode is shown in Figure 4-4(a). Details of these electrodes have been reported previously.[13]

Apparatus

The molecules were trapped between the nano-gap electrodes by applying alternating potentials between the electrodes using a function generator (NF Co., Wave Factory). The electrical properties of the devices were measured with a high vacuum low temperature four prober instrumentation (Nagase Electric Instrumentation Co.) at 10^{-4} ~ 10^{-5} Pa, equipped with a multi-electric source / meter (Advantest, R6246). SEM images were taken with a JEOL JSM-6700F instrument. Gel permeation chromatography was performed using the JASCO MD-2015 plus apparatus with three columns of Shodex GPC KF-805L serially connected.

References

1. Xiao, X. Y.; Xu, B. Q.; Tao, N. J. *J. Am. Chem. Soc.* **2004,** *126*, 5370-5371.
2. Xiao, X. Y.; Xu, B. Q.; Tao, N. J. *Nano Lett.* **2004,** *4*, 267-271.
3. Smit, R. H. M.; Noat, Y.; Untiedt, C.; Lang, N. D.; van Hemert, M. C.; van Ruitenbeek, J. M.. *Nature* **2002,** *419*, 906-909.
4. Otsuka, Y.; Naitoh, Y.; Matsumoto, T.; Kawai, T. *Appl. Phys. Lett.* **2003,** *82*, 1944-1946.
5. Otsuka, Y.; Naitoh, Y.; Matsumoto, T.; Kawai, T., A nano tester: A new technique for nanoscale electrical characterization by point-contact current-imaging atomic force microscopy. *Jpn. J. Appl. Phys.* **2002,** *41*, L742-L744.
6. Tanaka, H.; Yajima, T.; Matsumoto, T.; Otsuka, Y.; Ogawa, T. *Adv. Mater.* **2006,** *18*, 1411-.
7. Tanaka, H.; Yajima, T.; Kawao, M.; Ogawa, T. *J. Nanosci. Nanotechno.* **2006,** *6*, 1644-1648.
8. Huang, W.; Masuda, G.; Maeda, S.; Tanaka, H.; Ogawa, T. *Chem. Eur. J.* **2005,** *12*, 607-619.
9. Ogawa, T.; Kobayashi, K.; Masuda, G.; Takase, T.; Maeda, S. *Thin Solid Films* **2001,** *393,* 374-378.
10. Ozawa, H.; Kawao, M.; Tanaka, H.; Ogawa, T. *To be published.*
11. Tuukkanen, S.; Kuzyk, A.; Toppari, J. J.; Hytonen, V. P.; Ihalainen, T.; Torma, P. *Appl. Phys. Lett.* **2005,** *87*,183102-183104.
12. Messmore, B. W.; Hulvat, J. F.; Sone, E. D.; Stupp, S. I. *J. Am. Chem. Soc.* **2004,** *126*, 14452-14458.
13. Araki, K.; Endo, H.; Masuda, G.; Ogawa, T. *Chem. Eur. J.* **2004,** *10*, 3331-3340.

Chapter 5. Synthesis of end-functionalized π-conjugated porphyrin oligomers

---

In this chapter, synthesis and characterization of end-functionalized π-conjugated porphyrin oligomer are described.

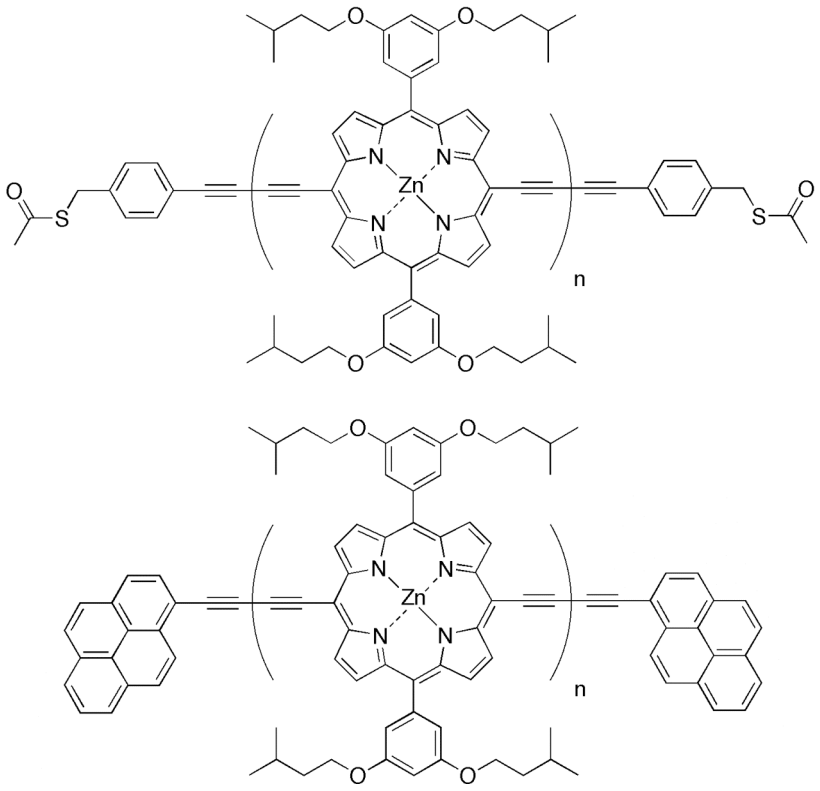

Ozawa, H.; Kawao, M.; Tanaka, H.; Ogawa, T., Synthesis of end-functionalized π-conjugated porphyrin oligomers. *Tetrahedron* **62**, 4749 (2006).

5-1. Introduction

Molecular electronics is a fascinating area of fundamental research with the potential for many future applications.[1-4] In recent years, studies on the conductance of single or small numbers of molecules were reported with intriguing results, exhibiting such interesting properties as switching,[5,6] the Coulomb-blockade phenomenon,[7-9] field-effect transistor[7-10] and the Kondo effect.[9,11] As an extension of these studies, the fabrication of larger nanostructures constructed from organic molecules as the functional moieties and conductive nanomaterials as the electron transport portion has been recognized as an important issue for future nano-devices (Figure 5-1). Various linear π-conjugated porphyrin polymers which linked neighbor porphyrin units by meso-meso[12] or diethynyl link[13,14] were reported. These polymers are of great interest by their electronic properties for applications to molecular wires because of small HOMO-LUMO energy gap.[13] Metal nanoparticles,[15,16] metal nanorods,[17] and carbon nanotubes[18,19] are promising candidates for conductive nano-materials. In order to construct such nanocomposites made from conductive materials and organic molecules,

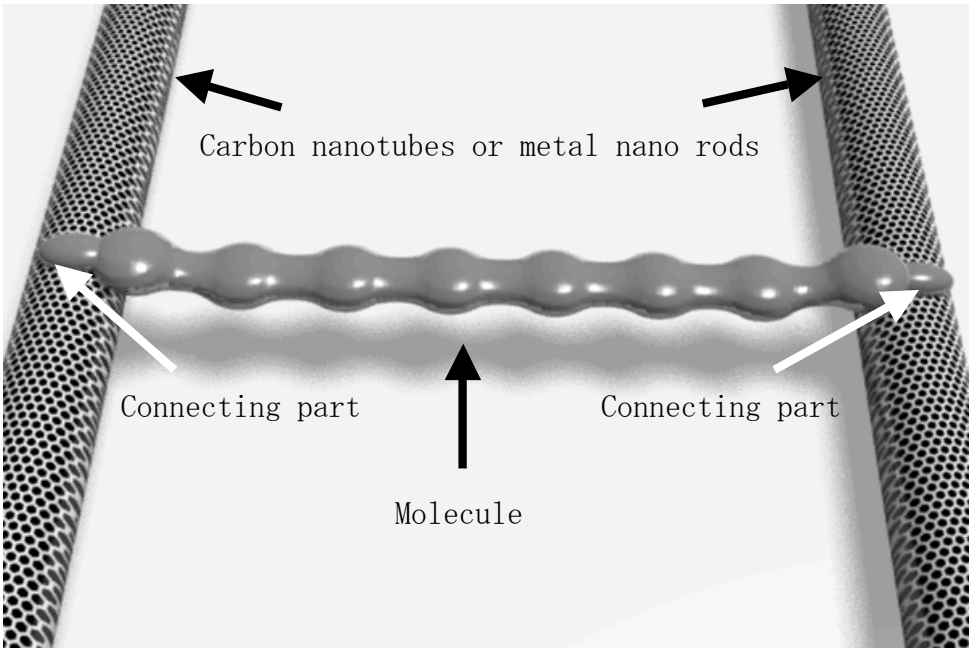

Figure 5-1. Schematic diagram of nanostructures consisting of end-functionalized oligomers and conductive materials.

functional groups are required to couple these moieties together. Mercapto or S-acetylthio groups are known to be good coupling groups to metals,[20] and aromatic hydrocarbons such as pyrene are known to adsorb to the surface of carbon nanotubes efficiently through π-π interactions.[21] For the purpose of constructing such nanocomposites[22-25] using a series of porphyrin oligomers as the organic portion, we synthesized a series of end-functionalized π-conjugated porphyrin oligomers. One series (**1a-g**) contains 1-[4-(S-acetylthiomethyl)phenyl]ethynyl groups and another series (**2a-g**) bears 2-pyrenylethynyl groups at the end of the molecules. Systematic spectroscopic studies of this series of oligomers were performed to study their electronic properties, especially to clarify the effects of the end-functional groups on the main π-conjugated electronic systems.

5-2. Synthesis of end-functionalized π-conjugated porphyrin oligomers

5-2-1. Syntheses

End-functionalized porphyrin oligomers **1a-g** and **2a-g** were synthesized by the synthetic route shown in Scheme 5-1. Functional alkynes **4** or **5** were used as the capping molecules. The oxidative coupling reaction of compound **3** and these capping molecules via copper catalysis gave a series of oligomers. The porphyrin-containing products were first purified by gel permeation chromatography (GPC) and further isolated by recycling high performance liquid chromatography GPC (HPLC-GPC). The purities of these

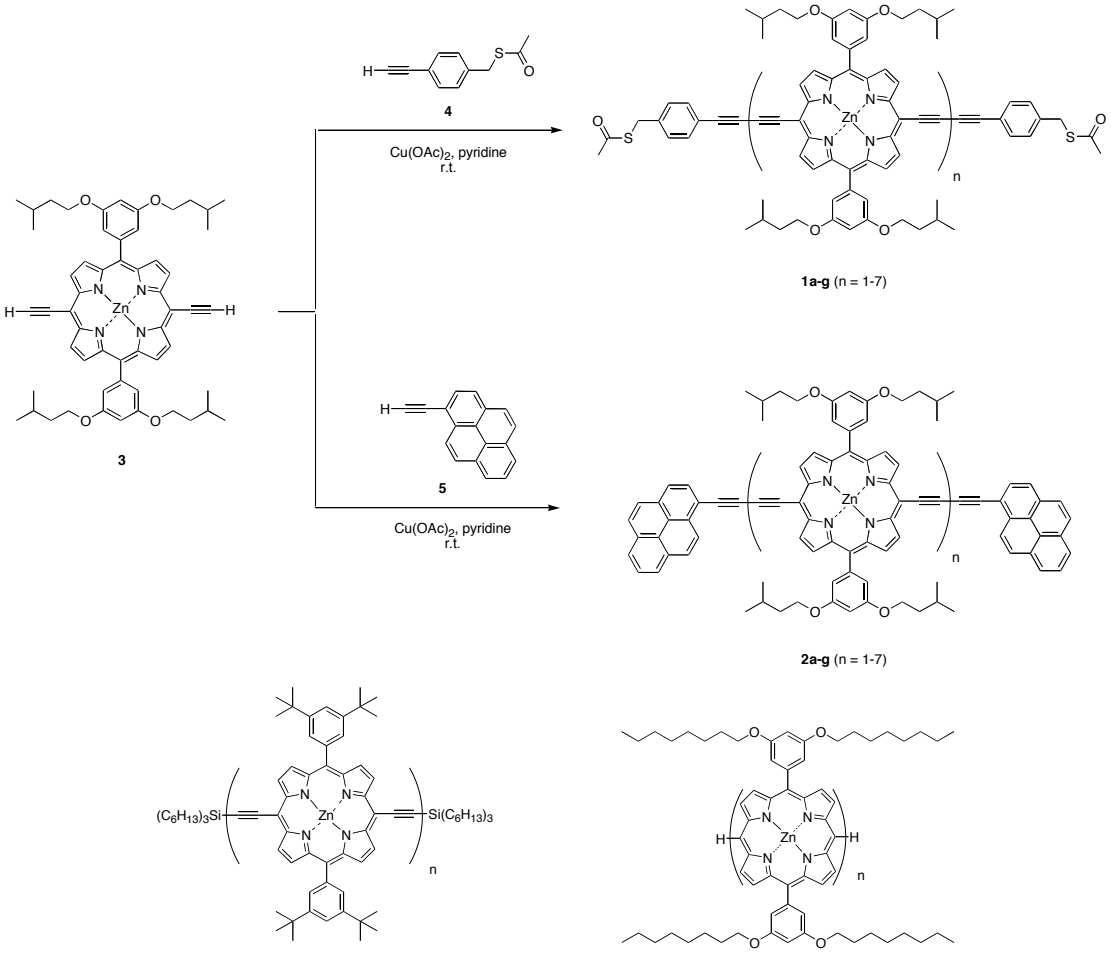

Scheme 5-1. Synthesis of end-functionalized porphyrin oligomers (**1a-g**, **2a-g**) and structures of silicon functionalized porphyrin oligomers (**6a-f**) and meso-meso linked porphyrin oligomers (**7a-g**).

oligomers were confirmed by ^{1}H NMR, MALDI-TOF-MS, and analytical GPC.

5-2-1. Control of product distribution

The distribution of oligomers could be controlled by changing the ratio of compound **3** to the capping molecules (**4** or **5**), as depicted in Figure 5-2. When the compound ratio of **3** to **4** was 1:2 (Entry 1), the main product was monomer. When the ratio was 5:2 (Entry 2), the major products ranged from tetramer to hexamer. When the ratio was 10:1 (Entry 3), the distribution peak of oligomers centered on a decamer.

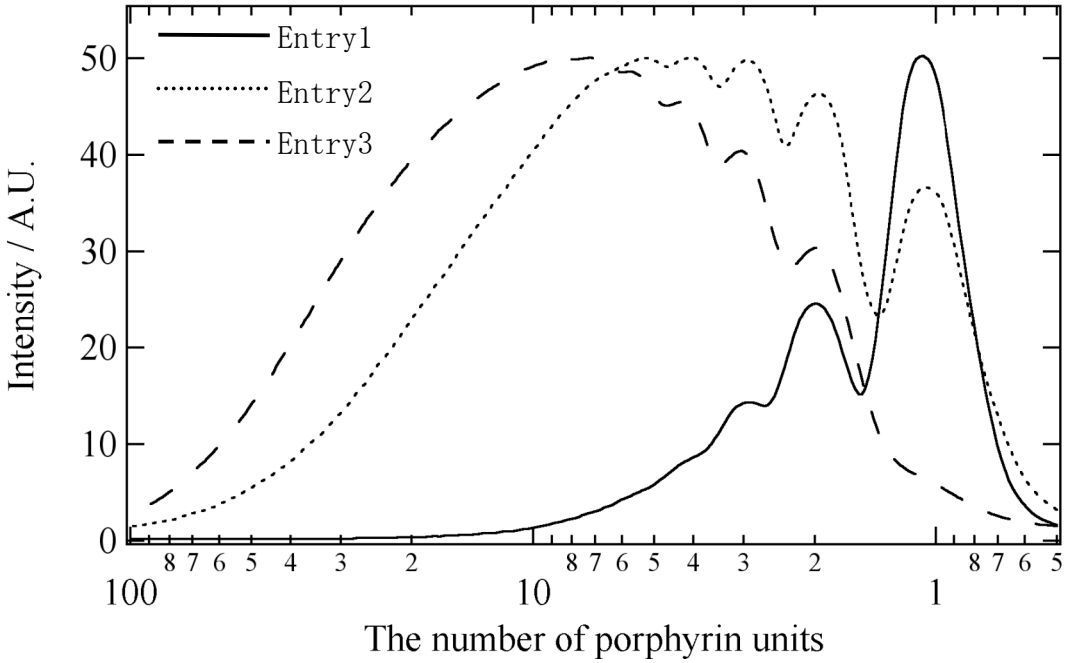

Figure 5-2. Analytical GPC data of porphyrin oligomers prepared by changing the compound ratio of **3** to **4**. The compound ratios of **3** to **4** were 1:2, 5:2, and 10:1 for Entries 1, 2 and 3, respectively.

5-3. Characterization of end-functionalized π-conjugated porphyrin oligomers

5-3-1. Molecular weight analysis of end-functionalized π-conjugated porphyrin oligomers

The molecular weight were strictly determined by matrix-assisted laser desorption ionization time of flight mass spectroscopy from monomer to heptamer and the data are shown Figure 5-3 (a) and (b). As another method, molecular weights were determined by HPLC-GPC. Calibrations were used polystyrene standard. From these results, each oligomer was separated and was pure.

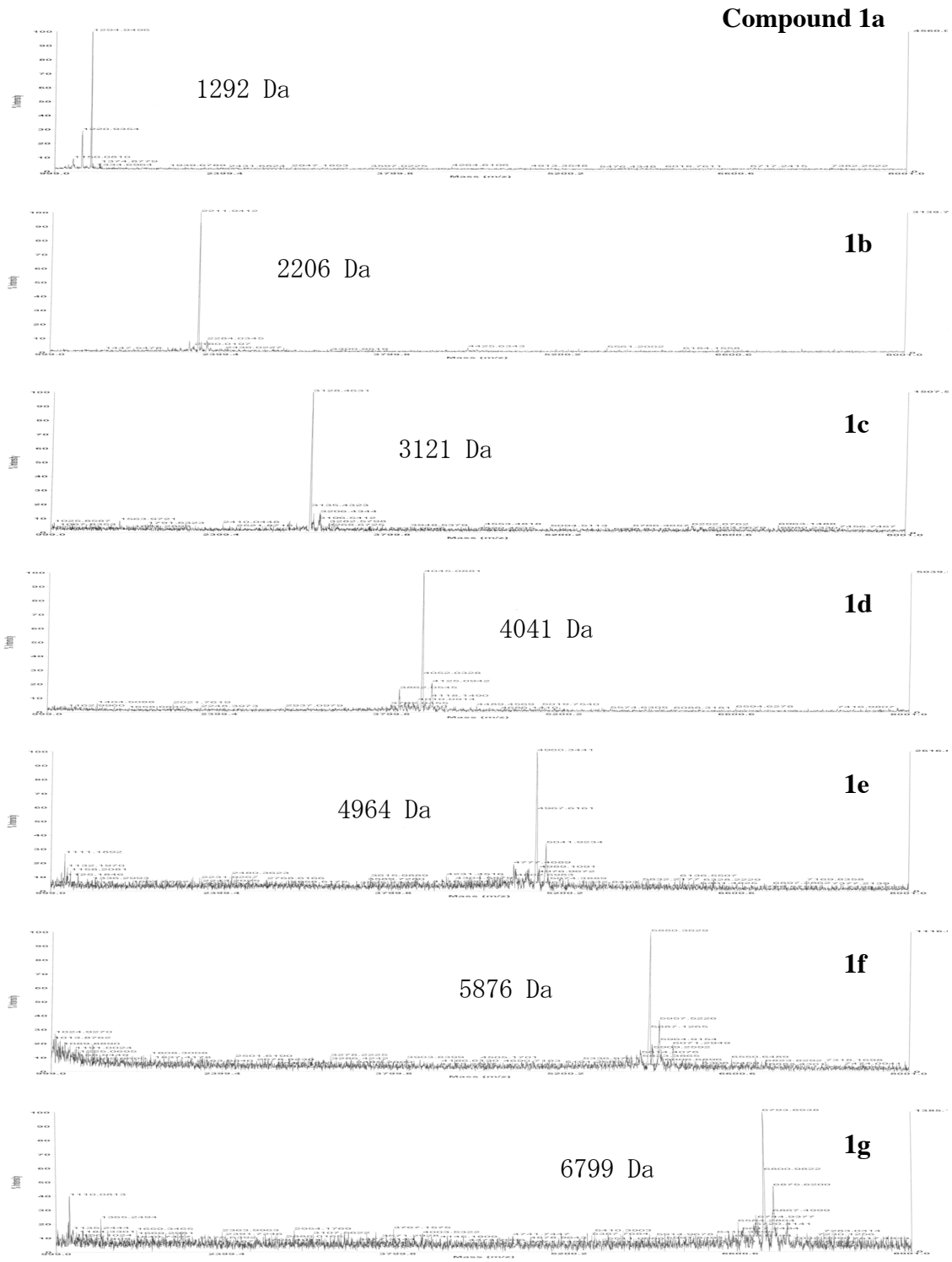

Figure 5-3. (a) MALDI-TOF-MS spectra of oligomer (**1a-g**).

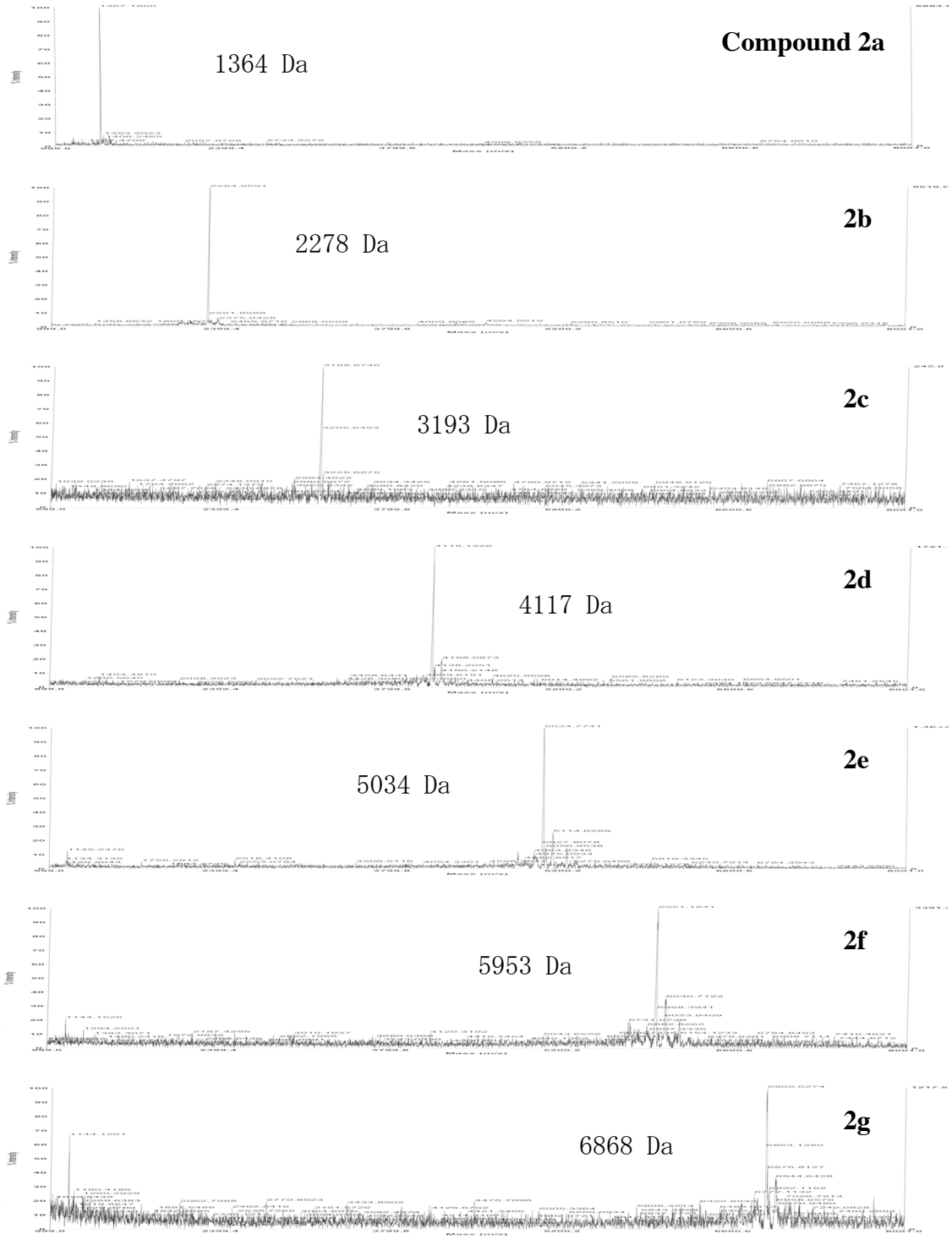

Figure 5-3. (b) MALDI-TOF-MS spectra of oligomer (**2a-g**).

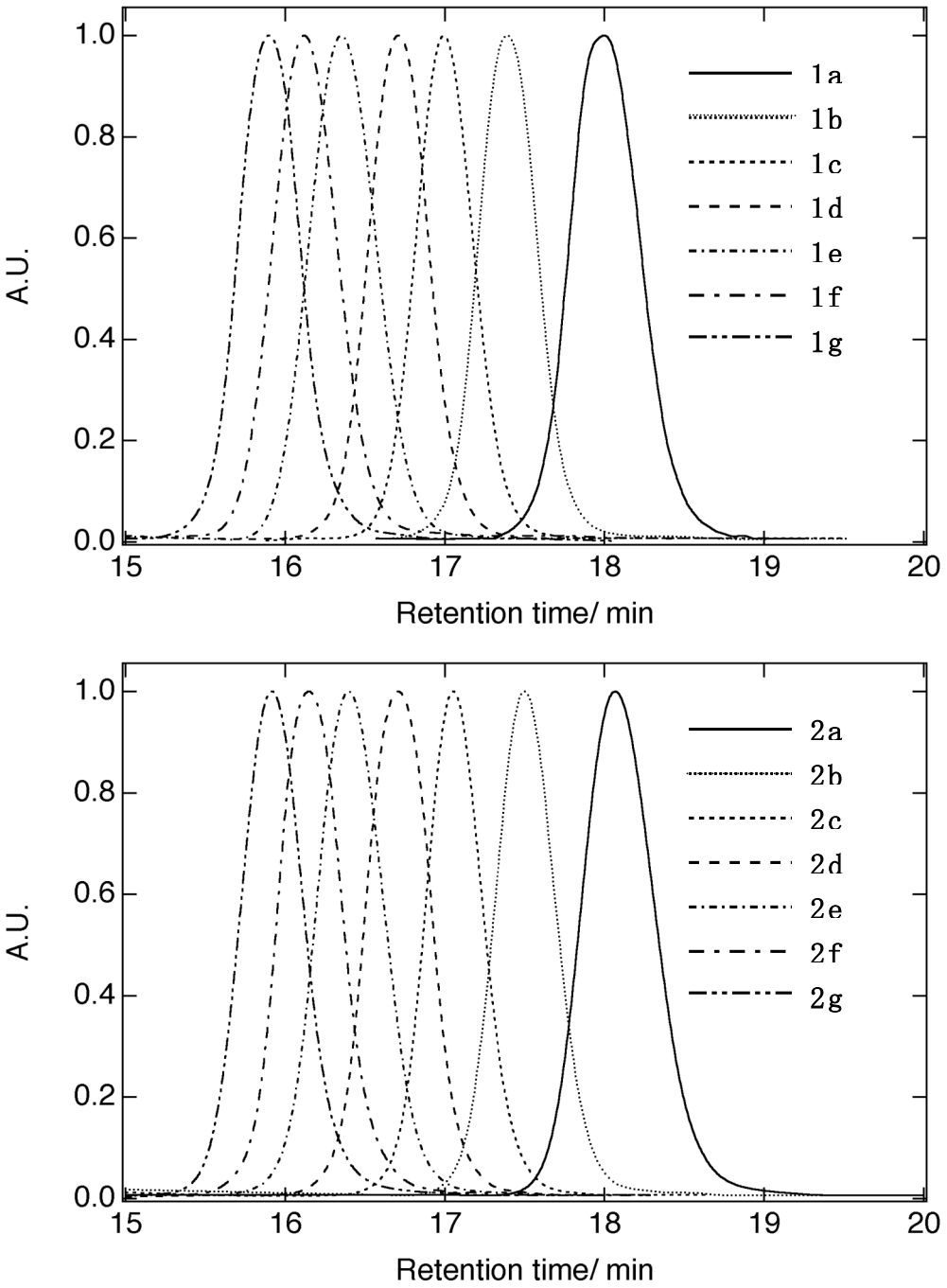

Figure 5-4. CPC-HPLC chromatograms of (a) oligomers (**1a-g**) and (b) oligomers (**2a-g**),

5-3-2. UV absorption and fluorescence spectra

UV-s absorption spectra of end-functionalized porphyrin oligomers **1a-g** and **2a-g** in THF are shown in Figures 5-5 (a) and 5-5 (b), respectively, and the peak wavelengths λ_{max} are tabulated in Table 1. The Soret peaks of the porphyrin oligomers were gradually red-shifted as the size of the oligomer increased. The Q bands were also red-shifted and intensified with increasing porphyrin units, indicating a high degree of conjugation. The Soret and Q band absorption maxima were dependent on the end-functional groups. Oligomers **2a-g** with pyrene end groups showed longer wavelength absorption compared to the corresponding oligomers **1a-g** with 4-(S-acetylthiomethyl)phenyl groups. The absorption coefficients of these oligomers became larger with the increasing number of porphyrin units. The absorption coefficients increased with a linear relationship to the number of porphyrin units with the exception of the monomer.

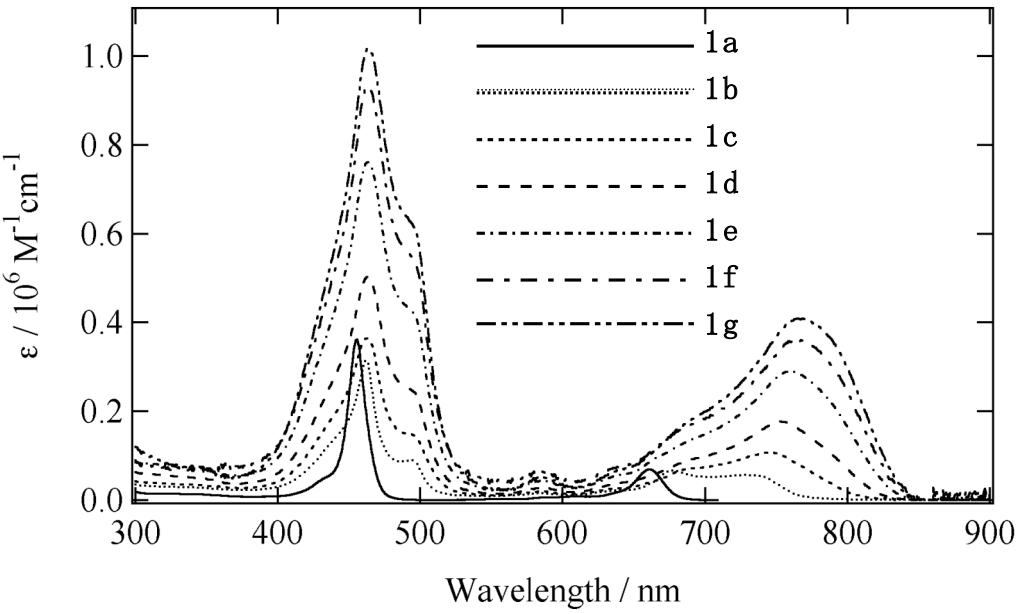

Figure 5-5. (a) UV-Vis spectra of acetylthiomethylbenzene-capped porphyrin oligomers **1a-g.**

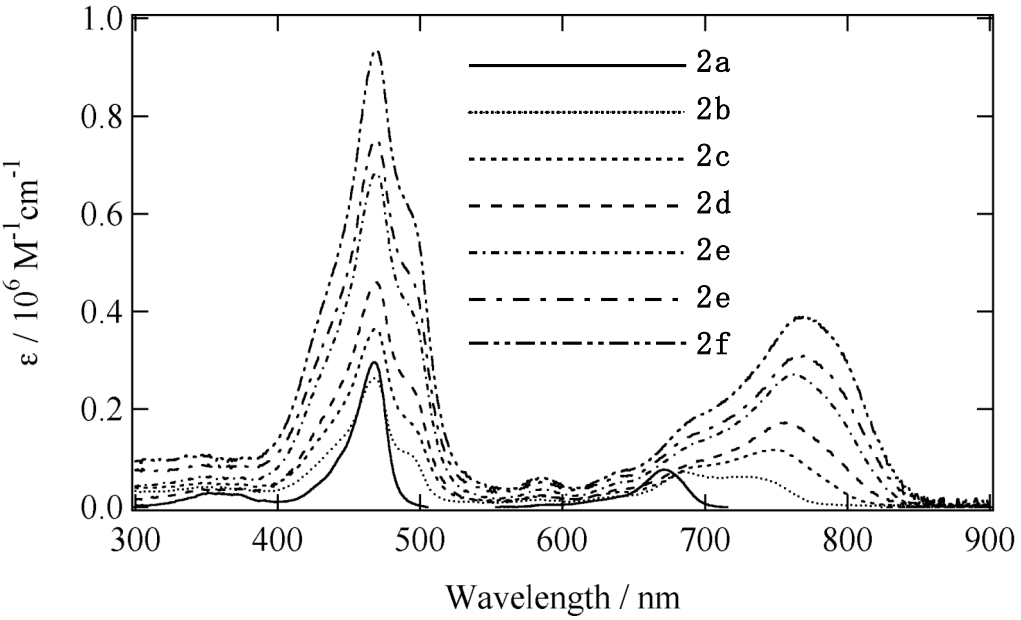

Figure 5-5. (b) UV-Vis spectra of pyrene-capped porphyrin oligomers 2a-g measured in THF.

Fluorescence data of these oligomers are also depicted in Table 5-1. These emission spectra show no dependency on excitation wavelength and the excitation spectra were coincident with the absorption spectra, which confirms that these emissions are not from any impurities. From the absorption and emission data, HOMO-LUMO energy gaps E_g were estimated. The values of E_g are plotted against the reciprocal of the number of porphyrin units ($1/N$) in Figure 5-6. These plots are linear, with no sign of saturation. The E_g value for **1a** obtained from absorption data (1.88 eV) is 0.03 eV larger than that for **2a** (1.85 eV), which is reasonably explained by the differences in the degree of resonance of the capping moieties. The E_g ($N =$) values obtained from the intercepts for a series of **1** and **2** were coincident to be 1.57 eV from the absorption data and 1.48 eV from the emission data. This means that might be though the optical properties of the monomer were highly influenced by the capping molecules, the effect decreased with an increasing number of porphyrin units. Therefore, we may conclude that the

optical properties of long oligomers were minimally influenced by the end-capping moieties. The reported E_g (N =) obtained from the emission of a series of **6** was 1.34 eV, which is significantly lower than the values obtained for **1** and **2**.[13] This can be attributed to a difference in the measurement conditions. Because of the low solubility of **6**, a small amount of pyridine was added to the solution. Most likely, the pyridine molecules coordinated to the zinc metal of each porphyrin unit, lowering the E_g values by the extended resonance.[14] In spite of such a condition, E_g values of non-functionalized porphyrin monomer **6a** was weak than that of end-functionalized porphyrin monomer **1a** and **2a**. However, the effect decreased with an increasing number of porphyrin units. It can be measure properties of porphyrin polymer without thinking of effect capping molecules expect for short oligomer such as monomer and dimer.

Table 5-1. The absorption λ_{max} (in THF), emission λ_{max} (in THF), and fluorescence quantum yield of porphyrin oligomers **1a-g** and **2a-g**.

Porphyrin oligomer	Absorption λ_{max}/nm	Emission[a] λ_{max}/nm	Φ_F[b]
1a	455, 661	674	0.09
1b	462, 493, 583, 677, 725	750	0.10
1c	463, 583, 744	780	0.07
1d	463, 584, 752	792	0.08
1e	463, 585, 758	800	0.07
1f	463, 585, 764	804	0.07
1g	463, 585, 768	808	0.07
2a	467, 671	688	0.09
2b	468, 583, 685, 730	758	0.12
2c	468, 584, 747	782	0.09
2d	469, 584, 756	796	0.09
2e	469, 584, 762	802	0.07
2f	469, 584, 766	806	0.07
2g	469, 583, 769	808	0.07

[a] Emission spectra were taken for excitation at Soret band.

[b] Tetraphenylporphyrin in benzene (TPP, Φ_F =0.11) was used as a standard.[26]

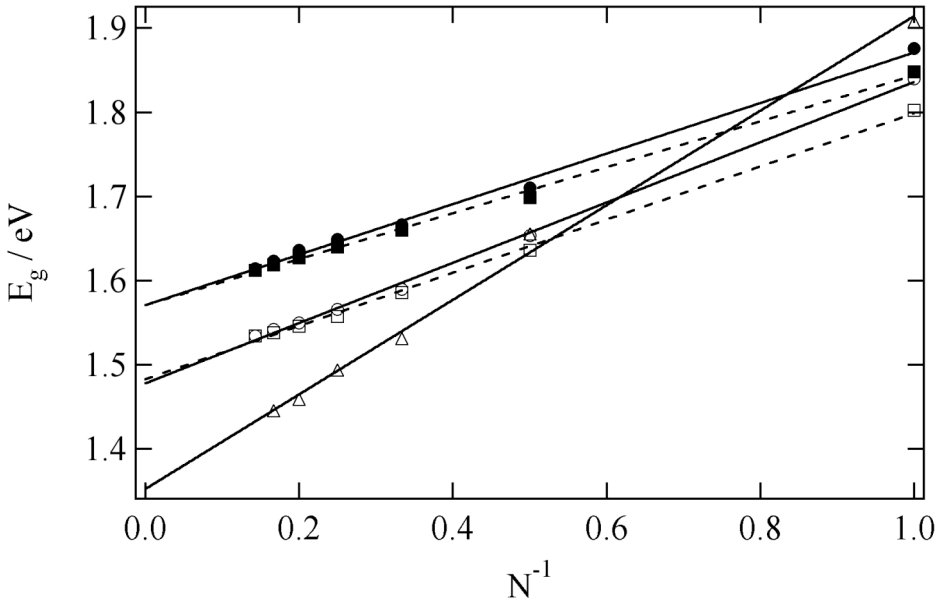

Figure 5-6. Plot of optical band gap energy E_g against the reciprocal of the number of porphyrin units 1/N for (●) **1a-g** (absorption), (■) **2a-g** (absorption), (○) **1a-g** (emission), (□) **2a-g** (emission) (△) **6a-f** with pyridine (emission).[13]

The relative fluorescence quantum yields were determined using tetraphenylporphyrin (H_2TPP) as the standard ($\Phi_F = 0.11$).[26] The quantum yield of the monomers (**1a** and **2a**) was 0.09, and this decreased gradually with the increase in the number of porphyrin units (Table 5-1 and Figure 5-7). The results shown are in sharp contrast with a report for meso-meso linked porphyrin oligomers **7**.[12,27,28] In the latter compounds, the quantum yield of the fluorescence for the monomer was 0.022 and increased as the number of porphyrin units increased in the arrays. This phenomenon is attributed to the increase of the rotational diffusion time by the anisotropic elongation of the molecules. As the rotational diffusion time increased, the natural radiative lifetime decreased, and consequently the fluorescence quantum yield increased. The reason for the difference between **7** and **1** or **2** is not clear at present, but the degree of conjugation between porphyrin moieties may be responsible.

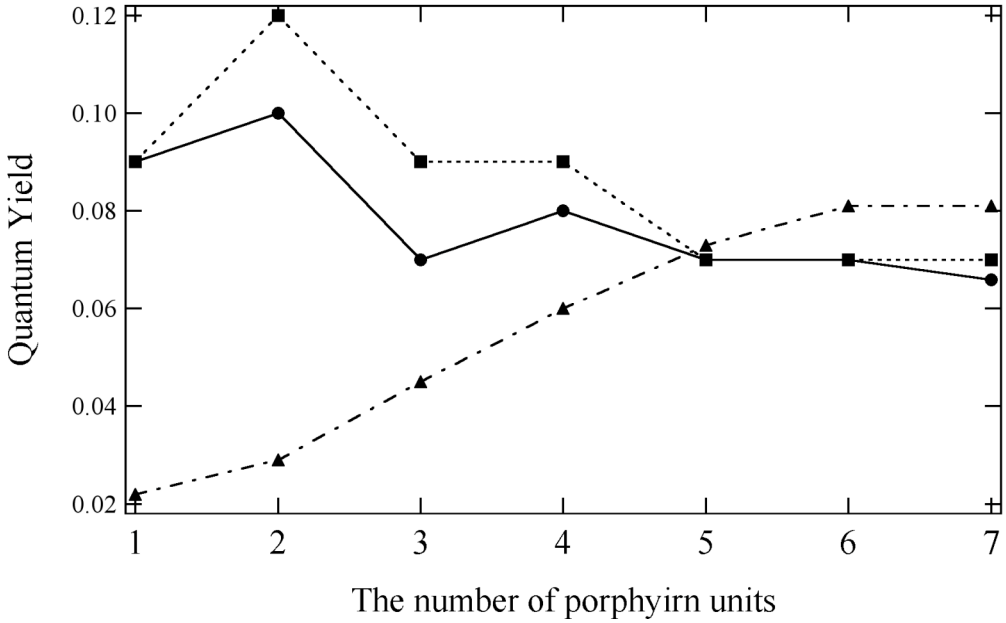

Figure 5-7. Plots of quantum yield versus the number of porphyrin units for (●) 1a-g, (■) 2a-g and (▲) 7a-g.[12]

5-4. Conclusion

We report the preparation and isolation of a series of end-functionalized porphyrin oligomers by a simple coupling reaction. The distribution of oligomers can be controlled by the ratio of porphyrin derivative to capping molecules. UV-Vis absorption and fluorescence spectra of the monomers were affected by the capping groups, however the effect decreased as the number of porphyrin units increased. The fluorescence quantum yield decreased as the number of porphyrin units increased, which showed a sharp contrast with a series of meso-meso coupled porphyrin oligomers. Construction of nanostructures consisting of these end-functionalized molecules and metal particles or carbon nanotubes is now in progress.

Experimental

Compounds **3**,[29,30] **4**[31] and **5**[32] were prepared according to published literature procedures. All solvents and reagents were commercial reagent grade and were used without further purification except where noted. ^{1}H NMR spectra were recorded on a JEOL JNM-LA400 spectrometer and chemical shifts were reported in the delta scale relative to an internal standard of TMS (δ = 0.00). Spectroscopic grade tetrahydrofuran (THF) and benzene were used as solvents for all spectroscopic measurements. UV-vis absorption spectra were recorded on a Shimadzu UV-3150 spectrophotometer. Fluorescence measurements were carried out with a JASCO FP-6600 spectrometer. Infrared spectra were obtained on a JASCO FT/IR-460plus. All MALDI-TOF-MS spectra were obtained using an Applied Biosystem Voyager DE-STR with 9-nitroanthracene and dithranol as the matrices. Analytical gel permeation chromatography (GPC) was carried out using Shimadzu LC-6A equipped with a diode array detector (MD-2015, JASCO) and two serially connected GPC KF-804L columns. THF was used as the eluent and the flow rate in all experiments was 1.0 mL/min. Recycling preparative GPC-HPLC was carried out on JAI LC-908 using serially connected preparative scale JAIGEL-2.5H, 3H and 4H columns. Preliminary separation of the oligomers was performed by open column chromatography-GPC using Bio-Beads S-X1 (BioRad) and THF as the eluent.

Preparation and isolation of 4-(S-acetylthiomethyl)phenyl functionalized porphyrin oligomers

In a round-bottomed flask, compounds **3** (52 mg, 57 μmol), **4** (11 mg, 57 μmol) and $Cu(OAc)_2$ (31 mg, 170 μmol) were dissolved in 5 ml of pyridine and the mixture was stirred at room temperature for 12 hours. Water was added to the reaction and the resulting precipitate was filtered and washed with methanol. The precipitate was dissolved in THF and passed through an open column chromatograph using Bio-Beads S-X1 (BioRad) to obtain a mixture of the products containing porphyrin oligomers. These oligomers were further

isolated by recycling GPC-HPLC to give **1a** (5 mg, 6%), **1b** (19 mg, 31%), **1c** (8 mg, 14%), **1d** (6 mg, 10%), **1e** (5 mg, 8%), **1f** (3 mg, 5%), **1g** (1 mg, 2%), and larger oligomers (6 mg). The purity of each homologue was checked by the following analyses. The ^{1}H NMR spectrum of each sample showed consistent integrations for all the resonances, and no evidence of impurities was observed. With the MALDI-TOF-MS spectra, no other homologues were detected for each isolated product. We conducted analytical GPC analyses of each product with simultaneous measurements of the absorption spectra using a diode array detector. All the isolated oligomers showed a single peak clearly distinguishable from other oligomers by its retention time and absorption spectrum.

Control of product distribution by changing the ratio of 3 to 4 (Entry 1)

In a round-bottomed flask, **3** (52 mg, 57 μmol), **4** (225 mg, 118 μmol) and $Cu(OAc)_2$ (30 mg, 167 μmol) were dissolved in 5 mL of pyridine and the mixture was stirred at room temperature for 12 hours. Water was added to the reaction and the resulting precipitate was filtered and washed with methanol. The precipitate was dissolved in THF and passed through an open column chromatograph using Bio-Beads S-X1 (BioRad) to obtain a mixture of the products containing porphyrin oligomers (55 mg). The distribution of the products was determined by analytical GPC of the mixture.

Control of product distribution by changing the ratio of 3 to 4 (Entry 2)

In a round-bottomed flask, **3** (51 mg, 55 μmol), **4** (4 mg, 21 μmol) and $Cu(OAc)_2$ (30 mg, 170 μmol) were dissolved in 5 mL of pyridine and the mixture was stirred at room temperature for 12 hours. Water was added to the reaction and the resulting precipitate was filtered and washed with methanol. The precipitate was dissolved in THF and passed through an open column chromatograph using Bio-Beads S-X1 (BioRad) to obtain a mixture of the products containing porphyrin oligomers (42 mg). The distribution of the

products was determined by analytical GPC of the mixture.

Control of product distribution by changing the ratio of 3 to 4 (Entry 3)

In a round-bottomed flask, **3** (51 mg, 56 μmol), a THF solution of **4** (52 μL solution of 10 mg/mL concentration, 2.8 μmol) and $Cu(OAc)_2$ (30 mg, 167 μmol) were dissolved in 5 mL of pyridine and the mixture was stirred at room temperature for 12 hours. Water was added to the reaction and the resulting precipitate was filtered and washed with methanol. The precipitate was dissolved in THF and passed through an open column chromatograph using Bio-Beads S-X1 (BioRad) to obtain a mixture of the products containing porphyrin oligomers (36 mg). The distribution of the products was determined by analytical GPC of the mixture.

Preparation and isolation of pyrenyl functionalized porphyrin oligomers

In a round-bottomed flask, **3** (51 mg, 56 μmol), **5** (13 mg, 56 μmol) and $Cu(OAc)_2$ (30 mg, 167 μmol) were dissolved in 5 mL of pyridine and the mixture was stirred at room temperature for 12 hours. Water was added to the reaction and the resulting precipitate was filtered, washed with methanol, and roughly purified by open column chromatography-GPC. The oligomers were isolated by a recycling GPC-HPLC to give **2a** (13 mg, 18%), **2b** (14 mg, 23%), **2c** (10 mg, 16%), **2d** (7 mg, 12%), **2e** (4 mg, 6%), **2f** (3 mg, 6%), **2g** (2 mg, 4%), and larger oligomers (4 mg).

Compound 1a. ^1H NMR (400 MHz, d_8-THF) δ 9.57 (d, J = 5 Hz, 4H, β-pyrrole), 8.96 (d, J = 5 Hz, 4H, β-pyrrole), 7.65 (d, J = 8.3 Hz, 4H, Ar), 7.40 (d, J = 8.3 Hz, 4H, Ar), 7.32 (d, J = 2 Hz, 4H, Ar), 6.95 (t, J = 2 Hz, 2H, Ar), 4.21 (t, J = 7 Hz, 8H, OCH_2), 4.18 (s, 4H, SCH_2Ph), 2.34 (s, 6H, $C(O)CH_3$], 1.92 (sext, J = 7 Hz, 8H, CH_2), 1.77 (m, J = 7 Hz, 4H, CH), 1.00 (d, J = 7 Hz, 24H, CH_3). HRMS (MALDI-TOF) calcd for $C_{78}H_{76}N_4O_6S_2Zn$ 1292.4492, found

1292.4489. UV-vis (THF) λ_{max} (logε) 455 (5.56), 661 (4.84) nm. Fluorescence (THF, λ_{ex} = 455 nm) λ_{em} 674 nm. IR (KBr) 2952, 2930, 2868, 2132, 2195, 1588, 1163 cm^{-1}.

Compound 1b. ^1H NMR (400 MHz, d_8-THF) δ 9.87 (d, J = 5 Hz, 4H, β-pyrrole), 9.60 (d, J = 5 Hz, 4H, β-pyrrole), 9.06 (d, J = 5 Hz, 4H, β-pyrrole), 9.00 (d, J = 5 Hz, 4H, β-pyrrole), 7.67 (d, J = 8 Hz, 4H, Ar), 7.41 (d, J = 8 Hz, 4H, Ar), 7.38 (d, J = 2 Hz, 8H, Ar), 6.97 (t, J = 2 Hz, 4H, Ar), 4.24 (t, J = 6.6 Hz, 16H, OCH_2), 4.18 (s, 4H, SCH_2Ph), 2.34 (s, 6H, $C(O)CH_3$), 1.92 (sext, J = 6.6 Hz, 16H, CH_2), 1.77 (m, J = 6.6 Hz, 8H, CH), 1.01 (d, J = 6.6 Hz, 48H, CH_3). HRMS (MALDI-TOF) calcd for $C_{134}H_{134}N_8O_{10}S_2Zn_2$ 2206.8241, found 2206.8234. UV-vis (THF) λ_{max} (logε) 462 (5.50), 493 (4.95), 583 (4.19), 677 (4.82), 725 (4.75) nm. Fluorescence (THF, λ_{ex} = 462 nm) λ_{em} 752 nm. IR (KBr) 2954, 2927, 2869, 2130, 2194, 1589, 1163 cm^{-1}.

Compound 1c. ^1H NMR (400 MHz, d_8-THF) δ 9.88 (m, 8H, β-pyrrole), 9.60 (d, J = 5 Hz, 4H, β-pyrrole), 9.08 (m, 8H, β-pyrrole), 9.00 (d, J = 5 Hz, 4H, β-pyrrole), 7.67 (d, J = 8 Hz, 4H, Ar), 7.41 (d, 4H, Ar), 7.38 (m, 12H, Ar), 6.97 (m, 6H, Ar), 4.24 (m, 24H, OCH_2), 4.19 (s, 4H, SCH_2Ph), 2.35 (s, 6H, $C(O)CH_3$), 1.92 (m, 24H, CH_2), 1.77 (m, 12H, CH), 1.02 (m, 72H, CH_3). HRMS (MALDI-TOF) calcd for $C_{190}H_{192}N_{12}O_{14}S_2Zn_3$ 3121.1991, found 3121.2266. UV-vis (THF) λ_{max} (logε) 463 (5.56), 583 (4.29), 744 (5.03) nm. Fluorescence (THF, λ_{ex} = 463 nm) λ_{em} 786 nm. IR (KBr) 2954, 2927, 2868, 2129, 2162, 1590, 1156 cm^{-1}.

Compound 1d. ^1H NMR (400 MHz, d_8-THF) δ 9.88 (m, 12H, β-pyrrole), 9.60 (d, J = 5 Hz, 4H, β-pyrrole), 9.08 (m, 12H, β-pyrrole), 9.00 (d, J = 5 Hz, 4H, β-pyrrole), 7.67 (d, J = 8 Hz, 4H, Ar), 7.41 (d, 4H, Ar), 7.38~7.44 (m, 16H, Ar), 6.97 (m, 8H, Ar), 4.24 (m, 32H, OCH_2), 4.19 (s, 4H, SCH_2Ph), 2.35 (s, 6H, $C(O)CH_3$], 1.92 (m, 32H, CH_2), 1.77 (m, 16H, CH), 1.02 (m, 96H, CH_3). MS (MALDI-TOF) calcd for $C_{246}H_{250}N_{16}O_{18}S_2Zn_4$ 4041.7, found 4041.5. UV-vis (THF) λ_{max} (logε) 463 (5.70), 584 (4.43), 752 (5.24) nm. Fluorescence (THF,

λ_{ex} = 463 nm) λ_{em} 800 nm. IR (KBr) 2953, 2927, 2869, 2128, 2162, 1588, 1163 cm^{-1}.

Compound 1e. ^1H NMR (400 MHz, d_8-THF) δ 9.88 (m, 16H, β-pyrrole), 9.60 (d, J = 5 Hz, 4H, β-pyrrole), 9.08 (m, 16H, β-pyrrole), 9.00 (d, J = 5 Hz, 4H, β-pyrrole), 7.67 (d, J = 8 Hz, 4H, Ar), 7.41 (d, 4H, Ar), 7.38~7.44 (m, 20H, Ar), 6.97 (m, 10H, Ar), 4.24 (m, 40H, OCH_2), 4.19 (s, 4H, SCH_2Ph), 2.35 (s, 6H, $C(O)CH_3$), 1.92 (m, 40H, CH_2), 1.77 (m, 20H, CH), 1.02 (m, 120H, CH_3). MS (MALDI-TOF) calcd for $C_{302}H_{308}N_{20}O_{22}S_2Zn_5$ 4964, found 4960. UV-vis (THF) λ_{max} (logε) 463 (5.88), 585 (4.63), 758 (5.46) nm. Fluorescence (THF, λ_{ex} = 463 nm) λ_{em} 814 nm. IR (KBr) 2953, 2926, 2868, 2128, 2162, 1588, 1162 cm^{-1}.

Compound 1f. ^1H NMR (400 MHz, d_8-THF) δ 9.88 (m, 20H, β-pyrrole), 9.60 (d, J = 5 Hz, 4H, β-pyrrole), 9.08 (m, 20H, β-pyrrole), 9.00 (d, J = 5 Hz, 4H, β-pyrrole), 7.67 (d, J = 8 Hz, 4H, Ar), 7.41 (d, 4H, Ar), 7.38~7.44 (m, 24H, Ar), 6.97 (m, 12H, Ar), 4.24 (m, 48H, OCH_2), 4.19 (s, 4H, SCH_2Ph), 2.35 (s, 6H, $C(O)CH_3$), 1.92 (m, 48H, CH_2), 1.77 (m, 24H, CH), 1.02 (m, 144H, CH_3). MS (MALDI-TOF) calcd for $C_{358}H_{366}N_{24}O_{26}S_2Zn_6$ 5881, found 5876. UV-vis (THF) λ_{max} (logε) 463 (5.97), 585 (4.81), 764 (5.56) nm. Fluorescence (THF, λ_{ex} = 463 nm) λ_{em} 816 nm. IR (KBr) 2954, 2926, 2868, 2126, 2162, 1588, 1163 cm^{-1}.

Compound 1g. ^1H NMR (400 MHz, d_8-THF) δ 9.88 (m, 24H, β-pyrrole), 9.60 (d, J = 5 Hz, 4H, β-pyrrole), 9.08 (m, 24H, β-pyrrole), 9.00 (d, J = 5 Hz, 4H, β-pyrrole), 7.67 (d, J = 8 Hz, 4H, Ar), 7.41 (d, 4H, Ar), 7.38~7.44 (m, 28H, Ar), 6.97 (m, 14H, Ar), 4.24 (m, 56H, OCH_2), 4.19 (s, 4H, SCH_2Ph), 2.35 (s, 6H, $C(O)CH_3$), 1.92 (m, 56H, CH_2), 1.77 (m, 28H, CH), 1.02 (m, 168H, CH_3). MS (MALDI-TOF) calcd for $C_{414}H_{424}N_{28}O_{30}S_2Zn_7$ 6799, found 6792. UV-vis (THF) λ_{max} (logε) 463 (6.01), 585 (4.72), 768 (5.61) nm. Fluorescence (THF, λ_{ex} = 463 nm) λ_{em} 816 nm. IR (KBr) 2953, 2927, 2869, 2121, 2166, 1588, 1162 cm^{-1}.

Compound 2a. ^1H NMR (400 MHz, d_8-THF) δ 9.57 (d, J = 5 Hz, 4H, β-pyrrole), 9.02 (d, J = 5 Hz, 4H, β-pyrrole), 8.83 (d, J = 9 Hz, 2H, pyrene), 8.42-8.05

(16H, m, pyrene), 7.38 (d, J = 2 Hz, 4H, Ar), 6.98 (t, J = 2 Hz, 2H, Ar), 4.23 (t, J = 7 Hz, 8H, OCH_2), 1.94 (sext, J = 7 Hz, 8H, CH_2), 1.79 (m, J = 7 Hz, 4H, CH), 1.01 (d, J = 7 Hz, 24H, CH_3). HRMS (MALDI-TOF) calcd for $C_{92}H_{76}N_4O_4Zn$ 1364.5152, found 1364.5150. UV-vis (THF) λ_{max} (logε) 467 (5.47), 671 (4.88) nm. Fluorescence (THF, λ_{ex} = 467 nm) λ_{em} 688 nm. IR (KBr) 2952, 2927, 2870, 2127, 2184, 1587, 1163 cm^{-1}.

Compound 2b. ^1H NMR (400 MHz, d_8-THF) δ 9.88 (d, J = 5 Hz, 4H, β-pyrrole), 9.72 (d, J = 5 Hz, 4H, β-pyrrole), 9.08 (d, J = 5 Hz, 4H, β-pyrrole), 9.05 (d, J = 5 Hz, 4H, β-pyrrole), 8.86 (d, J = 9 Hz, 2H, pyrene), 8.44-8.06 (m, 16H, pyrene), 7.40 (d, J = 2 Hz, 8H, Ar), 6.99 (t, J = 2 Hz, 4H, Ar), 4.25 (t, J = 7 Hz, 16H, OCH_2), 1.94 (sext, J = 7 Hz, 16H, CH_2), 1.80 (m, J = 7 Hz, 8H, CH), 1.02 (d, J = 7 Hz, 48H, CH_3). HRMS (MALDI-TOF) calcd for $C_{148}H_{134}N_8O_8Zn_2$ 2278.8902, found 2278.8881. UV-vis (THF) λ_{max} (logε) 468 (5.42), 580 (4.18), 685 (4.86), 730 (4.79) nm. Fluorescence (THF, λ_{ex} = 468 nm) λ_{em} 758 nm. IR (KBr) 2953, 2927, 2869, 2127, 2184, 1588, 1164 cm^{-1}.

Compound 2c. ^1H NMR (400 MHz, d_8-THF) δ 9.91 (m, 8H, β-pyrrole), 9.73 (d, J = 5 Hz, 4H, β-pyrrole), 9.10 (m, 8H, β-pyrrole), 9.05 (d, J = 5 Hz, 4H, β-pyrrole), 8.86 (d, J = 9 Hz, 2H, pyrene), 8.44-8.00 (16H, m, pyrene), 7.42 (m, 12H, Ar), 6.99 (m, 6H, Ar), 4.25 (m, 24H, OCH_2), 1.96 (m, 24H, CH_2), 1.82 (m, 12H, CH), 1.03 (m, 72H, CH_3). HRMS (MALDI-TOF) calcd for $C_{204}H_{192}N_{12}O_{12}Zn_3$ 3193.2651, found 3193.2678. UV-vis (THF) λ_{max} (logε) 468 (5.56), 584 (4.35), 747 (5.07) nm. Fluorescence (THF, λ_{ex} = 468 nm) λ_{em} 782 nm. IR (KBr) 2954, 2928, 2868, 2125, 2167, 1587, 1162 cm^{-1}.

Compound 2d. ^1H NMR (400 MHz, d_8-THF) δ 9.91 (m, 12H, β-pyrrole), 9.73 (d, J = 5 Hz, 4H, β-pyrrole), 9.10 (m, 12H, β-pyrrole), 9.05 (d, J = 5 Hz, 4H, β-pyrrole), 8.86 (d, J = 9 Hz, 2H, pyrene), 8.45-8.00 (m, 16H, pyrene), 7.42 (m, 16H, Ar), 6.99 (m, 8H, Ar), 4.26 (m, 32H, OCH_2), 1.96 (m, 32H, CH_2), 1.82 (m, 16H, CH), 1.03 (m, 96H, CH_3). MS (MALDI-TOF) calcd for $C_{260}H_{250}N_{16}O_{16}Zn_4$ 4117, found 4116. UV-vis (THF) λ_{max} (logε) 469 (5.66), 584 (4.37), 756 (5.24)

nm. Fluorescence (THF, λ_{ex} = 469 nm) λ_{em} 796 nm. IR (KBr) 2954, 2925, 2869, 2126, 2167, 1588, 1163 cm^{-1}.

Compound 2e. ^1H NMR (400 MHz, d_8-THF) δ 9.91 (m, 16H, β-pyrrole), 9.73 (d, J = 5 Hz, 4H, β-pyrrole), 9.10 (m, 16H, β-pyrrole), 9.05 (d, J = 5 Hz, 4H, β-pyrrole), 8.86 (d, J = 9 Hz, 2H, pyrene), 8.45-8.00 (m, 16H, pyrene), 7.42 (m, 20H, Ar), 6.99 (m, 10H, Ar), 4.26 (m, 40H, OCH_2), 1.96 (m, 40H, CH_2), 1.82 (m, 20H, CH), 1.03 (m, 120H, CH_3). MS (MALDI-TOF) calcd for $C_{316}H_{308}N_{20}O_{20}Zn_5$ 5034, found 5031. UV-vis (THF) λ_{max} (logε) 469 (5.84), 584 (4.55), 762 (5.43) nm. Fluorescence (THF, λ_{ex} = 469 nm) λ_{em} 802 nm. IR (KBr) 2951, 2927, 2870, 2126, 2167, 1588, 1162 cm^{-1}.

Compound 2f. ^1H NMR (400 MHz, d_8-THF) δ 9.91 (m, 20H, β-pyrrole), 9.73 (d, J = 5 Hz, 4H, β-pyrrole), 9.10 (m, 20H, β-pyrrole), 9.05 (d, J = 5 Hz, 4H, β-pyrrole), 8.86 (d, J = 9 Hz, 2H, pyrene), 8.45-8.00 (m, 16H, pyrene), 7.42 (m, 24H, Ar), 6.99 (m, 12H, Ar), 4.26 (m, 48H, OCH_2), 1.96 (m, 48H, CH_2), 1.82 (m, 24H, CH), 1.03 (m, 144H, CH_3). MS (MALDI-TOF) calcd for $C_{372}H_{366}N_{24}O_{24}Zn_6$ 5953, found 5948. UV-vis (THF) λ_{max} (logε) 469 (5.88), 584 (4.71), 766 (5.49) nm. Fluorescence (THF, λ_{ex} = 469 nm) λ_{em} 806 nm. IR (KBr) 2956, 2927, 2869, 2126, 2162, 1588, 1163 cm^{-1}.

Compound 2g. ^1H NMR (400 MHz, d_8-THF) δ 9.91 (m, 24H, β-pyrrole), 9.73 (d, J = 5 Hz, 4H, β-pyrrole), 9.10 (m, 24H, β-pyrrole), 9.05 (d, J = 5 Hz, 4H, β-pyrrole), 8.86 (d, J = 9 Hz, 2H, pyrene), 8.45-8.00 (m, 16H, pyrene), 7.42 (m, 28H, Ar), 6.99 (m, 14H, Ar), 4.26 (m, 56H, OCH_2), 1.96 (m, 56H, CH_2), 1.82 (m, 28H, CH), 1.03 (m, 168H, CH_3). MS (MALDI-TOF) calcd for $C_{428}H_{424}N_{28}O_{28}Zn_7$ 6868, found 6861. UV-vis (THF) λ_{max} (logε) 469 (5.97), 583 (4.78), 769 (5.59) nm. Fluorescence (THF, λ_{ex} = 469 nm) λ_{em} 808 nm. IR (KBr) 2954, 2927, 2869, 2126, 2162, 1588, 1163 cm^{-1}.

Reference

1. Reed, M. A.; Lee, T. *Molecular Nanoelectronics*; American Scientific Publishers: Los Angeles, California, 2003.
2. Flatt, A. K.; Dirk, S. M.; Henderson, J. C.; Shen, D. E.; Su, J.; Reed, M. A.; Tour, J. M. *Tetrahedron* **2003**, *59*, 8555-8570.
3. Tour, J. M.; Rawlett, A. M.; Kozaki, M.; Yao, Y. X.; Jagessar, R. C.; Dirk, S. M.; Price, D. W.; Reed, M. A.; Zhou, C. W.; Chen, J.; Wang, W. Y.; Campbell, I. *Chem. Eur. J.* **2001**, *7*, 5118-5134.
4. Reed, M. A. *Proc. IEEE* **1999**, *87*, 652-658.
5. Donhauser, Z. J.; Mantooth, B. A.; Kelly, K. F.; Bumm, L. A.; Monnell, J. D.; Stapleton, J. J.; Price, D. W.; Rawlett, A. M.; Allara, D. L.; Tour, J. M.; Weiss, P. S. *Science* **2001**, *292*, 2303-2307.
6. Blum, A. S.; Kushmerick, J. G.; Long, D. P.; Patterson, C. H.; Yang, J. C.; Henderson, J. C.; Yao, Y. X.; Tour, J. M.; Shashidhar, R.; Ratna, B. R. *Nature Materials* **2005**, *4*, 167-172.
7. Kubatkin, S.; Danilov, A.; Hjort, M.; Cornil, J.; Bredas, J. L.; Stuhr-Hansen, N.; Hedegard, P.; Bjornholm, T. *Nature* **2003**, *425*, 698-701.
8. Park, J.; Pasupathy, A. N.; Goldsmith, J. I.; Chang, C.; Yaish, Y.; Rinkoski, M.; Sethna, J. P.; Abruna, H. D.; McEuen, P. L.; Ralpa, D. C. *Nature* **2002**, *417*, 722-725.
9. Park, H.; Park, J.; Lim, A. K. L.; Anderson, E. H.; Alivisatos, A. P.; McEuen, P. L. *Nature* **2000**, *407*, 57-60.
10. Xu, B. Q.; Xiao, X. Y.; Yang, X. M.; Zang, L.; Tao, N. J. *J. Am. Chem. Soc.* **2005**, *127*, 2386-2387.
11. Liang, W. J.; Shores, M. P.; Bockrath, M.; Long, J. R.; Park, H. *Nature* **2002**, *417*, 725-729.
12. Kim, Y. H.; Jeong, D. H.; Kim, D.; Jeoung, S. C.; Cho, H. S.; Kim, S. K.; Aratani, N.; Osuka, A. *J. Am. Chem. Soc.* **2001**, *123*, 76-86.
13. Taylor, P. N.; Huuskonen, J.; Rumbles, G.; Aplin, R. T.; Williams,

E.; Anderson, H. L. *Chem. Commun.* **1998**, 909-910.

14. Screen, T. E. O.; Thorne, J. R. G.; Denning, R. G.; Bucknall, D. G.; Anderson, H. L. *J. Mater. Chem.* **2003**, *13*, 2796-2808.

15. Chi, L. F.; Hartig, M.; Drechsler, T.; Schwaack, T.; Seidel, C.; Fuchs, H.; Schmid, G. *Appl. Phys. A.* **1998**, *66*, S187-S190.

16. Brust, M.; Bethell, D.; Schiffrin, D. J.; Kiely, C. J. *Adv. Mater.* **1995**, *7*, 795-797.

17. Mbindyo, J. K. N.; Mallouk, T. E.; Mattzela, J. B.; Kratochvilova, I.; Razavi, B.; Jackson, T. N.; Mayer, T. S. *J. Am. Chem. Soc.* **2002**, *124*, 4020-4026.

18. Thess, A.; Lee, R.; Nikolaev, P.; Dai, H. J.; Petit, P.; Robert, J.; Xu, C. H.; Lee, Y. H.; Kim, S. G.; Rinzler, A. G.; Colbert, D. T.; Scuseria, G. E.; Tomanek, D.; Fischer, J. E.; Smalley, R. E. *Science* **1996**, *273*, 483-487.

19. Ebbesen, T. W.; Lezec, H. J.; Hiura, H.; Bennett, J. W.; Ghaemi, H. F.; Thio, T. *Nature* **1996**, *382*, 54-56.

20. Nuzzo, R. G.; Zegarski, B. R.; Dubois, L. H. *J. Am. Chem. Soc.* **1987**, *109*, 733-740.

21. Chen, R. J.; Zhang, Y. G.; Wang, D. W.; Dai, H. *J. Am. Chem. Soc.* **2001**, *123*, 3838-3839.

22. Ogawa, T.; Kobayashi, K.; Masuda, G..; Takase, T.; Maeda, S. *Thin Solid Films* **2001**, *393*, 374-378.

23. Huang, W.; Masuda, G.; Maeda, S.; Tanaka, H.; Ogawa, T. *Chem. Eur. J.* **2006**, *12*, 607-619.

24. Tanaka, H.; Yajima, T.; Matsumoto, T.; Ogawa, T. *Adv. Mater.* **2006**, *18*, 1411.

25. Tanaka, H.; Yajima, T.; Masahiro, K.; Ogawa, T. *J. Nanosci. Nanotechnol.* **2006**, *6, 1644.*

26. Seybold, P. G.; Gouterman, M. *J. Mol. Spectro.* **1969**, *31*, 1-13.

27. Ogawa, T.; Nishimoto, Y.; Yoshida, N.; Ono, N.; Osuka, A. *Angew. Chem. Int. Ed.* **1999**, *38*, 176-179.

28. Ogawa, T.; Nishimoto, Y.; Yoshida, N.; Ono, N.; Osuka, A. *Chem.*

Commun. **1998**, 337-338.

29. Kawao, M.; Ozawa, H.; Tanaka, H.; Ogawa, T. *Thin Solid Films* **2005**, *499*, 23-28.

30. Plater, M. J.; Aiken, S.; Bourhill, G. *Tetrahedron* **2002**, *58*, 2405-2413.

31. Gryko, D. T.; Clausen, C.; Roth, K. M.; Dontha, N.; Bocian, D. F.; Kuhr, W. G.; Lindsey, J. S. *J. Org. Chem.* **2000**, *65*, 7345-7533.

32. Hissler, M.; Harriman, A.; Khatyr, A.; Ziessel, R. *Chem. Eur. J.* **1999**, *5*, 3366-3381.

Chapter. 6 Thesis Summary

In this thesis, the synthesis, the structure on solis surfaces and optical properties of dendron portected porphyrin polymers were described. The porphyrin polymer are interested in the field of materials chemistry and moleclar electronics. The lengths of dendron protected porphyrin polymer were more than 100 nm and the heights were higher than non-dendron protected porphyrin polymers. It is easy to observe by AFM. Dendron protected porphyrin polymer may be useful for measurment of condactance on single molecule using PCI-AFM and double probe SPM.

As inorganic materials, we used gold nanoparticles. The gold nanoparticles were capped by 4-pyridineethanethiol were synthesized by ligand exchange method. The pyridine capped gold nanoparticles (py-AuNPs) were charactrized by UV-Vis absorption spectra, FT-IR, ^{1}H NMR and TEM.

We prepared a one-dimensional assemlbies of AuNPs chemically linked to porphyrin polymer.the assembies were observation by AFM and SEM. These results imply that AuNPs connected to every four-porphyrin unit. New organic-inorganic materials will bring us the new materials chemistry.

The I-V measurements and photo responses of assemblies were measured. The assemblies were trapped between gap electrodes using AC current. Photo responses were observed from devices, which were porphyrin polymer and AuNPs assemblies.

End-functionalized porphyrin polymers were synthesized and the effect of end capping groups to main π-systems were investigated. UV-Vis absorption and fluorescence spectra of the monomers were affected by the capping groups, however the effect decreased as the number of porphyrin units increased. The studies described here open a new area for construction of organic-inorganic materials.

List of publication

Takuji Ogawa, Hiroaki Ozawa, Masahiro Kawao, Hirofumi Tanaka.
"Photo-response behavior of Au nano-particle/porphyrin polymer composite device with nano-gapped electrodes"
J. Mat. Sci., in press.

Hiroaki Ozawa, Masahiro Kawao, Hirofumi Tanaka, Takuji Ogawa.
"Synthesis of Dendron Protected Porphyrin Wires and Preparation of a One-Dimensional Assembly of Gold Nanoparticles Chemically Linked to the π-Conjugated Wires"
Langmuir, in press.

Hiroaki Ozawa, Masahiro Kawao, Hirofumi Tanaka, Takuji Ogawa.
"Synthesis and end-functionalized π-conjugated porphyrin oligomers"
Tetrahedron, **62**, 4749-4755 (2006).

Hiroaki Ozawa, Takuji Ogawa.
"Synthesis of thick porphyrin molecular wires by a palladium catalyzed oligomerization"
Int. J. Nanosci., **1**, 483-487 (2002).

The following paper is related to the present work, but not included.

R. Negishi, T. Hasegawa, H. Tanaka, K. Terabe, H. Ozawa, T. Ogawa, M. Aono.
"Size-dependent single electron tunneling effect in Au nanoparticles"
Surf. Sci., in press.

Masahiro Kawao, Hiroaki Ozawa, Hirofumi Tanaka, Takuji Ogawa.
"Synthesis and self-assembly of novel porphyrin molecular wires"
Thin Solid Films **499**, 23-28 (2006).

List of presentations

○小澤　寛晃、　河尾　真宏、　田中　啓文、　小川　琢治
「末端に金微粒子を導入したポルフィリンポリマーの作製」
日本化学会第８７春季年会
大阪 (2007/3/28)

○Hiroaki Ozawa, Masahiro Kawao, Hirofumi Tanaka, Takuji Ogawa
“PREPATATION OF SUPRAMOLECULAR ASSEMBLIES OF GOLD NANOPARTICLES WITH PORPHYRINS”
Asian Conference on Nanoscience & Nanotechnology
Busan, Korea (2006/11/02)

○小澤　寛晃、　河尾　真宏、　田中　啓文、　小川　琢治
「π-共役ポルフィリンポリマーに化学結合した金微粒子の一次元集合体の作製」
日本化学会第８６春季年会
千葉 (2006/3/27)

○Hiroaki Ozawa, Masahiro Kawao, Hirofumi Tanaka, Takuji Ogawa
“Preparation of One-Dimensional Assembly of Gold Nanoparticles Chemically Linked to □-Conjugated Porphyrin polymers”
International Symposium on Molecular Scale Electronics
Tsukuba (2005/12/05)

○小澤　寛晃、　河尾　真宏、　田中　啓文、　小川　琢治
「LB法を用いたポルフィリンワイヤーの基板状での自己組織化」
日本化学会第８５春季年会
横浜 (2005/3/26)

○Hiroaki Ozawa, Masahiro Kawao, Hirofumi Tanaka, Takuji Ogawa
“The homogeneous deposition of dendron protected porphyrin wires on

various substrates using Langmuir-Blodgett method”
The 6th International Conference on Nano-Molecular Electronics
Kobe (2004/12/15)

○小澤　寛晃、　河尾　真宏、　田中　啓文、　小川　琢治
「デンドロン保護ポルフィリンワイヤーの単分子物性計測」
第５３回　高分子学会
北海道 (2004/9/15)

○小澤　寛晃、　河尾　真宏、　田中　啓文、　小川　琢治
“AFM observation of dendron protected porphyrin wires”
有機分子材料討論会
静岡 (2004/8/8)

○小澤　寛晃、　河尾　真宏、　小川　琢治
「デンドロン保護されたポルフィリンワイヤーとその電気伝導性」
分子エレクトロニクス研究会
愛知 (2004/4/9)

○Hiroaki Ozawa, Takuji Ogawa
“Synthesis and characterization of dendrimer protected conjugated porphyrin wires”
New Horizons in Molecular Science and Systems: An Integrated Approach
Okinawa (2003/10/16)

○小澤　寛晃、　河尾　真宏、　小川　琢治
「直径の大きなポルフィリンワイヤーの合成と AFM における測定」
日本化学会第８３春季年会
東京 (2003/3/18)

○Hiroaki Ozawa, Takuji Ogawa
“Synthesis of thick porphyrin molecular wires by a palladium catalyzed

oligomerization”
Asian Symposium on Nanotechnology and Nanoscience
Tokyo, (2002/11/27)

○小澤　寛晃、　小川　琢治
「デンドロン保護されたポルフィリンワイヤーの合成」
第１８回若手化学者のための化学道場愛媛２００２
愛媛　(2002/7/31)

○小澤　寛晃、小川　琢治
「デンドリマー保護されたポルフィリンワイヤーの合成」
日本化学会第８１春季年会
東京　(2002/3/26)

Acknowledgement

The author wishes to express his gratitude to Professor Takuji Ogawa at Institute for Molecular Science (IMS), for his invaluable guidance and encouragement throughout this study.

The author is deeply grateful to Dr. Hirofumi Tanaka at IMS and all the members of Ogawa group.

The author would like to give thanks to Dr. Hirokazu Sato and Dr. Osamu Tsutsumi at Ebara Research Co., Ltd. for their help and suggestion throughout this work.

The author gratefully acknowledges to Dr. Koiti Araki at Sao Paulo university, Dr. Wei Huang at Nanjing university, Dr. Takashi Nakanishi at NIMS, and Dr. Ryota Negishi at NIMS for their help in the experiments.

The author also wishes to thank Professor Hidemitsu Uno at Ehime university, Assistant professor Toshi Nagata at IMS and Dr. Toshiyuki Nagasawa at IMS for their help in the experiment of organic synthesis and valuable discussions.

Finally, the author wishes to thank his parents for their patience and healthful encouragement.